

Lars Oftedal Bjørum

Development of a Digital Twin for Condition Monitoring, Focusing on Electrical Propulsion Systems for Marine Application

Master's thesis in Marine Technology

Supervisor: Amir Nejad

June 2019

Lars Oftedal Bjørum

Development of a Digital Twin for Condition Monitoring, Focusing on Electrical Propulsion Systems for Marine Application

Master's thesis in Marine Technology
Supervisor: Amir Nejad
June 2019

Norwegian University of Science and Technology
Faculty of Engineering
Department of Marine Technology

 **NTNU**
Norwegian University of
Science and Technology

Abstract

This thesis considers the concept of digital twins for condition monitoring purposes, which is becoming an integral part of the simulation, testing and operation of different products. The technology has great potential for improving operation and cost efficiency of vessels. This report discusses the possible applications of digital twins in the maritime industry and gives an introduction to the digital twin of NTNU's research vessel RV Gunnerus.

The idea explored in the thesis is the possibility of using a digital twin as a condition monitoring tool of the Permanent Magnet Azimuth (PM-AZ) thrusters propelling R/V Gunnerus. As the world fleet is moving towards electric propulsion and automation, condition monitoring of these critical systems will become increasingly important. The thesis includes a study on condition monitoring and fault detection techniques targeting vessel propulsion systems. State-of-the-art electric propulsion systems are discussed, giving an overview of contributors to downtime of these systems. Research shows that bearing faults, stator faults, broken rotor bars and eccentricity-related faults are to be given serious attention regarding fault detection and maintenance.

Several condition monitoring approaches are researched through a literature review. Techniques focusing on Permanent Magnet Synchronous Motors (PMSM) are given the most attention. Given a complete and high-resolution stream of sensor data from R/V Gunnerus, it is debated that a combination of a signal-based and model-based approach monitoring the power signals would be a good approach. However, in light of the low quality of the sensor data, a thermal modelling approach combined with a statistical fault detection algorithm has been conducted in the case study.

Results from the electromagnetic analysis in RMXprt were used in a Lumped Parameter Thermal Network to simulate the thermal behaviour of a PMSM. This model simulates the temperature in the stator core, the armature copper windings, the permanent magnets and the rotor core. The results of the temperature simulations seem realistic and are within the expected range. Still, the lack of experimental or historical data from the vessel makes it hard to verify the accuracy of the results. The results of the simulations show that the winding temperature under overload scenarios can cause temperatures to exceed the maximum allowed limit. The distribution of the data was analysed in terms of normality, and the results show that the winding temperatures at different operating points are within the range of normality. A fault detection algorithm was modelled to detect changes in the mean and standard deviation of a time series. The results were promising, and an overload scenario was detected. A simple lifetime estimation model based on the winding insulation damage was built to predict the remaining lifetime of the motor. The results show that operation over the temperature limit will have a large effect on the remaining lifetime of the motor.

The method used in this thesis has been a physics-based modelling approach in combination with a data-driven fault detection algorithm. The literature shows that non-invasive Motor Current Signature Analysis (MCSA) is the most useful technique to identify faults in rotating electric motors. The low cost and efficiency of data driven-methods based on artificial intelligence are key elements of future condition monitoring. However, for vessels without proper data infrastructure, a combination of model-based and data-driven condition monitoring can serve as a good tool for monitoring, fault detection and lifetime estimation of electrical machinery.

Sammendrag

Denne oppgaven omhandler bruk av digitale tvillinger for tilstandsovervåking, som har utviklet seg til å bli en integrert del av simulering, testing og drift av ulike produkter. Teknologien viser stort potensial for å forbedre driften og kostnadseffektiviteten av skip. Denne rapporten drøfter mulige anvendelser av digitale tvillinger i den maritime industrien, og gir en introduksjon til den digitale tvillingen av NTNUs forskningsfartøy R/V Gunnerus.

Ideen utforsket i avhandlingen er muligheten for å bruke en digital tvilling som et tilstandsovervåkingsverktøy for Permanent Magnet Azimuth (PM-AZ) thrustere som driver R/V Gunnerus. Etter hvert som verdensflåten beveger seg mot elektrisk fremdrift og automatisering vil tilstandsovervåking av disse kritiske systemene bli stadig viktigere. Avhandlingen inneholder en undersøkelse av tilstandsovervåking og feildetekteringsteknikker rettet mot fartøyets fremdriftssystem. Toppmoderne elektriske fremdriftssystemer diskuteres, noe som gir en oversikt over bidragsyttere til nedetid på disse systemene. Forskning viser at feil på drev, stator, ødelagte rotorstenger og eksentrisitetsrelaterede feil må gis oppmerksomhet ved feilsøking og vedlikehold.

Flere tilstandsovervåkningsmetoder undersøkes gjennom en litteraturstudie. Teknikker som fokuserer på Permanent Magnet Synkron Motorer (PMSM) får mest oppmerksomhet. Gitt en komplett og høyoppløselig flyt av sensordata fra R/V Gunnerus, vil en kombinasjon av en signalbasert og en modellbasert metode som overvåker signalene være en god tilnærming. I lys av den lave kvaliteten på sensordataen ble imidlertid en termisk modelleringsmetode kombinert med en statistisk feildetekteringsalgoritme gjennomført.

Resultatene fra den elektromagnetiske analysen i RMxpRT ble brukt i en matematisk modell for å simulere den termiske oppførelsen til en PMSM. Denne modellen simulerer temperaturen i stator kjernen, kobberviklingene, permanent magnetene og rotorkjernen. Resultatene fra temperatursimuleringene virker realistiske og ligger innenfor det forventede intervallet. Likevel gjør mangelen på eksperimentelle eller historiske data fra fartøyet det vanskelig å bekrefte nøyaktigheten av resultatene. Resultatene av simuleringene viser at viklingstemperaturen under overbelastningsscenarier kan føre til at temperaturene overskrider den maksimalt tillatte grensen. Sannsynlighetsfordelingen av dataene ble analysert i forhold til normalitet, og resultatene viser at viklingstemperaturene ved forskjellige driftspunkter ligger innenfor normalitetsområdet. En algoritme for detektering av feil ble modellert ved å lete etter endringer i gjennomsnitt og standardavvik for en tidsserie. Resultatene var lovende, og et overbelastningsscenario ble oppdaget. En enkel estimeringsmodell av levetid basert på skade av kobberisolasjonen ble laget for å forutsi gjenværende levetid på motoren. Resultatene viser at drift over temperaturgrensen vil ha stor effekt på motorens gjenværende levetid.

Metoden som brukes i denne oppgaven har vært en fysikkbasert modelleringsmetode i kombinasjon med en data-drevet feildetekteringsalgoritme. Litteraturen viser at en signaturanalyse av strømmen i motoren er den mest nyttige teknikken for å identifisere feil i roterende elektriske motorer. Effektiviteten av data-drevne metoder basert på kunstig intelligens vil være sentrale elementer i fremtidig tilstandsovervåking. For skip uten riktig datainfrastruktur kan imidlertid en kombinasjon av modellbasert og data-drevet tilstandsovervåking fungere som et godt verktøy for overvåking, feilsøking og estimering av levetid.

Preface

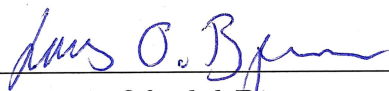
This paper is a master thesis and a part of the study programme Marine Technology at the Norwegian University of Science and Technology (NTNU).

The work was carried out during the spring semester of 2019 for the course *TMR4930 Marine Technology, master thesis*, at the Department of Marine Systems Design/Machinery. The workload and the weighting are 30 ECTS and the supervisor for this thesis is Amir Rasekhi Nejad. The work in this thesis is a continued work of the project thesis that was written in the fall semester of 2018. Chapter 2, 3 and 4 is based on the work done in the project thesis.

The focus in this thesis has been aimed towards modelling of a digital twin of an electric motor for the purpose of condition monitoring. This is motivated to be an integrated part of a complete digital twin of R/V Gunnerus, functioning as a fault detection tool for monitoring the permanent magnet azimuth thrusters. The work has been done by employing state-of-the-art tools and methods to model and simulate the behaviour of permanent magnet motors for marine application. The motor used for analysis was modelled in RMXprt and MATLAB with simulations done in MATLAB/Simulink. The literature studies have been conducted to gain insight into the various solutions for electrical propulsion systems, as well as methods for modelling and performing fault detection for such systems.

Conducting different modelling and simulation approaches has been very interesting and educational. With a background as a marine engineer, modelling of electrical systems have been challenging but rewarding. As the maritime industry is turning towards electrification and digitalization, I have tried to give a holistic perspective to some of the challenges and solutions for using digital twins for condition monitoring. I believe this has been a valuable time for me and that the knowledge I have attained in this project will be beneficial in the future.

Trondheim, 11th June 2019


Lars Oftedal Bjørum

Acknowledgment

This research is supervised by Amir Rasekhi Nejad, and I would like to thank him for his guidance and fruitful discussions around the topic. He has steered me in the right direction both theoretically and in terms of structuring the outline of the thesis. His door is always open and he is glad to share his thoughts and knowledge, as well as introducing you to other resourceful people at NTNU and from the industry.

Furthermore, I would like to thank PhD candidate Farid Khazaeli Moghadam for providing me with the model in RMXprt, for his valuable help with the electromagnetic simulations and the thesis work in general. I am thankful for his help and comments on my work. Finally, I would like to thank my colleagues in office C1.062 for always keeping the coffee warm and for providing input and discussing the subject of this project.

Contents

Abstract	i
Sammendrag	iii
Preface	v
Acknowledgment	vii
List of tables	xi
List of figures	xiii
Acronyms	xvi
1 Introduction	1
1.1 Motivation	1
1.2 Objective	2
1.3 Outline	2
2 Digital Twins	4
2.1 Application of Digital Twins in Maritime	6
2.2 Digital Twin of R/V Gunnerus	8
2.2.1 Gunnerus Sensor Data	11
3 Electric Propulsion in Maritime	13
3.1 Introduction	13
3.2 State-of-the-art	13
3.2.1 Conventional Fixed Pitch Propeller	13
3.2.2 Synchronous Azimuth/Azipod Propulsion	15
3.2.3 Asynchronous Azimuth Propulsion	17
3.2.4 Permanent Magnet Azimuth Thrusters	18
4 Fault Detection and Condition Monitoring	21
4.1 General	21
4.2 State-of-the-art in Condition Monitoring	22
4.3 Condition Monitoring of Permanent Magnet Machines	23
4.4 Signature-based Approach	24
4.5 Knowledge-based Approach	25
4.6 Model-based Approach	27
4.6.1 Thermal Modelling of PMSM	28
5 Case Study	31
5.1 Introduction	31
5.2 Motor	32
5.3 Approach	33
6 Modelling and Analysis Theory	34

6.1	Thermal Modelling	34
6.1.1	Lumped Parameter Thermal Network	36
6.1.2	Lower Order Models	37
6.2	Gaussian Processes	38
6.2.1	Gaussian Processes for regression	39
7	Methodology	41
7.1	Software	41
7.2	Electromagnetic Model	42
7.3	Thermal Model	43
7.3.1	Lower Order Model	45
7.4	Thermal Simulation	47
7.5	Modelling Faults	47
7.6	Fault Detection Algorithm	48
7.7	Lifetime Estimation	49
8	Results and Discussion	51
8.1	Electromagnetic Simulation - Power losses	51
8.1.1	Results	52
8.2	Temperature Results	58
8.3	Distribution of Temperature Data	62
8.4	Fault Detection	65
8.5	Lifetime Estimation	66
8.6	Uncertainty	68
8.7	CM Methods	68
9	Conclusions and Recommendations for Further Work	70
9.1	Concluding Remarks	70
9.2	Recommendations for Further Work	71
	References	73
	APPENDICES	I
	A Gunnerus Sensors	I
	B Motor Model	V

List of Tables

- 4.1 Fault types and percentage of occurrence in induction motors [42] 23
- 5.1 General design data 32
- 6.1 Analogy between electrical and thermal parameters 34
- 7.1 Thermal barriers and conductivities 45
- 7.2 Resistances [K/W] of the seven node thermal network 45
- 7.3 Capacitances [J/K] of the four node thermal network 46
- 8.1 Power losses at 20, 160 and 200 kW 51
- 8.2 Temperatures in $[C^o]$ at rated voltage and speed for different power output 58
- 8.3 Descriptive statistics of winding temperatures at different power outputs . 63

List of Figures

- 1.1 Flow chart of thesis structure 3
- 2.1 Virtual doppelganger of RV Gunnerus 4
- 2.2 Breakdown of the Digital Twin [68] 5
- 2.3 Digital twin in manufacturing [57] 7
- 2.4 Historic and projected development of digital twins in maritime [21]. 8
- 2.5 Workflow of digital twin development 9
- 2.6 Building blocks of Gunnerus Digital Twin 9
- 2.7 Overview of vessel in Digital Twin viewer 10
- 2.8 Location of sensors and other data sources embedded in the visual ship model 11
- 2.9 Detailed view of azimuth thruster with sensor and metadata from product model. 12
- 2.10 Power BI dashboard visualizing some of the sensor data from Gunnerus. . . 12
- 3.1 Propulsion system of an LNG carrier [36] 14
- 3.2 Synchronous motor rotor [38] 14
- 3.3 Podded propulsor [38] 16
- 3.4 Examples of azipod variants [28] 17
- 3.5 Axial view of an induction motor [38] 18
- 3.6 Induction motor [38] 18

3.7	Cross section of a permanent magnet synchronous machine [15]	19
3.8	Rolls Royce permanent magnet thruster [56]	19
3.9	Gunnerus fitted with two PM-AZ thrusters [56]	19
3.10	Propulsion curve, operating profile and efficiency [56]	20
4.1	A diagram of PMSM usual faults [84]	24
4.2	Neural Network Node [14]	26
4.3	Structure of Neural Network proposed in [14]	27
4.4	Park transformation [44]	28
4.5	(a) Shafted PMSM. (b) Heat flow diagram [16]	29
5.1	Figure of PMSM [61]	32
5.2	Illustration of the motor used for analysis in ANSYS electronics	33
6.1	Analogy between electric and thermal networks [16]	35
6.2	Example of a LPTN representing the heat flow in a PMSM motor	36
6.3	Three-node LPTN equivalent circuit [67]	38
6.4	Gaussian process for 2 training points and 1 testing point [50].	38
6.5	Gaussian function plots	39
7.1	Snippet of the motor in Maxwell 2D	42
7.2	LPTN representing the heat flow within the motor	44
7.3	LPTN equivalent circuit simplified for symmetry reasons	44
7.4	Four-node LPTN equivalent circuit	46
7.5	Descriptive statistics tool in Excel	48
8.1	IC loss vs rpm at 20kW	52
8.2	IC loss vs voltage at 20kW	52
8.3	IC losses at 20 kW, 3D-Plot	52
8.4	AC loss vs rpm at 20kW	53
8.5	AC loss vs voltage at 20kW	53
8.6	AC losses at 20kW, 3D-Plot	53
8.7	IC loss vs rpm at 160kW	54
8.8	IC loss vs voltage at 160kW	54
8.9	IC losses at 160 kW, 3D-Plot	54
8.10	AC loss vs rpm at 160kW	55
8.11	AC loss vs voltage at 160kW	55
8.12	AC losses at 160kW, 3D-Plot	55
8.13	IC loss vs rpm at 200kW	56
8.14	IC loss vs voltage at 200kW	56
8.15	IC losses at 200 kW, 3D-Plot	56
8.16	AC loss vs rpm at 200kW	57
8.17	AC loss vs voltage at 200kW	57
8.18	AC losses at 200kW, 3D-Plot	57
8.19	Temperature in 4 nodes at 20 kW	59
8.20	Simulations of winding temperature at 20 kW for different V and rpm	59
8.21	Temperature in 4 nodes at 160 kW	60
8.22	Simulations of winding temperature at 160 kW for different V and rpm	61
8.23	Temperature in 4 nodes at 200 kW	61
8.24	Simulations of winding temperature at 200 kW for different V and rpm	62

8.25	Distribution of winding temperatures at 20 kW	63
8.26	Distribution of winding temperatures at 160 kW	64
8.27	Distribution of winding temperatures at 200 kW	64
8.28	Simulation of temperature with overload scenario	65
8.29	Score representing deviation from Gaussian distribution at normal operation	66
8.30	Cumulated winding damage	67
8.31	Residual lifetime for winding	67
A.1	Spreadsheet describing enabled sensors	II
A.2	Gunnerus sensor chart	III
A.3	Gunnerus operational profile 12 h	IV
B.1	Design sheet of PMSM	VI
B.2	Circuit of PMSM in Maxwell	VII

Acronyms

AC Armature Copper.

AI Artificial Intelligence.

AIS Automatic Identification System.

ANN Artificial Neural Network.

AR Augmented Reality.

AZ Azimuth.

CM Condition Monitoring.

DP Dynamic Positioning.

DQ0 Direct-Quadrature-Zero Transformation.

EMD Empirical Mode Decomposition.

FFT Fast Fourier Transform.

GDQ Generalized DQ Model.

HHT Hilbert-Huang Transform.

IC Iron Core.

IoT Internet of Things.

LCC Low Computational Cost.

LNG Liquid Natural Gas.

LPTN Lumped Parameter Thermal Network.

MCSA Motor Current Signature Analysis.

MRO Maintenance, Repair and Overhaul.

OSV Offshore Supply Vessel.

PLM Product Lifecycle Management.

PM Permanent Magnet.

PM-AZ Permanent Magnet Azimuth.

PMOD Vessel Product Model.

PMSM Permanent Magnet Synchronous Motor.

PSO Particle Swarm Optimization.

PWM Pulse Width Modulation.

R/V Research Vessel.

RTDS Real Time Digital Simulator.

STFT Short-Time Fourier Transform.

TF Time Frequency.

VR Virtual Reality.

WT Wavelet Transform.

WVD Wagner-Ville Distribution.

Chapter 1

Introduction

1.1 Motivation

The growth and pressure of digitalization in the shipping industry are increasing. The development is rapid, and the amount of data collected from vessels are enormous. However, to fully utilize the collected data, it needs to be combined with existing models to describe a clear picture of the system.

Detailed vehicle simulations based on sensor data dynamics as well as physical and dynamic models make the building blocks for a “digital twin”. This digital twin refers to a comprehensive physical and functional description of a component, product or system, which includes more or less all information that can be useful in later lifecycle phases.

In the maritime industry, there are a lot of possibilities with using digital twins. Large and complex vessels are dependent on high reliability and operability when sailing around the world. A digital twin for life cycle monitoring and management could be very advantageous for a more energy efficient and smart ship design. For instance, the digital twin of a vessels machinery system can be modelled. When including sensor data, the condition of the system can be monitored. This requires creating a sufficiently high-fidelity model of these types of systems, as well as formulating algorithms for fault diagnosis. In order to get an accurate twin, the design would have to be very sophisticated, containing several subsystems.

During the summer of 2018, NTNU, DNV GL and Digitread collaborated on a project aimed at developing a digital twin of R/V Gunnerus. This resulted in a detailed 3D model of the entire vessel, a tool for displaying the different systems and components in addition to visualized sensor data from the vessel itself. The propulsion system on Gunnerus is diesel-electric, with three generator sets supplying the different systems with electric power. This type of electrical propulsion system is a growing segment in the maritime industry, as vessels become more and more electrified. In order to increase the performance and reliability of these systems, a tool for fault detection and performance monitoring should be developed. The idea for this thesis is to explore the possibilities of improving the digital twin of Gunnerus with a dynamic representation of a system. The existing digital twin is a static representation of shape, attributes and sensor data. Simulation will be an enabler to determine the behaviour of the system, making the digital twin dynamic.

1.2 Objective

The aim of the thesis is to study and evaluate different condition monitoring techniques related to electrical propulsion systems on vessels. Another aim is to identify the requirements needed to build a dynamic model of such a system. This includes a mapping of the required sensors as well as the different tools and methods to be used. The thesis aims to build on some of the work done in the “Gunnerus Digital Twin Project”, and a detailed description of this project will be included. As of 2015, Gunnerus was equipped with two new Rolls Royce Permanent Magnet Azimuth Thrusters (PM-AZ). As these thrusters are based on state-of-the-art technology while being such crucial components with available sensor data, this assignment will focus on studying different techniques to model these types of electric propulsion systems.

A case study will include the description and building of a physics-based model of the electric motor. This model will mainly focus on thermal behaviour, but also include other types of analysis. The results from the model will be used to perform condition monitoring and lifetime estimation of the PM-AZ thrusters based on the winding temperature. The case study will be used to describe how such a model can become an integrated part of the digital twin. This is a step towards using a digital twin to perform condition monitoring.

1.3 Outline

This section is an explanation of the structure of the thesis. Figure 1.1 is a visualization of the connection between the chapters.

Chapter 2: Digital Twins

This chapter is an introduction to the concept of digital twins. An overview of the application of digital twins in the maritime industry is given, and its advantages and challenges are presented. The digital twin of R/V Gunnerus is described in detail, and the available data from sensors on board is discussed.

Chapter 3: Electric Propulsion in Maritime

Chapter 3 presents an overview of the state-of-the-art electric propulsion systems used in the maritime industry. The most popular solutions are described in detail, and research and literature on advantages and challenges with the different systems are reviewed.

Chapter 4: Fault Detection and Condition Monitoring

This chapter is an overview of the research and literature as well as the state-of-the-art techniques within fault detection and condition monitoring of rotating electric motors. Methods for condition monitoring of Permanent Magnet Synchronous Machines are discussed in detail. A model-based approach for thermal monitoring is reviewed.

Chapter 5: Case Study

In this chapter, the objective and approach of the case study are presented. The motor used for analysis is also described.

Chapter 6: Modelling and Analysis Theory

The theories behind the methods of thermal modelling and Gaussian processes are described in chapter 6. Lumped Parameter Thermal Networks are described, and the theory

behind using Gaussian processes for regression is presented.

Chapter 7: Methodology

The methodology chapter describes the approach used to obtain the results of the case study. The relevant software is presented, and the approach of the RMxprt analysis is shown. The thermal modelling method is described, and simulation approaches are planned. Faulty stated to be detected is described, and the method for estimating motor lifetime estimation based on winding temperature is presented.

Chapter 8: Results and Discussion

Results from analysis, simulations etc. are presented and discussed in chapter 8. In addition to this, uncertainties of the results and the different condition monitoring methods are discussed.

Chapter 9: Conclusions and Recommendations for Further Work

Key findings from chapter 8 are presented and briefly discussed along with recommendations for further work.

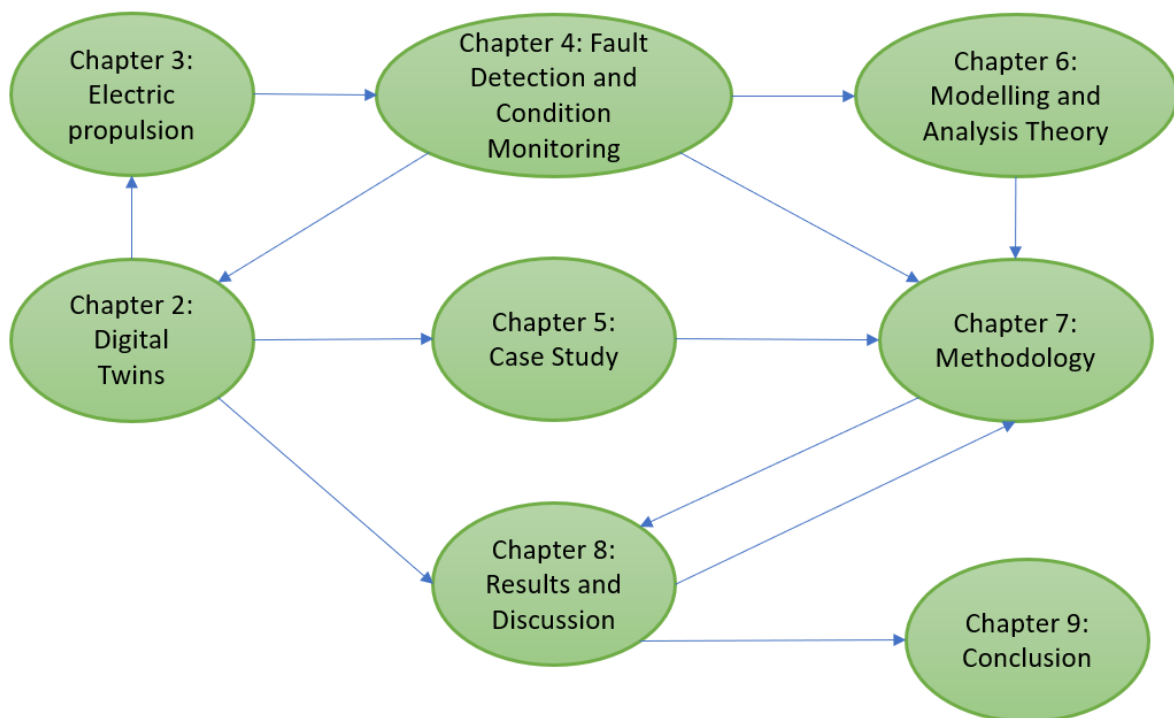


Figure 1.1: Flow chart of thesis structure

Chapter 2

Digital Twins

In recent years, digital twins have started to show their potential in the marketplace. Digital twins are not a new idea, however. Several car manufacturers and the US Air Force have used them in different stages of a product's lifecycle, with a goal to reduce cost and man-hours. In the maritime industry, the examples of fully utilizing integrated digital twins are lacking. Several tools and models for simulating different systems on a vessel already exists. A digital twin of a ship will combine all of these available models and information throughout its lifecycle. A variety of operations can be performed, including system design, simulation, condition monitoring and predictive maintenance as a tool to enable greater pro-activity to avoid risks and maximize profitability [68].



Figure 2.1: Virtual doppelganger of RV Gunnerus

In general, the digital twin is a virtual doppelganger of the vessel itself, call it a complex ecosystem of connected things, such as an autonomous vessel in the Trondheim fjord. The digital twin is more than just a 3D model. It's a model that sees the ship as a system of complex systems like propulsion, navigation, electronics and communication. The idea is that one can analyze the performance of the vessel under every condition and over its entire lifecycle, from conceptual design to decommissioning. Digital twins are being used to model the physical performance, but also how more complex systems will behave together as a whole [39].

The enablers of digital twins are three emerging technologies:

- Simulation software and tools
- IoT and sensors
- Power of machine learning and predictive analytics

The simulation software and tools represent the heart of the digital twin. Today, state of the art tools can replicate and virtualize the performance of products and systems based on the laws of physics. Digital twins are essentially simulations of components in action, based on operational data generated over long periods of time by sensors from critical parts. The Internet of Things, enabled by sensors and increasing connectivity allows us to capture real-time data, send it to the cloud, and store it in large quantities. We can then set the emerging power of machine learning and predictive analytics to work on all those data streams. This serves as a critical tool, providing capabilities that were previously accomplished through costly trial and error [39].

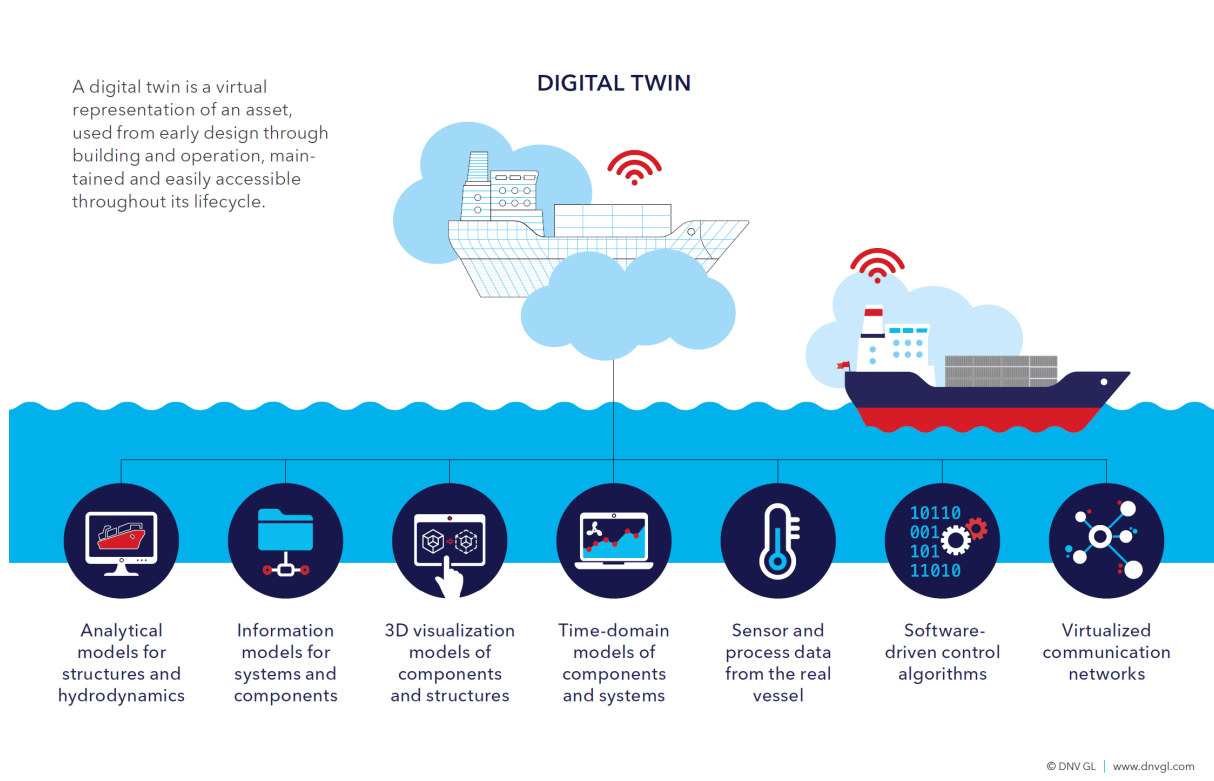


Figure 2.2: Breakdown of the Digital Twin [68]

The digital twins can bring a lot of value to different industries. The question is how it will bring value to the maritime industry, and how it will affect the way we build and operate ships. Optimally the digital twin will be constructed before the design and building of the real vessel. This will allow designers to start modelling and verifying how the vessel will perform under different operations and conditions. Building the twin might start with evaluating different, already existing components together. Data on e.g. type of propulsion, propeller, main dimensions and hull shapes will then be used to analyze the interaction between the different systems. Other data layers such as operational data from similar models, control system software or AIS and weather data can be added to improve the model. The ship designers can then use this data in combination with

machine intelligence tools to optimize the design against the requirements, long before the steel is cut [39].

Then comes the Product Lifecycle Management (PLM) part of the digital twin. Engineers will be able to see what is happening, and why. They can speed up the simulation in order to find when, why and how faults will occur. This will allow designers, builders, operators and other stakeholders to reduce costs, improving efficiency and bettering safety throughout the lifecycle of the vessel [68]. Another point is in regards to the development of autonomous ships. To quote Øyvind Smogeli at DNV GL; "Industries such as maritime are moving over to cyber-physical systems, and you cannot verify and classify these only on the basis of documentation - these systems need to be tested in a simulated environment"[39].

2.1 Application of Digital Twins in Maritime

GE has a vision of a digital twin model including all necessary aspects of the physical asset or larger system including thermal, mechanical, electrical, chemical, fluid dynamic, material, lifting, economic and statistical models [22]. These models are also meant to accurately represent the vessel under different variations related to operations. Using these models combined with techniques like optimization, control and forecasting, the digital twin can be used to predict outcomes along different axes. In conjunction with the sensor data, the model will have the ability to predict the vessel's performance, evaluate different scenarios, understand trade-offs and enhance efficiency [22]. The digital twin models are continuously updated as the vessel is operated. At any moment the twin will represent a faithful representation of the current state.

One potential application for vessels is optimizing efficiency by adjusting operational settings and finding the best possible load for different operations. Such an optimizer uses an online performance model together with real-time optimization to give periodic recommendations for operation. Another application that will be discussed further is having an asset life optimizer. This application will use different models to predict the remaining time left before maintenance is required. Maintenance schedules can be altered if a component experiences an unforeseen anomaly. These anomalies can be caused by failed components, deviations from the design operating profile etc. The goal of these models will be to reduce unplanned maintenance and optimize scheduled maintenance based on condition rather than fixed dates [22].

Digital Twins also has the potential to play a part of all ship manufacturing processes, achieving optimized ship design, manufacturing and MRO (Maintenance, Repair and Overhaul) etc. [72]. In the design phase, it involves interaction between the virtual and the physical world. A digital twin will enable iterative optimization of the design, helping designers to iteratively adjust and improve the design. Also, digital twins can be used to predict and verify product functions, behaviour, structures and manufacturability etc. [66]. The digital twin can accurately find defects in designs through virtual simulations, make the necessary improvements and thus avoiding tedious verification and testing [57]. Figure 2.3 is a good illustration of digital twin integration of manufacturing processes.

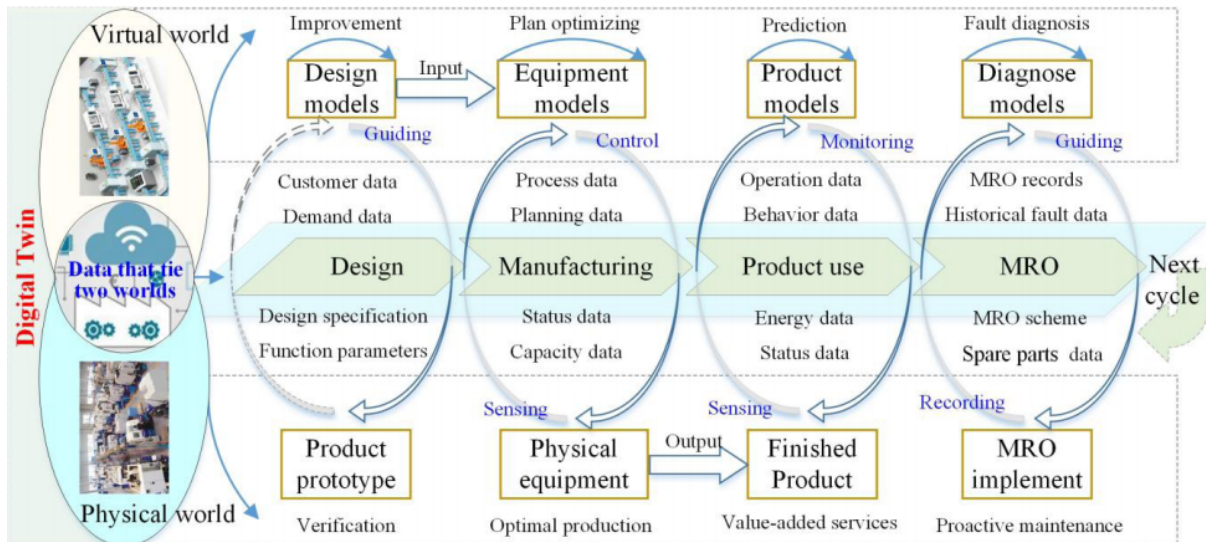


Figure 2.3: Digital twin in manufacturing [57]

Next, the proven ship design is sent to the yard for manufacturing. From the input of raw material, steel cutting and to the output of finished vessels, the whole manufacturing process is managed and optimized through a digital twin [62]. The virtual yard can simulate and evaluate the different manufacturing strategies until the best planning is found. In the building phase of the project, real-time monitoring and adjustment of manufacturing processes can be done through virtual-physical interaction and iteration. The virtual models will be updated based on data from the yard, staying updated in case of changes. Using simulation of the virtual yard, the manufacturing process can be adjusted to achieve optimal manufacturing [57].

As discussed earlier, the virtual model of the vessel will have an as-built standard when the vessel is completed. The digital twin will then follow the vessel throughout its lifecycle to provide value-added services. Users can see the latest state and position of the vessel, as well as any potential faults and warnings. Walkthrough MRO strategies can be executed in VR or AR in order to evaluate the effectiveness and execution of a plan. Lastly, the data from the different stages of the vessels lifecycle can be accumulated and inherited to contribute to the construction and operation of the next generation vessels [57].

The key enablers of digital twins within the maritime industry is presented by Erikstad in [21]. Figure 2.4 presents the historic and projected development for using digital twins in maritime.

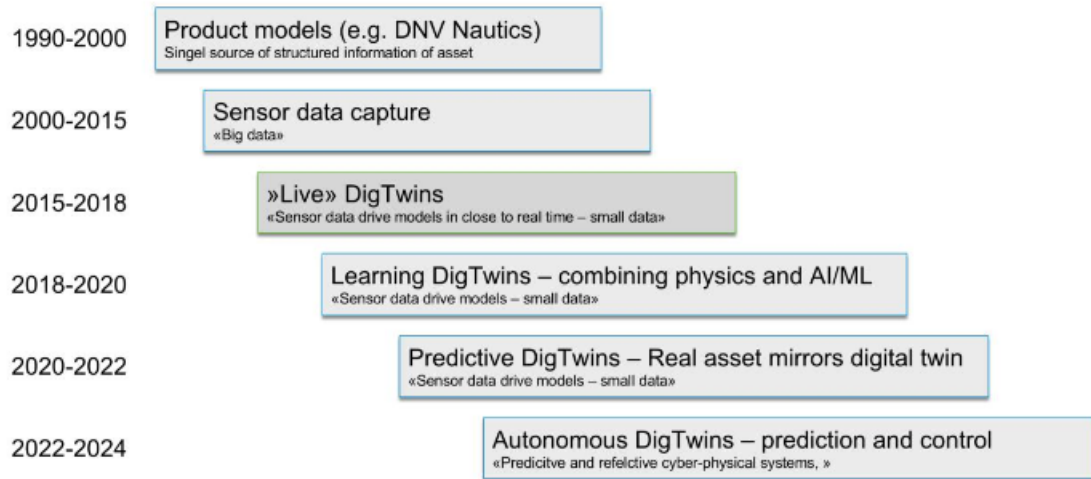


Figure 2.4: Historic and projected development of digital twins in maritime [21].

2.2 Digital Twin of R/V Gunnerus

The basis for a digital twin of R/V Gunnerus was developed in a collaborative project between NTNU, DNV GL and Digitread. The summer of 2018, five NTNU students, including myself, were involved in a student project aimed at developing the digital twin of R/V Gunnerus. The purpose of the project was among other things to increase the knowledge relevant for digitalization within marine technology. This included the chain from measurement techniques, sensors, data capture from systems and equipment on board a ship, via structuring and analysis of data, to use the derived information for decision support.

The summer project contributed to the foundations for an architecture of the R/V Gunnerus digital twin. The digital twin consists of different building blocks that are integrated on a shared platform. These building blocks are:

1. A detailed 3D-model of R/V Gunnerus
2. Vessel/component information and documentation
3. Sensor data information

The detailed 3D-model of the vessel was modelled in Siemens NX. This model was connected to sensor information and data, as well as the vessel product model (PMOD) that provides information about the different components and systems on board. These elements were managed and connected through DNV GL's Veracity data platform. A digital twin viewer that is supported in Veracity, is integrating and connecting all building blocks and is where the user can interact with the end product. The workflow connecting these building blocks is shown in figure 2.5.

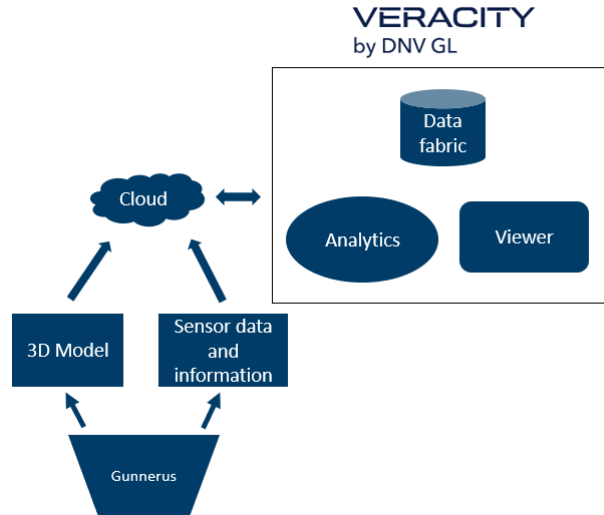


Figure 2.5: Workflow of digital twin development

Figure 2.6 shows another illustration of the building blocks that are a part of the Gunnerus digital twin. There is a lot more to a digital twin than this, but we have built a basis to build on in the future. When comparing with figure 2.2, we see that we have covered more or less 3 of the 7 building blocks in DNV GL’s breakdown of a digital twin. The information models for systems and components are collected from the vessel PMOD and connected with the visualized model. The Gunnerus PMOD has been updated this summer and contains information and parameters on the key components and systems on board the vessel.

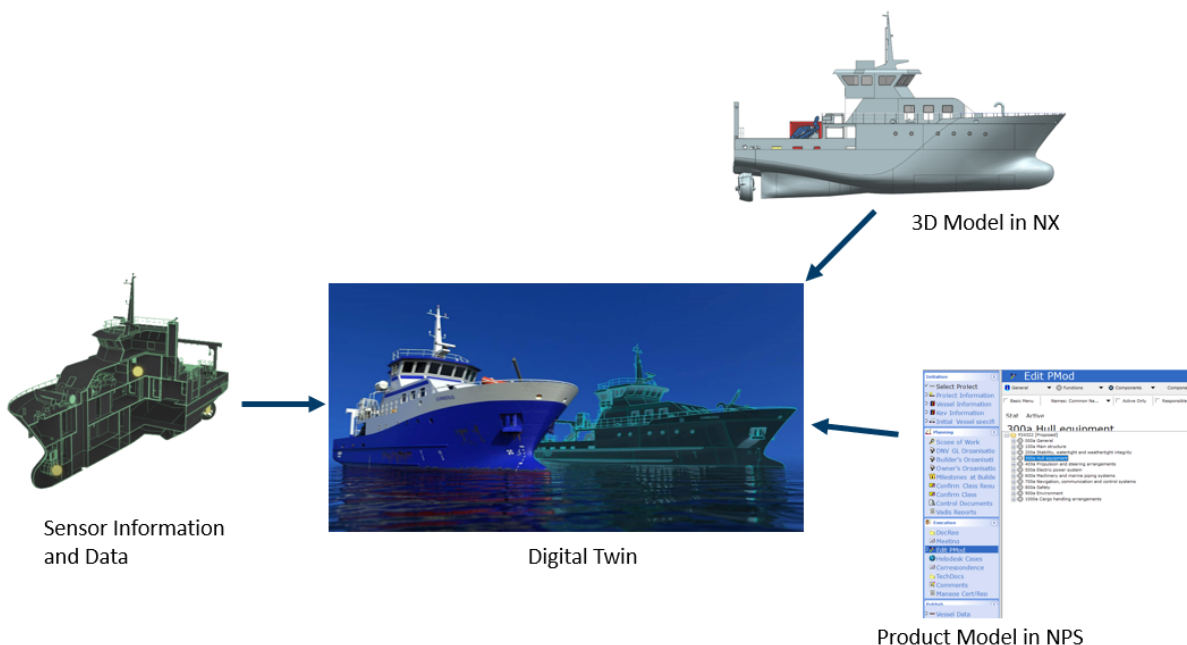


Figure 2.6: Building blocks of Gunnerus Digital Twin

The 3D visualization models of components and structures are very important for having a visual and intuitive digital twin. Therefore, a lot of hours was spent doing robust modelling in Siemens NX. The model consists in part of several smaller assemblies with

already created components, whereas other systems have to be explicitly modelled. Besides modelling the vessel, the location of the different sensors in the vessel was defined as a layer on top of the 3D-model. The finished 3D-model was exported to the digital twin viewer and connected to the vessel information model. An overview of the vessel in the digital twin viewer can be seen in figure 2.7 below:



Figure 2.7: Overview of vessel in Digital Twin viewer

My task in the project was to connect the 3D model to the information and data available from the vessel. This required a detailed mapping of the sensors, where each signal was given a description, a code, and the data from the given sensor was reviewed. Data from the functioning sensors were filtered in Python and stored in the cloud. Another part of the task was to update the PMOD of Gunnerus, making sure all useful information about the different systems and components was available and correct. This PMOD was then integrated with Veracity as a web-based viewer accessing the PMOD database. This made it possible to integrate the PMOD information with the digital twin. The next part of the process was to visualize the filtered sensor data. A dashboard in Power BI was made for Gunnerus, and this was also made available as a Veracity application. A continuous dialogue with the 3D-viewer developers helped us connect the PMOD and dashboard with the 3D-model.

The digital twin of R/V Gunnerus as of now can be used for a variety of purposes, even though it is far from complete. It serves as a simple platform for learning about basic naval architecture and terminology related to ships. It can serve as an interactive and good visualization of the vessel for the crew and users. Key components and system information can also be easily accessed by clicking a selected ship component.

In addition to the vessel overview and access to metadata, the sensors are shown as clickable spheres. Like with the vessel components, relevant metadata can be accessed and links to visualized data from the selected sensor are included. The user functionality can be seen in figure 2.8, showing some of the sensors found on the vessel. Note the colour coding of the spheres, allowing the sensor node to display any type of status or faulty condition at the given position.

Different Sensors Installed for Demo

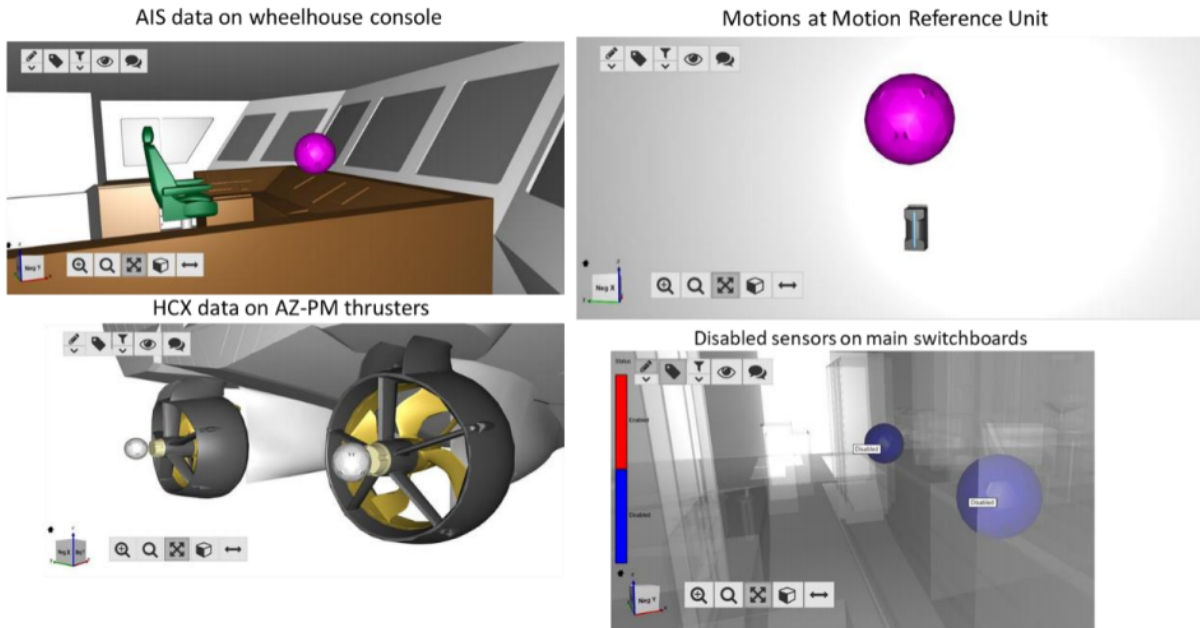


Figure 2.8: Location of sensors and other data sources embedded in the visual ship model

A summary video of the project can be found by following this link:
http://folk.ntnu.no/asbjorns/Gunnerus_Demo_Video.mp4

2.2.1 Gunnerus Sensor Data

As described in the objective, the Permanent Magnet Azimuth thrusters are equipped with a number of sensors. Historical data from these are available for evaluation and analysis. This is the reason why the case study in this thesis focuses on the thruster system. The study will research how the digital twin of Gunnerus can be developed further to include condition monitoring and simulation in order to give a health status of the system. The R/V Gunnerus digital twin already presents a detailed overview of the PM-AZ thrusters. This can be seen in figure 2.9.

In the same detail view as in figure 2.9, a link to the Power BI dashboard is provided. This dashboard visualizes sensor data time series and AIS data. Figure 2.10 shows one part of the dashboard, displaying different signals from Gunnerus while in operation. For the Digital Twin summer project, a Non-Disclosure Agreement was signed between NTNU and Rolls-Royce Marine in order to use historical data from the AZ-PM Thrusters. Appendix A displays a spreadsheet and illustration describing the different sensors from where data is available. From this illustration, it is clear that there exists data from some but not all of the interesting vessel subsystems

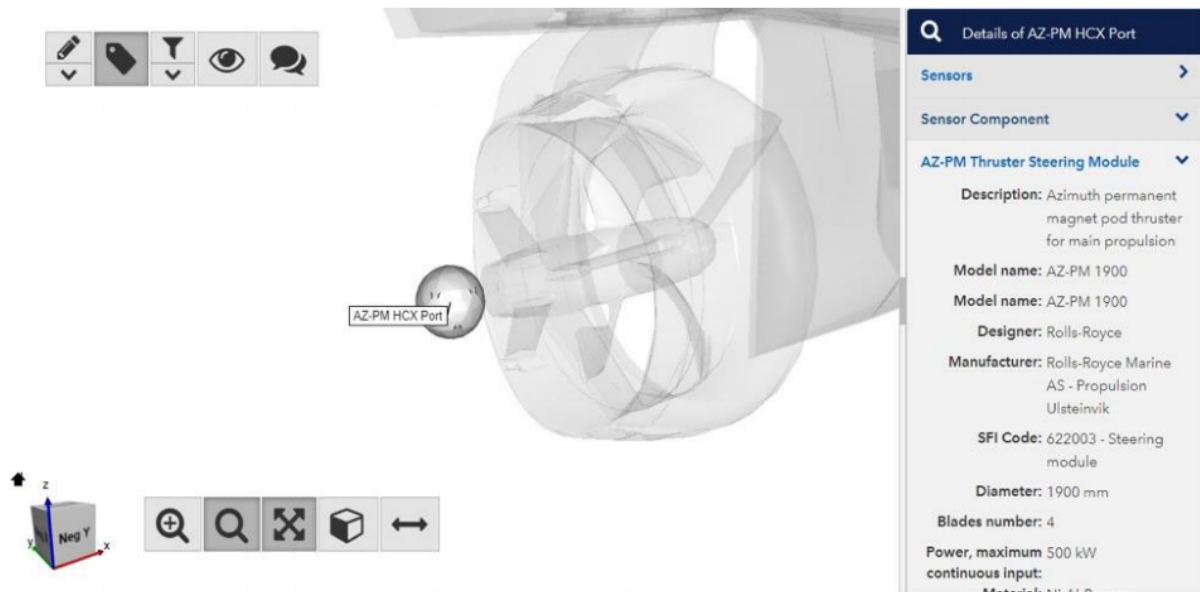


Figure 2.9: Detailed view of azimuth thruster with sensor and metadata from product model.

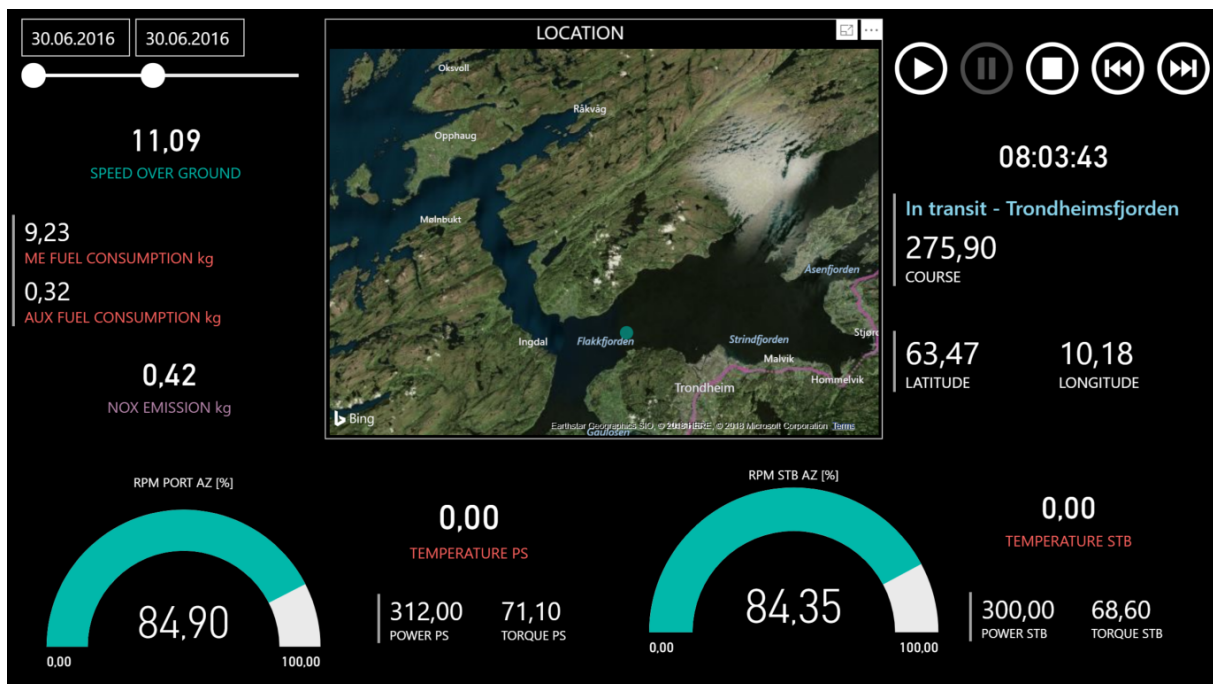


Figure 2.10: Power BI dashboard visualizing some of the sensor data from Gunnerus.

Making sense of the available sensor data can also be a challenge, as there exists little standardization in the naming of sensor signals, with data coming from systems delivered by several vendors. Many signals were ambiguous or nonsensical, and some signals gave little insight into the physical state of the vessel but only triggered some other control system function. Other signals, like temperature, did not seem to give any nonzero value at all. This is discussed further in chapter 5.

Chapter 3

Electric Propulsion in Maritime

3.1 Introduction

Electric propulsion has developed into one of the most efficient propulsion arrangements for several vessel types over the last decade [28]. The development of semiconductor switching devices has opened up for full rpm control of propellers and thrusters, enabling simplification of the mechanical structure. Electric propulsion also has the potential for fuel savings compared to direct drive propulsion. This potential lies with the highly varying operational profile of commercial vessels, who are seldom running at design speed. This favours electrical production of power that can be produced and stored with the optimum running of prime movers. Vessels such as icebreakers, cruise vessels, DP off-shore vessels, LNG carriers and other special vessels etc. are being designed with electric propulsion [54].

3.2 State-of-the-art

There has been developed a lot of different variants of electrical propulsion systems in recent years. In the following sections, some of the most common systems will be presented along with the most common faults and condition monitoring techniques for the given system. The main types described are conventional fixed pitch systems and different types of azipod and azimuth propulsion systems, including permanent magnet azimuth thrusters like the ones installed on R/V Gunnerus.

3.2.1 Conventional Fixed Pitch Propeller

Dual fuel electric vessels have become more or less standard for newbuilding of LNG Carriers lately. These have a configuration of either single or double fixed pitch propeller systems powered by two electric motors each via a twin input/single output reduction gearbox. This is basically the same mechanical single shaft-line configuration as for traditional steam or diesel ships [36]. The reduction gear enables the use of medium speed electric motors of less physical size than corresponding slow speed motors [28]. Figure 3.1 shows such a single-screw propulsion system.

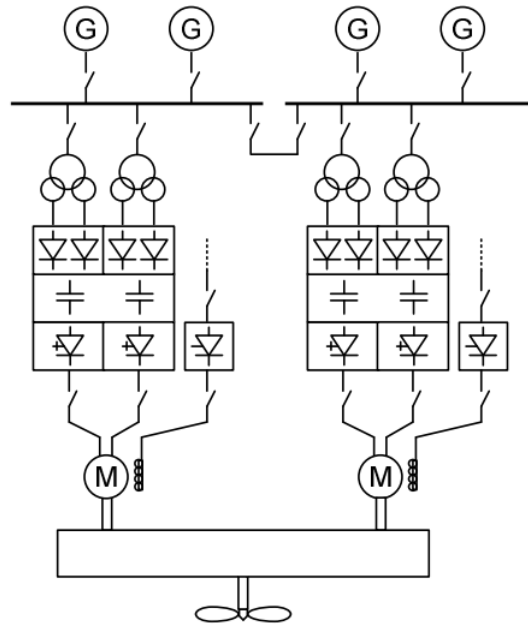


Figure 3.1: Propulsion system of an LNG carrier [36]

Regardless of the number of propellers, these are typically equipped with four or five dual fuel engines powering the electric plant. This plant consists of switchboards, transformers, converters and two synchronous propulsion motors. This system will provide a gain in efficiency, especially in the lower power range. Synchronous propulsion motors provide high efficiency and low weight to power ratio. The motors come with two stator windings, because of the power level that requires double inverter units in the frequency converter. These sort of systems have a high level of redundancy given the possibility of running on one stator winding [36].

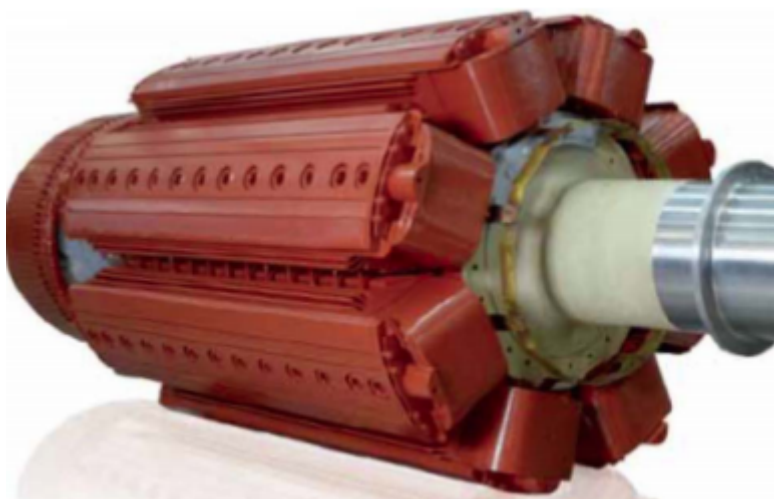


Figure 3.2: Synchronous motor rotor [38]

Synchronous motors have been the preferred propulsor for application above 10 MW since the 1980s. For direct slow speed propulsion, synchronous propulsors can be selected

down to 5 MW application [28]. The synchronous motor has an inner rotor with a number of poles with field windings around them. Figure 3.2 shows a photograph of a synchronous motor rotor. The stator of the machine is wound with coils consistent with the number of poles in the rotor. Synchronous motors require dc current to be supplied to the rotor, which typically requires slip rings and brushes. These are vulnerable in a marine application given the contact between the rotating parts while the motor is subjected to high variation in loads. However, slip rings may be avoided by providing dc to the rotor with a brushless exciter.

The drivetrain and gearbox of this sort of system will be critical components to monitor. Failures in gearboxes are costly both due to high repair downtime and the cost of the gearbox. In [52], the components with a higher probability of failure and lower level of reliability are detected based on their fatigue damage. This sort of "vulnerability map" can be used to pinpoint where it is most effective to install condition monitoring devices on the drivetrain. Acceleration measurements can be used to detect and prevent faults as fast as possible [25]. Methods to analyze vibration data for fault detection are many in numbers and well documented. In [53], a frequency based detection scheme is presented to detect potential faults in a wind turbine gearbox. Statistical methods like the one used in [25] can also be used for this purpose. This method detects a statistical change to the data coming from the gearbox.

Other possible faulty components in the system shown in figure 3.1 are the synchronous propulsion motors. Common faults and fault detection methods for these motors will be discussed in the next section.

3.2.2 Synchronous Azimuth/Azipod Propulsion

The introduction of podded propulsion and azimuthing thrusters has been a benefit for electric propulsion. In an Azipod thruster, the electric motor can be mounted directly on the propeller shaft in a submerged 360° steerable pod. This adds to the efficiency, improve manoeuvring and reduces installation space and cost [28]. The Azipod has proven well for ice going vessels and later also for cruise vessels and OSV's etc. Mechanically, an electric pod is simple in construction with a low number of rotating parts. The electric motor, often synchronous, is integrated with the thrust and propeller bearing. A synchronous electric motor is an AC motor in which, at steady state, the rotation of the shaft is synchronized with the frequency of the supply current [81]. The electric transmission is done via slip rings, and the pod is rotated by a steering unit placed directly above the pod [28]. See figure 3.3 below.

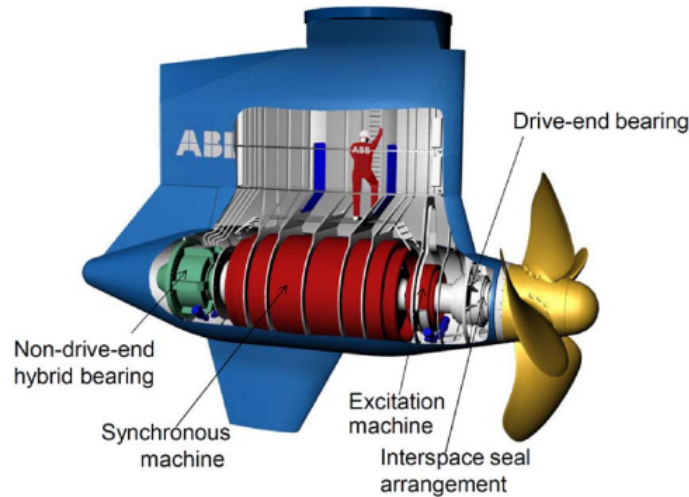


Figure 3.3: Podded propulsor [38]

Azimuth thrusters are, like the azipods, rotational devices for the production of thrust in any direction. The electric motor is usually vertically mounted on top of the thruster and drives an L-shaped gear transmission. Azimuth thrusters have a variable speed thruster motor drive and a fixed pitch type propeller that simplifies the underwater mechanical construction and reduces low-thrust losses significantly [1]. Today the propulsion motor for most azipod and many azimuth thrusters are dual-stator synchronous machines with a brushless excitation system. The synchronous motor has two stator windings with a 30-degree phase shift. As mentioned in section 3.2.1, the phase-shifted configuration with two separate stator windings provides redundancy and fault tolerance, because the motor also can operate with one stator winding. Commercial shipbuilding still prefers these traditional synchronous motors because of the efficiency, power factor, reliability and experience with previous vessels [36].

The most prevalent faults of synchronous propulsion motors can be summed up to four types [51]:

1. Bearing fault
2. Stator or armature faults
3. Broken rotor bar
4. Eccentricity related faults

For the purpose of detecting these faults, many diagnostic methods have been developed. These methods involve several different fields of science and technology. The most utilized methods are [51]:

1. Electromagnetic field monitoring
2. Temperature measurements
3. Infrared recognition
4. Radio-frequency emission monitoring

5. Noise and vibration monitoring
6. Chemical analysis
7. Acoustic noise measurements
8. Motor-current signature analysis
9. Model, artificial intelligence, and neural-network-based techniques

Many of these faults and their diagnosis techniques are the same for both synchronous, induction and permanent magnet propulsion motors, with some exceptions.

3.2.3 Asynchronous Azimuth Propulsion

At lower powers, a competitive solution to the synchronous motor is using asynchronous (induction) azimuth propellers. An induction motor is an AC electric motor in which the electric current in the rotor needed to produce torque is obtained by electromagnetic induction from the magnetic field of the stator winding [79]. The selection of induction motors has historically been for application below 5 MW. For power rating between 5 and 10 MW, the rated RPM is the decisive factor, indicating asynchronous for medium speed geared propulsion/thruster application up to 10MW. Recently, also asynchronous motors are introduced for larger ocean-going vessels, and the selection of motor type is mostly based on vendor preferences. Drilling vessels and OSVs require excellent dynamic positioning (DP) abilities. These are usually equipped with several thrusters and propulsion units at both the stern and the bow. In this category, induction motors are usually used. The thrusters are typically mechanical with an inboard electric motor or a podded unit with a submerged electric motor [28]. Figure 3.4 shows examples of azipod variants.

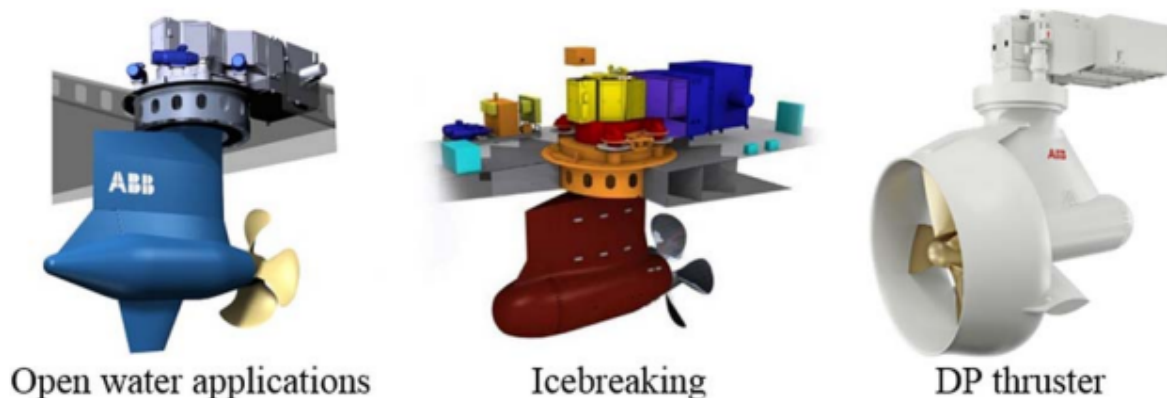


Figure 3.4: Examples of azipod variants [28]

When it comes to induction motors, they are very common in industrial, commercial and residential applications. They are simple, cheap, rugged, compact and efficient. The stator consists of windings just like in a synchronous machine, while the rotor might have a winding or a number of conductors around the periphery of the rotor ("squirrel cage"). Figure 3.5 and 3.6 show illustrations of an induction motor. The stator is connected to a voltage source, and the rotor is closely coupled to the stator while turning with a

rotational speed ω_m . The voltage source produces a rotating flux wave in the stator and air gap of the motor. The speed of this flux wave is given by

$$\Omega_s = \frac{\omega}{p} \quad (3.1)$$

where ω is the electrical frequency and p is the number of pole pairs. The motion of the flux wave with respect to the rotor induces currents in the rotor. These interact in turn with the flux wave to produce torque [38].

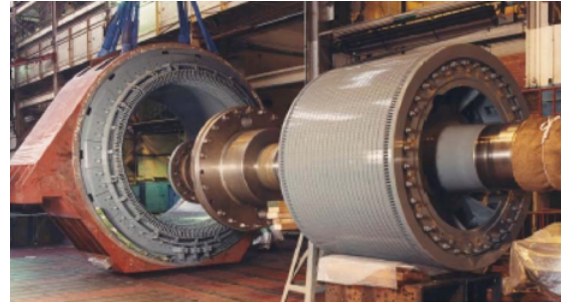
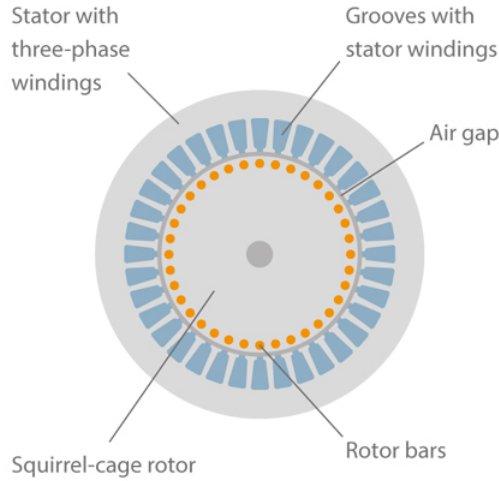


Figure 3.5: Axial view of an induction motor [38] **Figure 3.6:** Induction motor [38]

One of the advantages of having induction motors as ship propulsors is that they are physically simple and quite rugged. There is no commutator or slip rings that demand maintenance. Other than the main shaft bearings, there is no particular component demanding regular attention. Like all electrical machines, however, they are subject to the faults listed in section 3.2.2.

3.2.4 Permanent Magnet Azimuth Thrusters

Permanent magnet azimuth thrusters are considered state-of-the-art technology in the maritime industry. The Permanent Magnet Synchronous Machines (PMSM) are cheap to manufacture, have a high power density, high efficiency and low cogging torque. The machines have shown a high fault tolerance, which is an important factor in ship design [47]. The cross-sectional layout of a surface mounted permanent magnet motor is shown in figure 3.7.

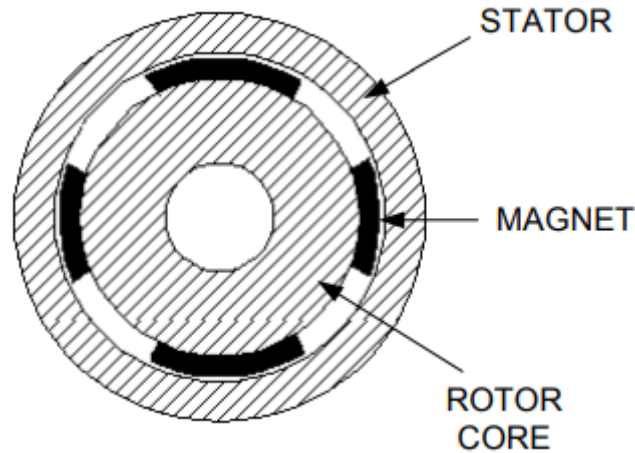


Figure 3.7: Cross section of a permanent magnet synchronous machine [15]

The machine consists of an outer stator, a set of permanent magnets and a rotational core. The stator carries a three-phase winding that produces a magnetic force based on the value of the stator current. The magnets are mounted on the surface of the rotor core and create a constant magnetic field [15]. When current is supplied to the stator the electromagnets are excited in a particular sequence and the resulting magnetic fields interact with the field from the rotor magnets creating a torque that turns the rotor and the propeller blades. These blades are joined to a hub in the centre of the thruster, which is meant to carry the bearings taking the thrust, provide the radial location of the rotor and improve hydrodynamics. Loads are transferred to the stator through struts, and both the rotor and stator are operating fully submerged sealed against water ingress [56]. See figure 3.8 below.

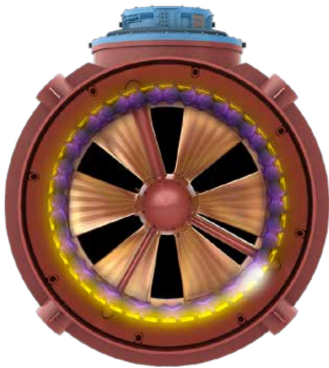


Figure 3.8: Rolls Royce permanent magnet thruster [56]



Figure 3.9: Gunnerus fitted with two PM-AZ thrusters [56]

In 2015, two PM-AZ thrusters were manufactured by Rolls Royce and installed on R/V Gunnerus for a long-term evaluation program. The two thrusters have a rating of 500kW to match the vessel's available power. In figure 3.9 one can see the vessel after being equipped with the new thrusters. A year after the conversion of the vessel, exact comparisons before and after were made. Bollard pull increased with 20 % and speed increased by about one knot for the same input power. Stability was good, and manoeuvrability greatly improved. The first year of testing, the thrusters ran more than 1500 hours

trouble-free [56]. See figure 3.10 below for results from the comparison between the old and the new propulsion system.

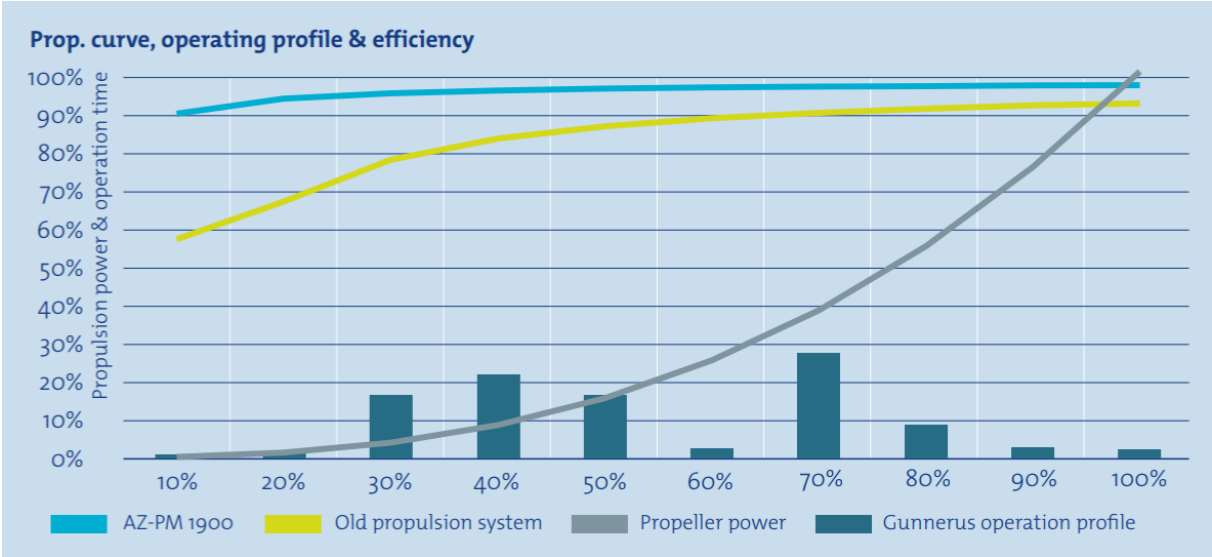


Figure 3.10: Propulsion curve, operating profile and efficiency [56]

Chapter 4

Fault Detection and Condition Monitoring

4.1 General

Fault detection is defined as the "determination of faults present in a system and time of detection" while faults are defined as "unpermitted deviation of at least one characteristic property or variable of the system" [34]. When it comes to maintenance, there are two different actions, corrective and preventive [55]. Corrective maintenance is a run-to-failure tactic, while a preventive maintenance tactic is to repair or replace system components before failure occurs. Corrective maintenance is considered more expensive, due to unforeseen downtime. However, there is no need for expensive monitoring systems, and therefore it may still be a preferred strategy. A preventive strategy could be the scheduling of maintenance or condition monitoring as a tool for fault detection [35].

Traditionally scheduled maintenance actions have been used to keep vessels operating at a desirable condition and to prevent system failure. This is typically scheduled using a probabilistic model of repairable system operation, failure and maintenance. However, this does not eliminate the risk of system failure and implies a risk of having unnecessary downtime due to maintenance. Therefore, condition-based maintenance policies have received more and more attention recently [82]. This type of method includes updated risks of failure and suggests maintenance action or inspection based on the system state [43]. The objective is to reduce wasted operating time and risk of failure associated with using a scheduled maintenance tactic.

Condition monitoring has been a technique of interest for a long time. It is a feature that has proven very valuable for any technical system. The principal objective of condition monitoring techniques is to construct a reliable mechanism for fault detection so that the system can be checked and repaired after being shut down in a controlled manner, avoiding excess downtime imposed by sudden breakdowns [42]. A condition monitoring system should be capable of monitoring the running machines while predicting the need for maintenance, identifying and locating the defects in detail and doing lifetime predictions. Four main parts should be included in a condition monitoring system [27]:

1. Sensors - converting physical quantities to electrical signals. Sensor selection relies on the monitoring method. On-line capability, sensitivity and cost are key requirements.
2. Data acquisition - data acquisition units are built to realize the amplification and pre-processing of sensor data.
3. Fault detection - detect an incipient fault appearing in the machine. Can be done by comparing the results from the sensors with predictive models. Another way is to use frequency and time-domain signal processing methods to obtain 'signatures' that represent normal or faulty performance.
4. Diagnosis - post-processing of the detected abnormal signals. Should include the name and location of each defect, the status of the machine, advises for maintenance etc.

4.2 State-of-the-art in Condition Monitoring

This section focus on giving a short summary of the recent developments in the field of condition monitoring and diagnosis of faults for determining the health of electric motors. This field of research has been attracting attention from researchers for more than three decades. Early research focuses on Acoustic Emission (AE) monitoring, vibration signature analysis and Motor Current Signature Analysis (MCSA), but these monitoring techniques are complex and require expensive sensors [49]. In [85] it is claimed that the major drawback with such CM techniques is the human interpretation and that automation of fault detection and diagnostics is a logical progression of the CM technologies.

These automatic fault diagnostic systems require an intelligent system such as artificial intelligence techniques, Genetic Algorithm (GA), Fuzzy Logic (FL), Artificial Neural Network (ANN) and expert systems [11]. ANN is a recent development in condition monitoring of electrical motors but has proven a powerful tool to estimate and predict the remaining useful lifetime more accurately [26]. Where machine learning algorithms are more suitable for big data gathering to draw conclusions about its operating state of health, ANN has been developed to effectively identify bearing faults in electrical rotating machines [11].

A comprehensive CM analysis based on motor signals must consider the inter-relationship between mechanical and electrical signals. Sources indicate that the use of stator current analysis techniques are considered most appropriate for the diagnosis of bearing faults [10]. Various non-contact methods are also widely discussed, and it has been found that Park vector analysis and instantaneous power analysis techniques are best suited for identifying motor fault signatures [11]. However, theoretical modelling analysis of machine faults is necessary to distinguish the faulty signatures, meaning the relevant component of the higher frequency spectrum that may be present due to machine saturation and harmonics distortion. In the next section, a review of condition monitoring of permanent magnet motors will be presented, and some of the most popular techniques will be presented in detail.

4.3 Condition Monitoring of Permanent Magnet Machines

Fault tolerance and reliability in electric propulsion systems are important design features besides functionality and efficiency for today’s modern vessels. The challenge is that a fault-tolerant design often requires more space and implies a higher cost. An alternative is to have more standardized machines and providing fault tolerance through sophisticated control methods. These sort of methods require detailed knowledge of the dynamic machine behaviour. For permanent magnet motors, this implies both electrical, magnetic and mechanical conditions [47].

Industrial surveys have revealed that a large percentage of faults in induction motors occur at stators, rotors, and bearings [37]. The statistical percentages of fault types and occurrence are listed in table 4.1.

Table 4.1: Fault types and percentage of occurrence in induction motors [42]

Fault type	Percentage	Category	Fault
Rotor faults	10 %	Electrical/Mechanical fault	Broken rotor bars Mass unbalance Air-gap eccentricity Rotor winding fault
Stator faults	37 %	Electrical fault	Unbalanced supply voltage Inter-turn fault Line-line fault Open short circuit SLG fault
Bearing faults	41 %	Mechanical fault	Air-gap eccentricity Bearing misalignment Single point defect
Other faults	12 %	Mechanical/Environmental	Colling fan breakage Vent clog by debris Ambient temp. External moisture

For these types of motors, as in most machines, faults occur in sequence. If a certain fault occurs at one point in the machine, it may cause a more severe fault at another location in the machine. This phenomenon makes it crucial to detect faults at the incipient stage [42]. A permanent magnet synchronous motor (PMSM) has many properties in common with an induction motor. Most of the faults listed in table 4.1 are problematic also for PMSM motors. In [84], such faults for these kinds of motors are described. As the permanent magnets of a PMSM are placed on the rotor, the rotor faults are in the category of demagnetization faults. The permanent magnets can be demagnetized by high temperatures, over-running load or two motors coupled to a single load. In figure 4.1 is a diagram of usual faults for a PMSM motor.

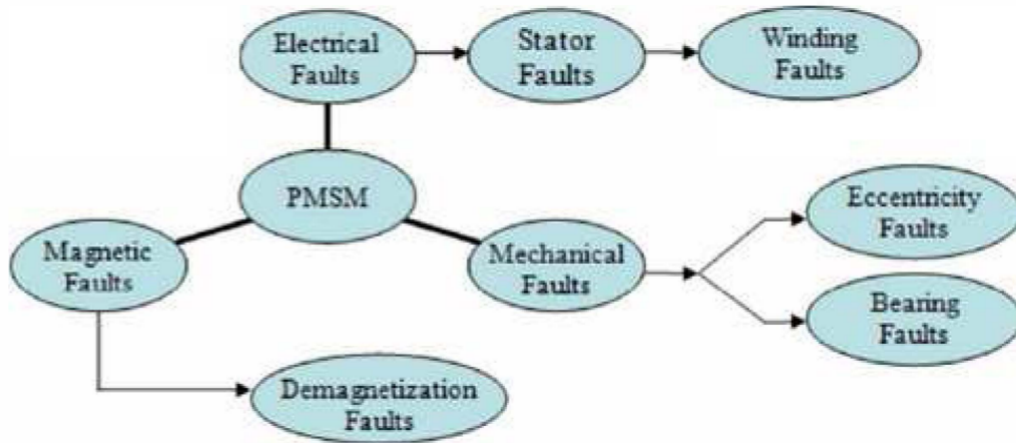


Figure 4.1: A diagram of PMSM usual faults [84]

Condition monitoring techniques can be divided into three fundamental categories [18]:

1. Signature extraction-based approach
2. Model-based approach
3. Knowledge-based approach

Looking at it from a broader perspective, condition monitoring techniques can be classified into two types: invasive and non-invasive. Where the invasive methods provide accurate and reliable results through the use of sensors, the non-invasive methods do not require installation of special sensors. The invasive methods are often complex and expensive but have a direct approach that does not require much expertise to understand. The non-invasive methods have a more economical approach with a relatively easy implementation procedure, but does require a more analytical approach and might require an expert's opinion [42].

Since the thrusters of RV Gunnerus are driven by permanent magnet synchronous motors, the next sections will give more extensive research on condition monitoring techniques for these types of motors. The three fundamental categories presented above will serve as subsections, and state-of-the-art approaches will be reviewed for potential use on this type of thruster. The objective will be to find effective methods to detect several critical conditions, such as the ones presented in table 4.1.

4.4 Signature-based Approach

Signature-based extraction involves analyzing properties of various output signals from sensors. Among various condition monitoring techniques, the monitored signals can be current, voltage, power, vibration, temperature and acoustic emission [42]. For instance, the frequency domain of the current signal can be used to detect several types of faults. These signal processing methods are widely used in the field of PMSM fault diagnosis. They are considered fast and efficient and does not require a specific model. These methods rely on knowledge of faulty signals from sensors. The faults are often detected by comparing the measured signals from a healthy and faulty system.

Joint time-frequency (TF) analysis is a common technique in signal processing. The problem with using some of these methods to analyze PMSM stator current, including Fast Fourier transform (FFT), is that some require stationary conditions. The stator current for PMSMs is easily influenced by torque and speed change, and obtaining stationary conditions for a PM thruster is unlikely given the constant change in vessel speed and varying loads [14].

Some methods, however, can cope with the non-stationary conditions. Short-time Fourier transform (STFT), wavelet transform (WT), Wigner-Ville distribution (WVD), Empirical Mode Decomposition (EMD) and Hilbert-Huang transform (HHT) are the most usual TF methods for fault diagnosis in PMSMs [84]. STFT is a useful and simple technique. This method needs a suitable window (Gaussian, Rectangle etc.) to match with specific frequencies in the signals. This window has to be chosen before analyzing and can influence the resolution of the frequency and time. STFT is defined by:

$$F_x(t, v, h) = \int_{\inf}^{\sup} x(u)h * (u - t)e^{-j2\pi v u} du \quad (4.1)$$

Where $x(t)$ is the signal to analyze and $h(t)$ is the selected window [84].

Wavelet transform (WT) has developed into one of the most popular tools to be applied in PMSM diagnosis, as it can analyze non-stationary time series at many different frequencies [64]. WT is different from STFT as it uses a variable-sized-regions windowing technique, allowing it to detect local features in signals like trends, breakdown points and discontinuities in higher derivatives [63].

Other methods like EMD and HHT are connected in a way that the analysis is adaptive, with no need for adaptive filters to follow non-stationary motor frequencies. Intrinsic Mode Functions (IMF) can be gained through EMD to decompose the signals at different frequency ranges. IMF can be transformed to Hilbert spectrum by using HHT, which is a simple technique for PMSM fault diagnosis. With the spectrum obtained by this method, one can get a full frequency-time energy distribution of the signal. HHT is defined as:

$$H[x(t)] = y(t) = \frac{1}{\pi} \int \frac{x(\tau)}{t - \tau} d\tau \quad (4.2)$$

Where $x(t)$ is the real component of the analytic function, and $y(t)$ is the imaginary component [30][83]. Signature-based methods can also be used to detect bearing faults. These faults are best detected with acoustic and vibration monitoring [14]. As of now, there are no data on vibration or acoustics available from the thrusters of Gunnerus. It seems that several signature-based approaches have been able to identify signatures of faulty states for a PMSM motor. However, these are often operating under stationary conditions.

4.5 Knowledge-based Approach

Knowledge-based methods/Artificial Intelligence (AI) use historical knowledge to determine faults. It is widely implemented in fault diagnosis and can improve the robustness and efficiency of this field. Artificial Neural Network (ANN), Fuzzy Logic and Particle

Swarm Optimization (PSO) are three AI methods that have been used for PMSM fault diagnosis [84]. These methods have produced excellent results for different types of faults [14]. However, they require extensive amounts of data, including data under various faulty modes. These methods are well suited for digital twins, as historical data can be collected and used to improve the AI-models [42].

Artificial Neural Network (ANN) is a method that can be applied to a lot of problems. The structure of such a method usually consists of an input layer, a hidden layer and an output layer. It can represent many kinds of systems such as non-linear by choosing different transfer functions [84]. See figure 4.2 for illustration of a single node in a network.

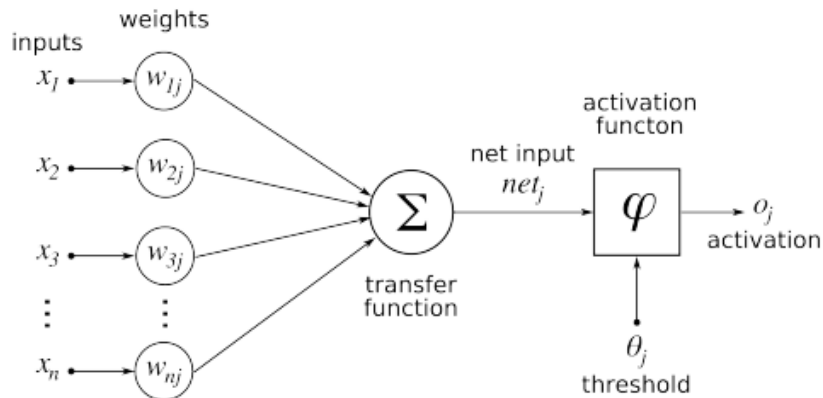


Figure 4.2: Neural Network Node [14]

The ANN technique is widely used in PMSM fault diagnosis. Such a network is structured into layers consisting of different nodes. The outputs from one layer typically become the inputs to the next layer. The final layer is the output, that contains the information about the condition and faults of the component. A full network used for condition monitoring of an induction motor can be seen in figure 4.3. The networks are trained by adjusting the weighting of the input at each node, based on the data provided to the network [14]. This training data is a set of inputs with an equivalent output reflecting a healthy or faulty state.

Examples of use are in fault detection of a single phase winding short, by using a multi-layer dynamic recurrent ANN [58]. In [14], two methods are implemented to support the digital twin of the autonomous model ReVolt. The first algorithm is a signature-based method using data from a functional motor, while the second relies on knowledge about faulty motors. The first method uses the current signal and speed of the motor at various setpoints. A model of acceptable measurements for each setpoint is calculated to create a zone that represents a normal functioning motor.

The second method in [14] is based on the ANN showed in figure 4.3. The input nodes are setpoint (PWM %), motor speed and motor current. When the output indicates a fault continually for a certain time interval, an alert is triggered. This helps prevent false positives when the motor is outside normal operation for a very short period. The network takes in labelled data from both non-functional and functional motors to train the network. The results from [14] showed that both algorithms were able to identify when the motors were functioning correctly, and also when one was broken. Results showed that the ANN was more consistent in detecting the faulty motor.

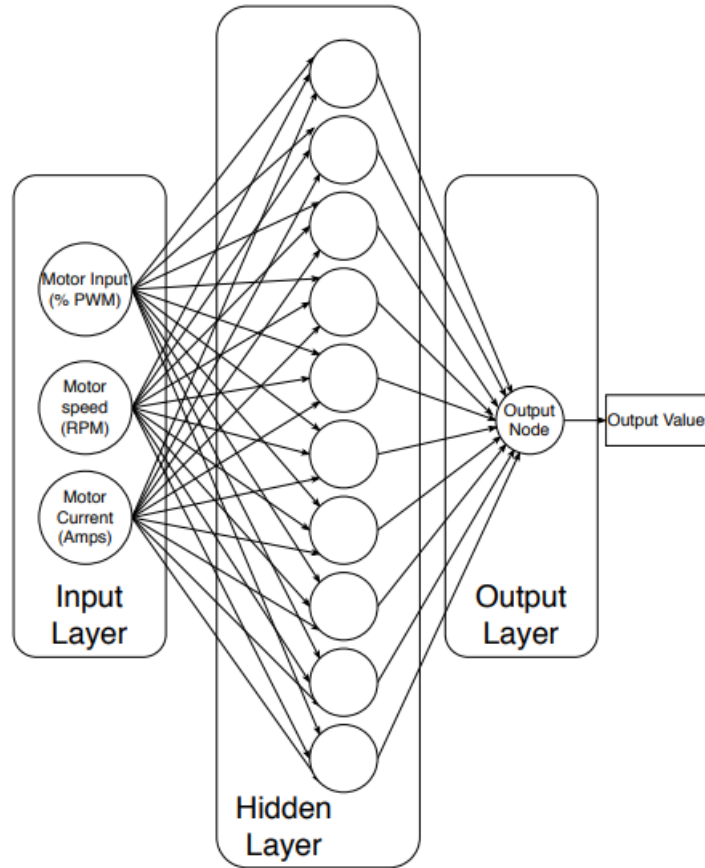


Figure 4.3: Structure of Neural Network proposed in [14]

Fuzzy logic is a method that translates the human perception of values. It consists of variables that are represented by words instead of numbers, fuzzy rules and fuzzy sets determined by practical experience. The advantages of fuzzy logic are good flexibility and tolerance to imprecise data [59]. There are examples of fuzzy logic being used to detect stator winding short circuit of a PMSM. The drawback of this method is that the results depend on the selection of rules and sets that are determined using practical experience [84].

Particle Swarm Optimization (PSO) is an evolutionary computation technique that uses swarm intelligent methodology. At first, a set of arbitrary solutions (particles) are found, before the optimal solution is discovered by iteration [86]. The PSO technique is fast, efficient and simple. It has been used for PMSM inter-turn short circuit fault identification in [45].

4.6 Model-based Approach

Model-based methods are another set of methods for condition monitoring of PMSMs. These methods use mathematical models of the motors in a healthy and faulty state. Enabled by powerful computers, various approaches have been proposed to model the behaviour of these types of motors under faulty conditions [5]. Many techniques have been presented for the use of the current signal from the motors [71]. The main drawback

of these approaches is their sensitivity to stator voltage unbalances. To overcome this, a solution based on the multiple reference frame theory has been suggested in [13]. Other methods are based on comprehensive mathematical models of PM motors and characteristic parameters of faults. These models need specified details of the fundamental motor parameters, as well as initial parameters that characterize the machine condition [5].

[15] presents two different approaches to model the permanent magnet synchronous machine in a real-time digital simulator (RTDS). This is the traditional dq0 model of the machine and the embedded phase domain model. The RTDS is a combination of specialized computer hardware and software designed specifically for the solution of power system electromagnetically transients in real time, much like the concept of digital twins. RTDS combines the real-time operational properties of analogue simulators with the flexibility and accuracy of digital simulation programs [15].

The dq0 transformation first presented in the late 1920s is widely considered as a sharp revolution of electric machine analysis [44]. In [44] a generalized dq model (GDQ) for a PMSM is presented based on an extended Park transformation. The dq0 transformation of a synchronous machine makes all sinusoidally varying inductance in the abc frame become constant in the dq frame. This transformation is also called Park transformation written in equation 4.3 and represented in figure 4.4 below.

$$T_p = \frac{2}{3} \begin{bmatrix} \cos\phi & \cos(\phi - 2\pi/3) & \cos(\phi - 4\pi/3) \\ -\sin\phi & -\sin(\phi - 2\pi/3) & -\sin(\phi - 4\pi/3) \\ 1/2 & 1/2 & 1/2 \end{bmatrix} \quad (4.3)$$

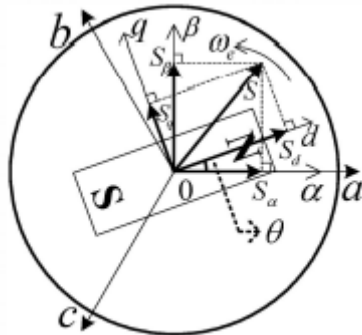


Figure 4.4: Park transformation [44]

Where T_p represents the Park transformation matrix. A lot of studies have shown that PMSM drives using the dq model edition based on the Park transformation have high performance. In [44], this sort of model produced promising results in modelling a healthy PMSM motor.

4.6.1 Thermal Modelling of PMSM

Overheating is one of the main reasons for permanent magnet synchronous motors breakdown, and the temperature is usually the main limiting factor for how much a PMSM can be loaded [41]. Damages can occur either by the breakdown of the stator winding

insulation or the demagnetization of the magnets if the thermal limit of a PMSM is exceeded [41]. A suitable temperature prediction method can prevent overheating, improve the utilization in normal operation, and give a good indication of the condition of the system in general. An ideal method for predicting temperature would be to have temperature sensors embedded into part of the motor structure. However, these sensors may in some cases affect the flow of current and cause problems regarding sensor assembling and maintenance. Another disadvantage is that most sensors have a relatively slow reaction time making them inadequate to the high speed of the heating process during motor acceleration [77].

An alternative to using temperature sensors are a real-time thermal model (RTTM) of the motor that can predict the thermal behaviours in time in order to protect the motor from high temperatures. If the motor is also equipped with temperature sensors, the results from the thermal model can be compared with the sensor data and give an indication of the motor condition. A trend in literature is that a considerable number of publications deal with thermal models for induction motors, but these analytical models can be applied to PMSM after some modifications [41]. The thermal model can also be combined with a standard lifetime model of the winding insulation to give an impression of the remaining lifetime of the motor.

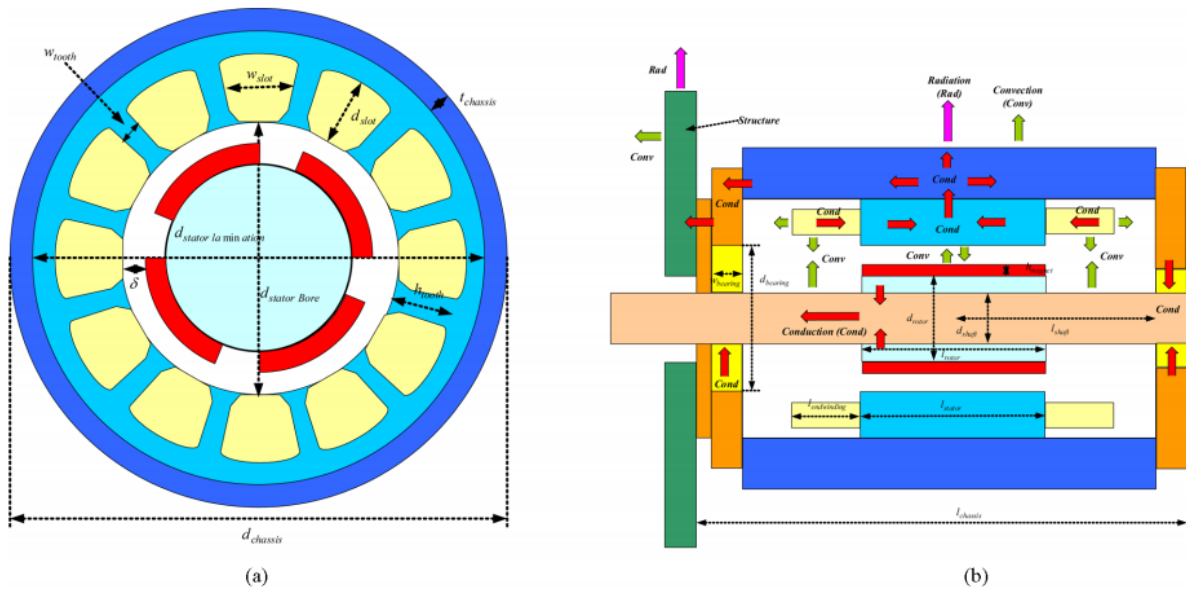


Figure 4.5: (a) Shafted PMSM. (b) Heat flow diagram [16]

Several approaches have been used to model the thermodynamics of a PMSM. Gerling and Dajaku [24] presents the most common equations for thermal analysis, and give a good overview of thermal modelling of electrical systems. In [7], Boglietti et al. develop a simplification of the thermal model presented in [48]. Despite the simplicity of this model, the accuracy of the resistances only deviates with 2.5%. This error is lower than uncertainty related to calculating the convective resistance itself [7]. Andersson [3] includes two different models of a PM motor, both simplified to some extent. One model uses optimized component parameters, while the other contains components based on real physical parameters [16]. Determination of the critical parameters in thermal models of electrical machines is studied in [8]. The work shows that parameters such as the convection heat transfer coefficient between winding and air gap, and thermal resistance

between frame and ambient are critical for the quality of the model. In figure 4.5(a), an example of a shafted PMSM is shown. Figure 4.5(b) shows the heat flow between the different parts of the motor. The red arrows represent the heat transport due to conduction, the green arrows the heat flow due to convection, and the purple due to radiation. Radiation has not been considered in this paper.

The behaviour of the machines can also be analyzed by combining thermal and electromagnetic analysis. In [17] and [2], finite-element method (FEM) analysis is used in combination with a thermal model, where a set of magnetic analyses is used to determine the parameters of the motor equivalent circuit [16]. Real-time thermal models (RTTM) are tools that aim to monitor temperatures to protect against thermal stresses and other faults. A considerable amount of literature can be found in this field, especially concerning stator winding temperature estimation [16]. In [40], an indicator of stator winding temperature is found by using an estimate of the stator resistance. The advantages of this method vs conventional thermal modelling are discussed, but it is also pointed out that the estimation of the stator resistance becomes difficult during high-speed operation. Neural networks have also been used to estimate the stator resistance, and in [46] a fuzzy logic estimator is used for accurate estimation.

In Demetriades et al. [16], a reduced RTTM is proposed. The model is a lumped-parameter configuration for a surface-mounted PMSM, using parameters based on the geometry of the different components of the motor. The model is discretized and reduced to minimize complexity. Sciascera et al. present a low computational cost (LCC) thermal model for online prediction of PMSM winding temperature. The model uses a polynomial approximation of the solution of a LPTN-model. The results show that the accuracy of the LCC is similar to the higher cost LPTN. The model only takes into account the Joule losses in the copper windings and is therefore well suited for applications where these losses are the main heat source. This is relevant to PMSM with high slot density and relatively low operational speed [67]. In [41], a simple RTTM with few variable parameters is presented to predict the real-time thermal behaviour of PMSM. This model includes the stator core losses besides the Joule losses for more accurate temperature estimation. The proposed model is a good alternative with a balance between the accuracy, complexity and computing load [41].

Chapter 5

Case Study

5.1 Introduction

Given the state-of-the-art technology of Permanent Magnet Azimuth thrusters, the critical part this system plays in the operation of the vessel and the access to historical sensor data, this system was selected early on for a case study. The case study aims to develop a condition monitoring tool for a specific PM electrical motor used in marine applications. As discussed in section 2.2, the historical sensor data is far from complete, and many signals are ambiguous, nonsensical and do not seem to give any nonzero value at all. In addition to this, the sampling frequency of the signals from the electrical drive system is 1 Hz. This sampling rate makes it impossible to conduct many of the analysis discussed in chapter 4. The Nyquist sampling theorem states that the sampling rate needs to be at least twice the maximum frequency of the signal of interest [80]. Signature- and knowledge-based approaches involving vibration or power signals will not give correct results with this sampling rate. As an example, a current spectrum analysis of the AZ-PM electrical motors would require a sampling rate of at least 200 Hz given the electric frequency of the current. With this in mind, the case study will look further into physical modelling of PMSM's.

Temperature detection has been a method that has been successful in use. It is a good global indicator of faulty states and deterioration of electrical machines but has been neglected more recently because of newer, more attractive methods. However, temperature measurements should still be monitored, especially in combination with a more modern technique. The problem with the temperature signals from Gunnerus is that, as mentioned earlier, they are zero values.

Based on the review of the different methods and the evaluation of data quality from R/V Gunnerus, the case study will intend to use a model-based approach to simulate the thermal behaviour of a PMSM. With the lack of correct temperature data and accurate geometric properties of the AZ-PM electrical motors on R/V Gunnerus, the case study will look at another motor for further analysis. This motor is already modelled in the program RMxpvt, with detailed geometry available and the possibility to perform electromagnetic analysis for different operational states.



Figure 5.1: Figure of PMSM [61]

5.2 Motor

The motor chosen for further analysis and modelling is intended for use in marine applications. The power rating of the motor is 200 kW. This is low compared to the 500 kW thrusters at R/V Gunnerus [56], but will make for a good case study. The design is an adjustable-speed permanent magnet synchronous motor, with a rated voltage of 400 volts and a rated speed of 699 rpm. The number of poles is 22 and the magnets are surface mounted. Table 5.1 shows the design data of the motor used in the case study, and figure 5.2 show illustrations of the motor design. The complete design sheet and electrical circuit of the motor can be found in Appendix B.

Table 5.1: General design data

Rated Output Power	[kW]	200
Rated Voltage	[V]	400
Number of poles	[-]	22
Number of stator slots	[-]	132
Frequency	[Hz]	128.15
Number of phases	[-]	3
Outer diameter of stator	[mm]	650
Depth	[mm]	260

Different operational states for the motor will be analysed, varying with $\pm 20\%$ of the rated voltage and rpm. This is assumed to represent the interval of normal operation.

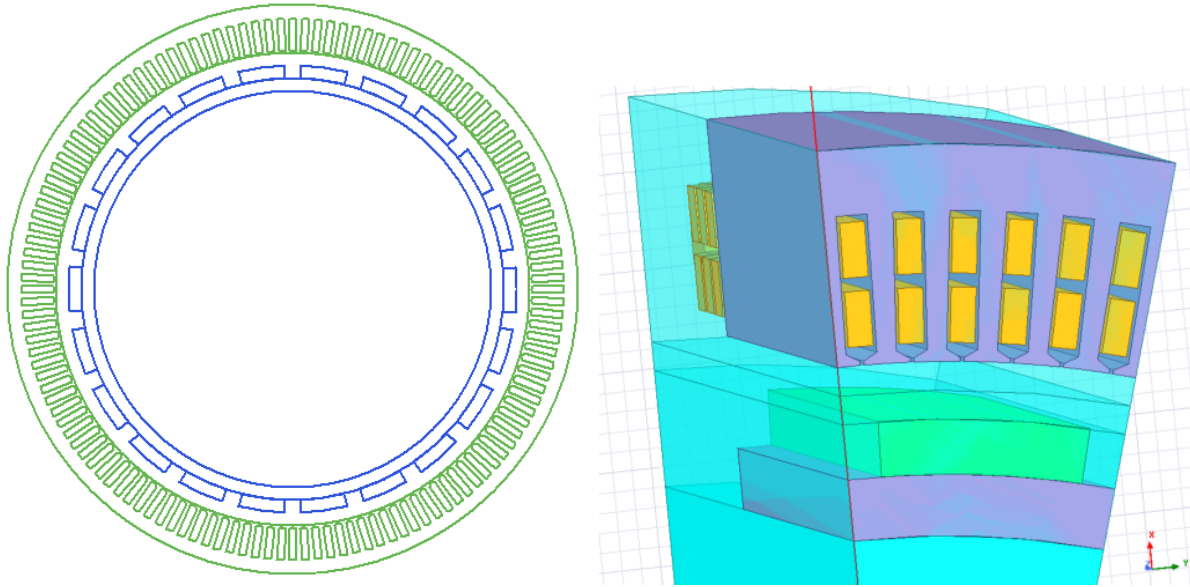


Figure 5.2: Illustration of the motor used for analysis in ANSYS electronics

5.3 Approach

The approach of the case study will be to develop a tool for condition monitoring of the PMSM, starting with combining different analysis to simulate the thermal behaviour of the motor. An electromagnetic analysis for all different "normal" operational states will be carried out. This analysis calculates the power losses in several parts of the motor. A polynomial fit of the losses will be made for different values of voltage and rpm. The losses can then easily be calculated for every operational state without having to perform time-consuming analysis.

The polynomial fit of the power losses will be integrated into a Lumped Parameter Thermal Network to simulate the thermal behaviour of the motor. This thermal model is meant to calculate the temperature in different parts of the motor for each time-step. Extensive thermal simulations will be carried out for every operational state in order to get a sufficient amount of temperature data.

The temperature data will be analysed with regards to distribution and normality, and this will be used to develop a state prediction algorithm using the measurement residuals and Gaussian processes. This will be done under the assumption that the faults can be characterized by changes in the mean and standard deviation of a time series. The incoming signals will be given a 'score' based on the deviation from the Gaussian distribution of a healthy motor at the same operating point. This score will then be used to detect and possibly predict faults.

Another use-case is to use the winding temperature for lifetime estimation of the motor. Winding insulation failure due to high temperatures is one of the most frequently occurring electrical faults in a PMSM [75]. Therefore, a simple lifetime estimation model based on the winding insulation temperature can serve as a handy tool and a good estimation for the remaining lifetime of the entire motor.

Chapter 6

Modelling and Analysis Theory

6.1 Thermal Modelling

Heat transfer in a PMSM can be modelled as a thermal network with thermal resistances in between its different parts. The model tries to simulate the behaviour of the heat transfer, by using the physical properties of the motor. This heat transfer is complex, and a model completely describing the thermal system of a PMSM would be very advanced [41]. The heat can be transported in two different ways, either by conduction or convection. Conduction occurs if two solid elements are in contact with each other, while convection is heat transfer between two elements via a fluid or gas. For thermal analysis of electrical components, electrical networks can be used in order to study the thermal behaviour of a system [16]. The analogies between electrical and thermal parameters are illustrated in table 6.1 below.

Table 6.1: Analogy between electrical and thermal parameters

Electrical Parameter	Thermal Parameter
Current (i) in [A]	Losses (P) in [W]
Voltage (u) in [V]	Temperature (T) in [$^{\circ}$ C]
Resistance (R) in [Ω]	Thermal Resistance (R_{th}) in [W/K]
Capacitance (C) in [F]	Thermal Capacitance (C_{th}) in [J/K]

Thermal resistances represent the thermal properties of different materials used as well as the thermal connection between different parts of the component. Similarly, stored thermal energy can be modelled as a thermal capacitance. Figure 6.1 illustrates the analogy between the electrical and the thermal circuits [16].

Heat transfer between two structures can be modelled by determining the thermal impedance of each material. Different parameters such as temperature distribution, mechanical complexity and material properties have to be considered. Conduction occurs when heat is transferred from one element to another due to a temperature gradient between the two elements [16]. The energy is transferred from the warmer region to a colder region, as described by Fourier's law

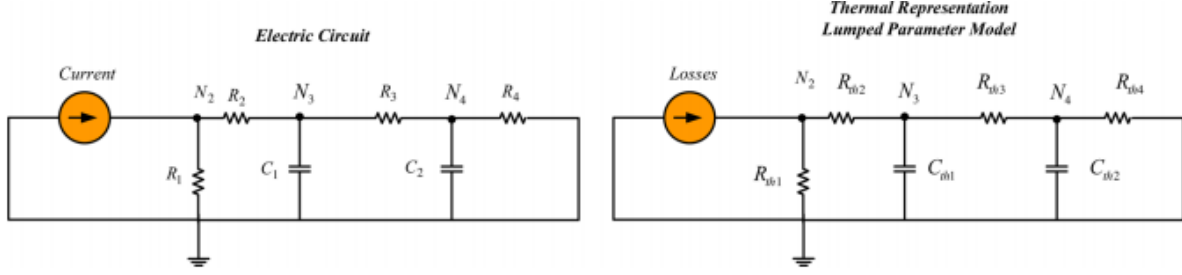


Figure 6.1: Analogy between electric and thermal networks [16]

$$q = -\lambda A \frac{\delta T}{\delta x} \quad (6.1)$$

where q is the heat transfer rate, $\delta T/\delta x$ is the temperature gradient describing the direction of the heat flow. λ is a positive constant called the thermal conductivity of the material, and A is the cross-section area. The thermal conductivity describes the material's ability to conduct heat. The conduction thermal resistance is defined as

$$R_{th} = \frac{t}{A\lambda} \quad (6.2)$$

where t is the thickness of the element [69]. In a similar fashion, convection occurs when heat is transferred to/from an element by a moving fluid or gas. The rate of heat transfer is described by

$$q = hA(T_w - T_{inf}) \quad (6.3)$$

where T_w is the temperature of the element, T_{inf} is the temperature of the fluid, A is the area of the surface and h is the convection heat transfer coefficient [6]. The thermal resistance for convection [69] is defined as:

$$R_{th} = \frac{1}{Ah} \quad (6.4)$$

There are two different types of convection: natural and forced convection. Natural convection occurs in the absence of an external source and is driven by buoyancy and gravity. Forced convection occurs when an external source like a fan or a pump is used to move fluids [9].

Stored energy in the different nodes of the thermal model is described by thermal capacitance C_{th} [69], and is calculated with the formula

$$C_{th} = mC_p \quad (6.5)$$

where m is the mass of the structure and C_p is the specific heat capacity.

The power losses in a PMSM will cause a temperature rise in the different parts of the motor. Power losses consist of different losses at different locations in the motor. The most important losses are winding losses and iron losses in the stator and rotor core.

6.1.1 Lumped Parameter Thermal Network

A LPTN models the heat flow and the temperature distribution inside a motor by using an equivalent thermal circuit composed of heat sources, thermal resistances and thermal capacitances [67]. A preliminary selection of the resistances and capacitances can be determined according to the geometry of the motor and from the physical properties of the materials used [48]. Figure 6.2 below is an example of a LPTN model schematic for a PMSM motor. The motor is modelled for only one slot section for symmetry reasons.

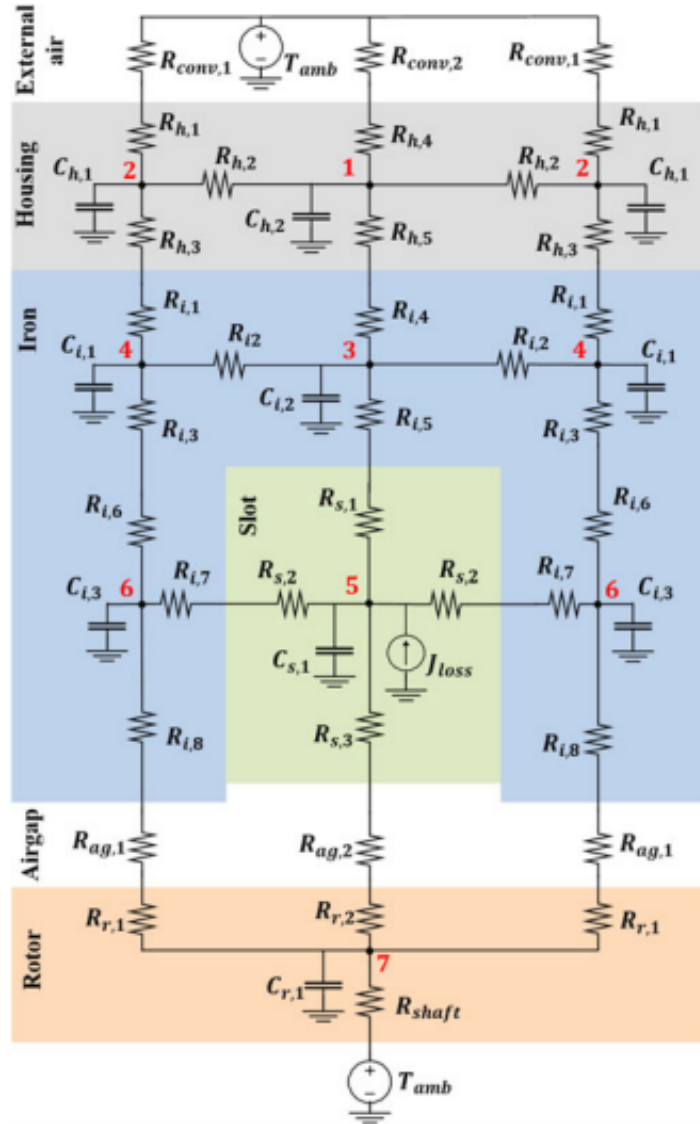


Figure 6.2: Example of a LPTN representing the heat flow in a PMSM motor

Some of the parameters in a LPTN are not easily determined. The thermal parameters in the slot are often uncertain due to a random wound winding configuration [67]. The external surface and airgap convection coefficients are also very significant parameters, as shown in [70] and described by equation 6.4. These uncertain and significant parameters are therefore often tuned based on experimental results [67].

The LPTN uses the node potential method for the resolution of circuits, representing the system by a set of first order differential equations. Vector T represents the unknown

temperatures in the different nodes, u is the inputs vector and the matrices A and B are the state coefficient matrix and the source coefficient matrix:

$$\begin{aligned}\dot{T} &= AT + Bu, \\ A &= C^{-1}A_1, \\ B &= C^{-1}B_1.\end{aligned}\tag{6.6}$$

Where matrices A_1 , B_1 and C are shown as follows for a simple 4 node network in series:

$$A_1 = \begin{bmatrix} a_{11} & R_2^{-1} & 0 & 0 \\ R_2^{-1} & a_{22} & R_3^{-1} & 0 \\ 0 & R_3^{-1} & a_{33} & R_4^{-1} \\ 0 & 0 & R_4^{-1} & a_{44} \end{bmatrix}\tag{6.7}$$

where a_{ii} represents all resistances connected to node i . The product of matrix B and vector u represents the losses in the different nodes of the network divided by the capacitance:

$$Bu = \begin{bmatrix} P_1 C_1^{-1} \\ P_2 C_2^{-1} \\ P_3 C_3^{-1} \\ P_4 C_4^{-1} \end{bmatrix}\tag{6.8}$$

Where C is a diagonal matrix of the capacitances:

$$C = \mathbf{diag}(C_1, \dots, C_4).\tag{6.9}$$

In the discrete-time domain, the set of equations above can be discretized using the forward Euler method [41].

6.1.2 Lower Order Models

Considering the benefits of reduced computational costs, the model can be reduced by removing less significant components without lowering the accuracy of the model considerably [67]. Using the model in figure 6.2 as an example, it can be reduced to a three-node circuit as shown in figure 6.3.

The new resistances and thermal capacitances can be calculated with the following formulas

$$R_I = \frac{R_i R_j}{R_i + R_j}\tag{6.10}$$

$$R_I = R_i + R_j\tag{6.11}$$

where formula 6.10 merges two parallel resistances, while formula 6.11 is for two resistances in series.

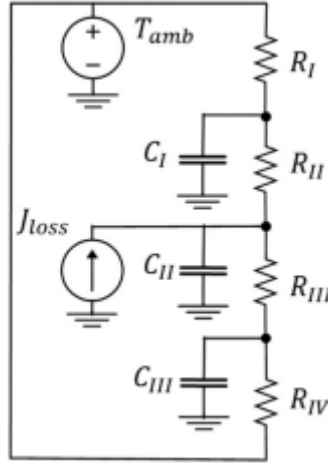


Figure 6.3: Three-node LPTN equivalent circuit [67]

6.2 Gaussian Processes

A Gaussian process is a generalization of the Gaussian probability distribution. One can think of a Gaussian process as defining a distribution over functions, and inference taking place in the space of functions [60]. Assuming we have some input \mathbf{x}_i and some outputs y_i , we assume that $y_i = f(\mathbf{x}_i)$, for some unknown function f . The approach is then to infer a distribution over functions given the data, $p(f|\mathbf{X},\mathbf{y})$, and then use this to make predictions given new inputs, i.e. to compute

$$p(y_*|\mathbf{x}_*, \mathbf{X}, \mathbf{y}) = \int p(y_*|f, \mathbf{x}_*)p(f|\mathbf{X}, \mathbf{y})df \quad (6.12)$$

where y_* are the test targets and x_* the test inputs. A Gaussian process assumes that $p(f(\mathbf{x}_1), \dots, f(\mathbf{x}_N))$ is jointly Gaussian, with some mean $\mu(\mathbf{x})$ and covariance $\Sigma(\mathbf{x})$ given by $\Sigma_{ij} = \kappa(\mathbf{x}_i, \mathbf{x}_j)$, where κ is a positive definite kernel function. The key point is that if \mathbf{x}_i and \mathbf{x}_j are deemed similar by the kernel, then the output of the function at those points are also expected to be similar [50]. See figure 6.4 for an illustration.

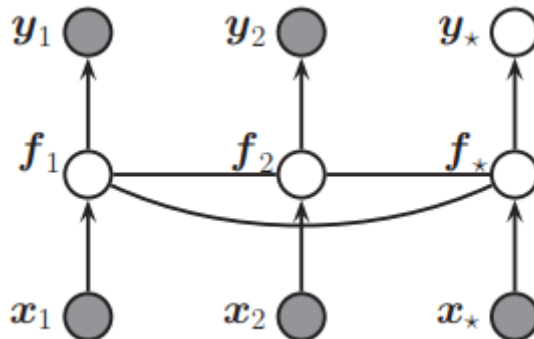


Figure 6.4: Gaussian process for 2 training points and 1 testing point [50].

6.2.1 Gaussian Processes for regression

A Gaussian process (GP) defines a probability distribution over functions and is denoted as:

$$f(\mathbf{x}) \sim GP(m(\mathbf{x}), \kappa(\mathbf{x}, \mathbf{x}')) \quad (6.13)$$

where $m(\mathbf{x})$ is the mean function and $\kappa(\mathbf{x}, \mathbf{x}')$ is the kernel or covariance, i.e.,

$$m(\mathbf{x}) = \mathbb{E}[(f(\mathbf{x}) - m(\mathbf{x}))(f(\mathbf{x}') - m(\mathbf{x}'))^T] \quad (6.14)$$

For any finite set of points, this process defines a joint Gaussian:

$$p(\mathbf{f}|\mathbf{X}) = \mathcal{N}(\mathbf{f}|\mu, \mathbf{K}) \quad (6.15)$$

where $K_{ij} = \kappa(\mathbf{x}_i, \mathbf{x}_j)$ and $\mu = (m(\mathbf{x}_1), \dots, m(\mathbf{x}_N))$ [50].

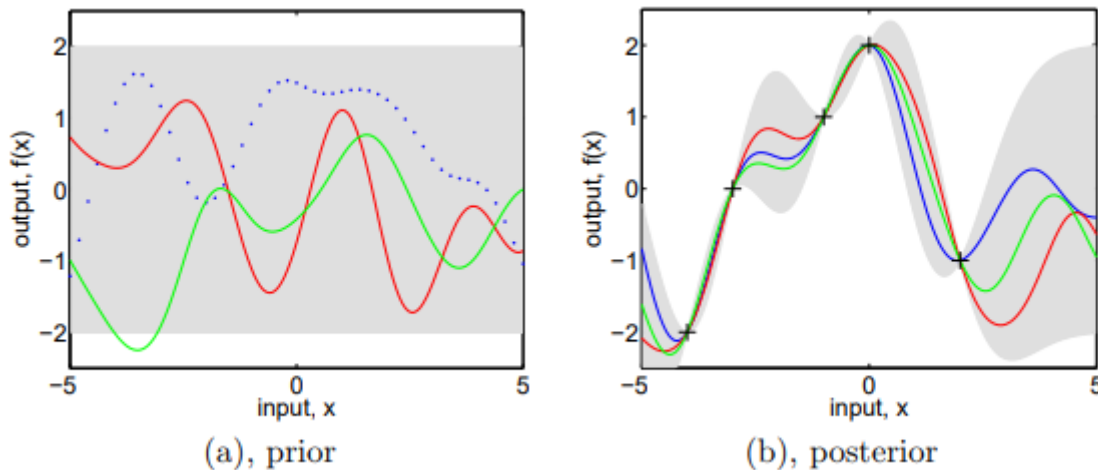


Figure 6.5: Gaussian function plots

Figure 6.5 above shows three functions drawn from a GP prior and posterior. The functions in figure (b) have been conditioned on five observations indicated. The shaded area in both plots represents the mean value with two times the standard deviation added and subtracted. This area corresponds to the 95% confidence region [60].

Suppose we observe a noise free training set $\mathcal{D} = \{(x_i, f_i), i = 1 : N\}$, where $f_i = f(x_i)$ is the observed value of the function evaluated at x_i . Given a test set X_* of size $N_* \times D$, the objective is to predict or evaluate a function output \mathbf{f}_* .

By definition of the GP, the joint distribution has the form of

$$\begin{pmatrix} \mathbf{f} \\ \mathbf{f}_* \end{pmatrix} = \mathcal{N} \left(\begin{pmatrix} \mu \\ \mu_* \end{pmatrix}, \begin{pmatrix} \mathbf{K} & \mathbf{K}_* \\ \mathbf{K}_*^T & \mathbf{K}_{**} \end{pmatrix} \right) \quad (6.16)$$

where $\mathbf{K} = \kappa(\mathbf{X}, \mathbf{X})$ is $N \times N$, $\mathbf{K}_* = \kappa(\mathbf{X}, \mathbf{X}_*)$ is $N \times N_*$, and $\mathbf{K}_{**} = \kappa(\mathbf{X}_*, \mathbf{X}_*)$ is $N_* \times N_*$. The form of the posterior is as follows:

$$p(\mathbf{f}_*|\mathbf{X}_*, \mathbf{X}, \mathbf{f}) = \mathcal{N}(\mathbf{f}_*|\mu_*, \Sigma_*) \quad (6.17)$$

$$\mu_* = \mu(\mathbf{X}_*) + \mathbf{K}_*^T \mathbf{K}^{-1}(\mathbf{f} - \mu(\mathbf{X})) \quad (6.18)$$

$$\Sigma_* = \mathbf{K}_{**} - \mathbf{K}_*^T \mathbf{K}^{-1} \mathbf{K}_* \quad (6.19)$$

Figure 6.5 illustrates this process, where the left figure show samples from the prior, $p(\mathbf{f}|\mathbf{X})$. The figure to the right show samples from the posterior, $p(\mathbf{f}_*|\mathbf{X}_*, \mathbf{X}, \mathbf{f})$. The model perfectly interpolates the training data, while the uncertainty of the prediction increases as we move further away from the observed data [50].

This can be used for condition monitoring purposes, as the learned model can be used to make temperature predictions based on the operational state. Another approach for fault detection is to assess the effect that new observed data have to the distribution of the training data. By doing this, a fault can be detected or predicted when a temperature measurement breaches a certain threshold.

Chapter 7

Methodology

7.1 Software

The different programs used for analysis, modelling and simulation in this thesis are ANSYS RMxpert, ANSYS Twin Builder, MATLAB/Simulink and Power BI. This section will give an overview of the software and how it has been used in the case study.

ANSYS RMxpert is a template-based design tool to create fully customized machine design flow very efficiently using lower cost machines. The program uses classical analytical motor theory and equivalent magnetic circuit methods, allowing a calculation of machine performance in a matter of seconds. RMxpert has the ability to automatically set up a complete Maxwell 2-D and 3-D project, including geometry, materials and boundary conditions. It automatically generates a reduced order model, considering the nonlinearities and eddy effects [32]. RMxpert also sets up customized driving circuit topology as a single component in ANSYS Twin Builder to be coupled with the corresponding electric machine reduced order model. This is critical for running co-simulation, and a step towards a fully integrated digital twin.

As mentioned in chapter 5, RMxpert is used in the case study to calculate the power losses in the PMSM for different operational states. It also provides a design sheet of the motor that lists all the relevant input parameters and calculated parameters. The resulting equivalent model is then explored and run in ANSYS Twin Builder, where it is possible to explore electronic control topologies, loads and interactions with drive-system and multi-domain components.

ANSYS Twin Builder is a new tool for building, validating and deploying complete systems simulations and digital twins for predictive maintenance. Twin Builder combines the power of a multi-domain systems modeller with extensive libraries, 3D-physics solvers and reduced-order model (ROM) capabilities. This allows you to reuse existing components and quickly create a systems model of the component. To connect the twin to test or real-time data, Twin Builder easily integrates with IIoT platforms and contains run-time deployment options, enabling predictive maintenance on the physical asset [33].

MATLAB/Simulink is used for many calculation and modelling purposes. The thermal model is made as a MATLAB function and is imported to Simulink for time series simulation. With Twin Builder it is possible to connect with a Simulink function, making

it possible to fully integrate the thermal model with the analysis in ANSYS. This is an enabler towards making the model real-time. In addition to the thermal model, MATLAB is used for the curve fitting of the power losses, the Gaussian Process Regression and several other functions for data handling and plotting.

7.2 Electromagnetic Model

The electromagnetic model briefly described in section 7.1 is a key part of the case study. Together with the thermal model, it creates a multi-physics environment of the motor. As discussed above, the electromagnetic model is made in RMXprt and is used to simulate the power losses of the motor. These losses are estimated purely by a physics-based mathematical model. The figure below shows a snippet of the motor in Maxwell 2D:

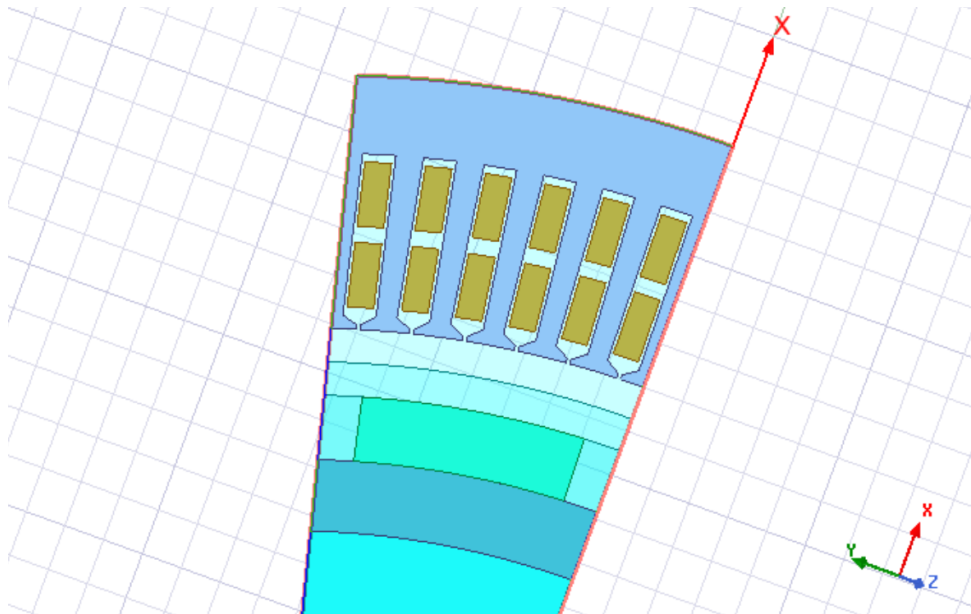


Figure 7.1: Snippet of the motor in Maxwell 2D

Simulations are run manually for different output power, starting at 20% of the rated power and ending at cases with overload above the rated power level. At each power setpoint, a number of simulations are done for $\pm 20\%$ of the rated voltage and rpm. The rated output power is 200 kW, the rated voltage is 400 V and the rated speed is 699 rpm, as can be seen in table 5.1. Multiple analyses are done at rated voltage with varying speed, at rated speed but with varying voltage, and with voltage and speed linearly increasing. This is done in order to get enough data-points to make an accurate curve fit of the losses.

This curve fit is done in MATLAB with the curve fitting tool, and the results can be seen in section 8.1. The 3-dimensional fit is the one used in the thermal model, as it covers all different values of voltage and rpm. The curve fit method best suited for the data is thin plate interpolation. This method is a spline-based technique for data interpolation and smoothing. The fit function is stored, and called upon by the thermal model, meaning that the time-consuming electromagnetic analysis and curve fit is only done one time for each operating point.

7.3 Thermal Model

As described in section 6.1, the heat transfer in a PMSM can be modelled as a thermal network composed of heat sources, thermal resistances and thermal capacitances. Based on the physical properties of the motor modelled in RMxpvt, the proposed thermal model try to simulate the heat flow in the PMSM. As mentioned earlier, a model that completely describes the thermal system of a PMSM would be very complex, therefore a reduced model is built with the following assumptions:

1. The different parts of the PMSM are symmetrical about the radial and axial direction.
2. The heat in the different parts of the PMSM is evenly distributed.
3. There is no axial heat flow.
4. The power losses are concentrated in the stator iron core, the rotor iron core and the stator windings.
5. The heat is removed by natural convection with water flowing around the motor.

Based on the lumped parameter method, a seven-node network is built by exploiting the motor symmetries. The schematic of the model is shown in figure 7.2. For symmetry reasons, only one slot section is modelled, with the motor having 136 slots. Notice that some nodes in the network have the same number due to circuit symmetries. Thus, the LPTN can be simplified to a seven-node LPTN depicted in figure 7.3. The capacitances C_i and resistances R_i of the seven-node LPTN can be calculated by using the computation of the equivalent series and parallel resistances and capacitances. [67].

Notice that the nodes at which the power is injected are coloured red. A selection of the resistances and capacitances can be determined according to the geometry of the motor and the physical properties of the materials used [48]. For the convective heat transfer between the housing and the ambient seawater, the resistance is calculated with formula 6.4, where A represents the contact surface and h is the heat transfer coefficient. The same equation is used for calculation of the resistance between the stator and rotor through the air gap. Here, h is the air gap heat transfer coefficient and A is a portion of the surface of the cylinder whose radius is equal to the air gap radius.

In the air gap, the heat transfer coefficient is

$$h = Nu \cdot \lambda / g \quad (7.1)$$

Where Nu is the dimensionless Nusselt number describing the flow of air through the air gap. Another quantity is the Taylor number which is used for convection calculation in the air gap:

$$Ta = Re^2 g / R_g \quad (7.2)$$

Where Re is the Reynolds number and R_g is the air gap radius. For a laminar shear flow with a low Taylor number, the Nusselt number is constant [4]. The relations between the Taylor and Nusselt numbers for different flow characteristics are described in [65]. The

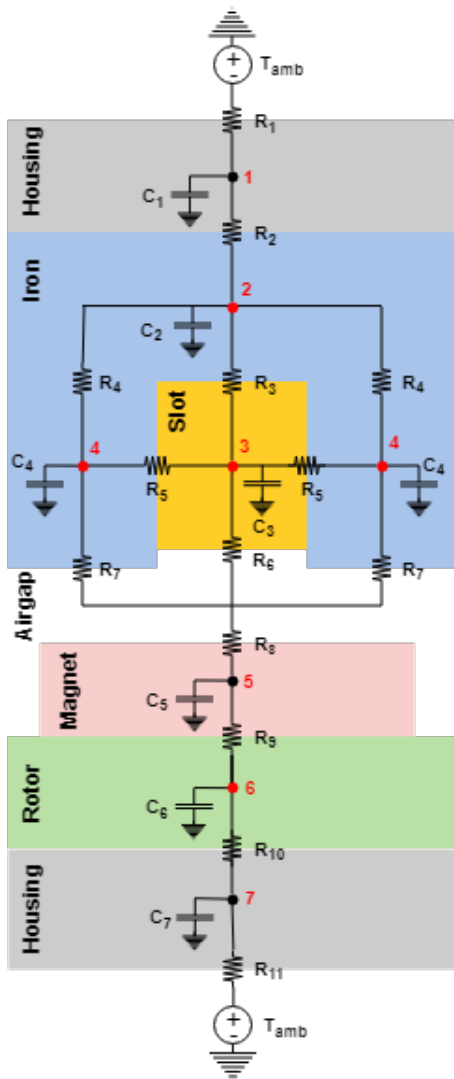


Figure 7.2: LPTN representing the heat flow within the motor

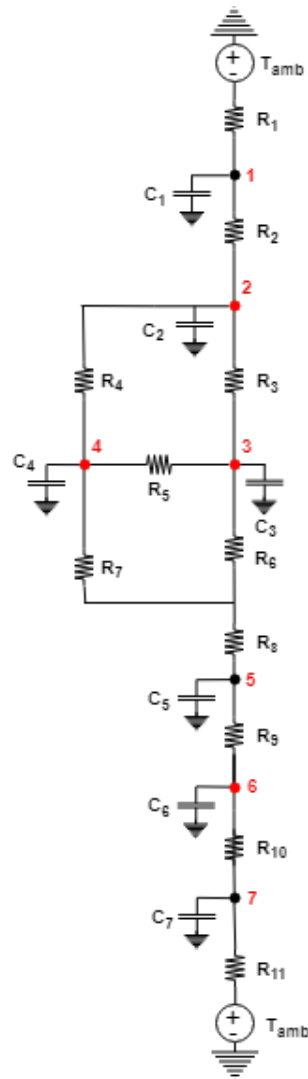


Figure 7.3: LPTN equivalent circuit simplified for symmetry reasons

air surrounding the end windings and end spaces is assumed to have a low velocity, and a heat transfer coefficient of $h = 14W/m^2K$ is used [29] to calculate the convection from air to the housing and windings.

For normal operation of the thruster, the motor is naturally cooled by the surrounding seawater travelling with a speed approximately similar to the vessel speed. The convection is assumed good enough that the surface temperature equals the seawater temperature set to $15^{\circ}C$. A heat transfer coefficient of $h = 500W/m^2K$ is used [19] for the seawater. Table 7.1 below lists the thicknesses and thermal conductivities of the various parts of the motor.

Table 7.1: Thermal barriers and conductivities

Description	Thickness	Conductivity
Housing (steel)	20 mm	40 W/Km
Magnet	14 mm	9 W/Km
Stator yoke	17 mm	38 W/Km
Stator tooth	35 mm	38 W/Km
Copper	35 mm	360 W/Km
Winding (axial)	8 mm	7 W/Km
Air	14.5 mm	0.023 W/Km

The external surface and airgap convection coefficients are significant parameters, as shown in [70]. These parameters are not easily determined, mainly because of the fluid dynamics and orientation of the electrical motor. The resistances obtained for the seven-node network are listed in table 7.2 below:

Table 7.2: Resistances [K/W] of the seven node thermal network

Parameter	Value
R_1	0.740
R_2	0.280
R_3	0.327
R_4	0.035
R_5	0.303
R_6	21.191
R_7	13.954
R_8	21.593
R_9	0.581
R_{10}	0.269
R_{11}	0.740

The capacitances, which model the thermal mass of the motor component represented, are calculated with equation 6.5 as the product of mass and specific heat capacity of the material. The capacitance is modelled by considering the total mass of the element in question. The masses available from the RMXprt model are for the stator core, rotor core, windings and the permanent magnets. Considering this, and the advantages of having a lower computational cost model, the LPTN can be reduced to a four-node network. This reduced model is derived from the original seven-node LPTN and is presented in the next section.

7.3.1 Lower Order Model

Considering that the capacitances can be calculated for the stator core, rotor core, windings and permanent magnets, these make out the four nodes in the new LPTN:

The new resistances are defined by using equation 6.10 for parallel resistances, and equation 6.11 for resistances in series:

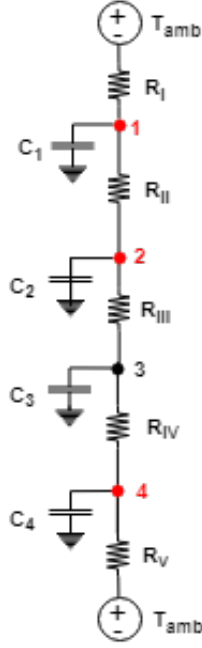


Figure 7.4: Four-node LPTN equivalent circuit

$$\begin{aligned}
 R_I &= R_1 + R_2 + R_4 & R_{II} &= R_3 + R_5 & R_{III} &= \frac{R_6 R_7}{R_6 + R_7} + R_8 \\
 R_{IV} &= R_9 & R_V &= R_{10} + R_{11}
 \end{aligned} \tag{7.3}$$

The capacitances of the four node network are found by using equation 6.5. The masses of the four different sections are found in the design sheet in RMxprrt, and the specific heat capacity of the metals are found at [20]. As the thermal model only looks at one slot section, the masses are divided by the number of slots to obtain the correct capacitance. The capacitances of the stator core, rotor core, windings and permanent magnets can be found in table 7.3 below:

Table 7.3: Capacitances [J/K] of the four node thermal network

Section	Value
Stator core	473.84
Rotor core	167.16
Windings	194.69
Permanent magnet	193.30

As seen in figure 7.4, three out of four nodes are coloured red, meaning that losses occur at these nodes. These losses are stator core losses in node I, windings copper losses in II and rotor core losses in IV. Using the equations in 6.6, and discretizing using the forward Euler method, the calculation algorithm for the PMSM temperature can be expressed as follows:

$$\begin{bmatrix} T_1(k) \\ T_2(k) \\ T_3(k) \\ T_4(k) \end{bmatrix} = \begin{bmatrix} 1 - \frac{\Delta t}{C_1} \left(\frac{1}{R_1} + \frac{1}{R_2} \right) & 0 & 0 & 0 \\ \frac{\Delta t}{C_2 R_2} & 1 - \frac{\Delta t}{C_2} \left(\frac{1}{R_2} + \frac{1}{R_3} \right) & 0 & 0 \\ 0 & \frac{\Delta t}{C_3 R_3} & 1 - \frac{\Delta t}{C_3} \left(\frac{1}{R_3} + \frac{1}{R_4} \right) & 0 \\ 0 & 0 & \frac{\Delta t}{C_4 R_4} & 1 - \frac{\Delta t}{C_4} \left(\frac{1}{R_4} + \frac{1}{R_5} \right) \end{bmatrix} \cdot \begin{bmatrix} T_1(k-1) \\ T_2(k-1) \\ T_3(k-1) \\ T_4(k-1) \end{bmatrix} + \begin{bmatrix} P_{ic} C_1^{-1} + T_{amb} R_1^{-1} \\ P_w C_2^{-1} \\ 0 \\ P_{rc} C_4^{-1} + T_{amb} R_5^{-1} \end{bmatrix} \quad (7.4)$$

Where k is the number of sampling times, Δt is the sampling time for the input signals, P_{ic} are the stator core losses, P_w are the winding losses, P_{rc} are the rotor core losses and T_{amb} is the ambient seawater temperature.

7.4 Thermal Simulation

The thermal simulations are done in MATLAB or Simulink by running the LPTN over time. A set of different simulations and scenarios have been evaluated, and the results can be seen in section 8.2. Each simulation at a set-point is run for at least 10^4 time-steps due to the transient phase of the temperatures. As the ambient temperature is set to $15C^\circ$, it takes some time for the temperature to stabilize. The temperatures at rated operation can quickly be found by running the LPTN for steady-state operation at the rated power, voltage and rpm. The time-consuming part of the simulations is when every possible combination of $\pm 20\%$ of voltage and rpm are to be simulated. For both $20kW$, $160kW$ and $200kW$, around 120 thermal simulations were done to get a sufficient amount of data.

Another type of simulation done is to compare the winding temperatures for different output power. This model has to include different loss values based on the power output. The last and final simulation model which also has been imported to Simulink is a model where the output power, the voltage level and the rpm are taken in at every time-step. By doing so, thermal simulations can be done with vessel data as input. This will give a good understanding of how the temperature in the motor behaves under normal and faulty operation.

7.5 Modelling Faults

This section will describe the faulty operation that is focused on, how it is modelled, and the connection to ship operation scenarios. In dynamic sailing conditions such as sailing in heavy weather, turning or operating in icy waters, the actual load of the motor fluctuates around the averaging operating point of the propeller curve [76]. The averaging point at cruising speed is normally around 80 % of maximum, or at 160 kW for the motor in this case study. This fluctuation around the average load can cause overloading. Because all loads experience the electrical network voltage and frequency, voltage and frequency swings under fault conditions can cause electrical systems to be switched off.

Particularly in power systems with a high amount of variable speed drives, constant power load instability can occur [23].

A combination of an overload scenario with a drop in voltage due to normal fluctuations can cause an overheating of the motor. This faulty operation will be the one focused on by the fault prediction algorithm. The winding temperature will be used to detect overload scenarios. Faulty modelling is done by calculating the power losses at maximum output power, in combination with a low voltage. This causes high copper losses that result in a rise in the winding temperature, possibly damaging the winding insulation.

7.6 Fault Detection Algorithm

In section 6.2.1 the computation of predictive distributions is shown for the outputs y_* corresponding to the novel test input x_* . The distribution of the prediction is Gaussian with a calculated mean and variance. For practical applications, a loss function can be utilized in order to make a decision about how to act. This loss function specifies a penalty incurred by comparing an observed value to the distribution of the test set [60].

The goal is to give a score to each observed temperature value based on the deviation from the predictive distribution. This score is normally used to improve the predictive model, while in a fault detection scenario it can be used to detect faulty states.

The method related to the case study is to use the results from the physics-based thermal model simulating the temperature in the motor at healthy states. The distribution of the temperature is first tested for normality before the distribution of the data at different operating points is found. This is done by using descriptive statistics in the data analysis tool in Microsoft Excel. This tool describes the data statistically and provides useful parameters like mean, standard error, median, standard deviation, sample variance, kurtosis, skewness and range. This is used to evaluate the normality of the data set by looking at skewness and kurtosis. These values are considered acceptable between ± 1.96 in order to prove normal univariate distribution.

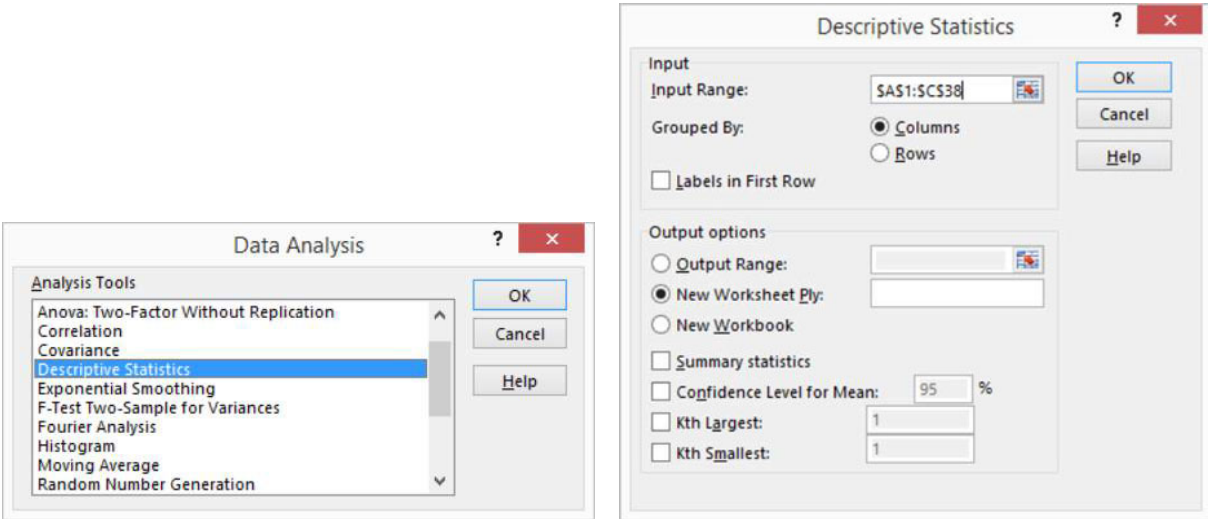


Figure 7.5: Descriptive statistics tool in Excel

The distribution of the temperature from simulations at rated power specifies the desired temperatures at that point of operation. The differences in temperature are because the simulations are done for different levels of voltage and rpm. The data set consists of over 100 simulations for different combinations of $\pm 20\%$ of rated voltage and rpm. This is assumed to be the range of normality for operation at rated power. The deviations in voltage and rpm can be a result of several factors and is a well-known problem for electrical power systems in ships [12].

Given a prediction method, we can evaluate the normality of the temperature data in several ways. The simplest method is the squared error loss, where we compute the squared residual $(y_* - \hat{f}(x_*))^2$ between the mean prediction and the target at each test point. This can be summarized by the mean squared error (MSE) by averaging over the test set. However, this method is sensitive, and a better option is to normalize by the variance of the targets of the test cases to obtain the standardized mean squared error (SMSE). Additionally, if we produce a probability distribution for each test input we can evaluate the negative log probability of the target under the model [78]. As GPR produces a Gaussian predictive density, one obtains

$$-\log p(y_* | \mathbf{D}, \mathbf{x}_*) = \frac{(y_* - \bar{f}(\mathbf{x}_*))^2}{2\sigma_*^2} \quad (7.5)$$

where the predictive variance σ_*^2 for GPR is the variance of the healthy data $\sigma_*^2 = \mathbb{V}(f_*)$ that is obtained in the descriptive statistics tool [60]. This model is tested on data from simulations of the faulty cases discussed in section 7.5. From this, it is possible to develop a threshold that can be used to detect faulty operation.

7.7 Lifetime Estimation

Experience from industrial applications shows that the bearings and windings insulation is most likely to fail. High power density leading to high winding temperatures accelerates thermal ageing additionally, and this is why several studies deal with lifetime calculation based on the winding insulation [31]. This section will briefly describe the lifetime prediction model of the PMSM based on winding temperature analysis. It is assumed that the same amount of damage appearing during one driving cycle will occur for every similar driving cycle. In practice, demagnetizing of magnets or ageing of insulation will lead to torque ripples, increasing losses and leading to higher temperatures that accelerate the ageing of the windings. The lifetime model for the winding insulation is combined with the results from the thermal model.

The deterioration of the winding insulation is a chemical process that can be approximated by a simple, logarithmic function:

$$L_w(\theta) = L_0 \cdot 2^{\frac{TI - \theta}{HIC}} \quad (7.6)$$

with $\theta[^\circ\text{C}]$ being the actual temperature, $TI[^\circ\text{C}]$ being the temperature index, which is the reference temperature for reference lifetime $L_0[h]$, and $HIC[K]$ being the half-life index describing the temperature difference for which the lifetime is halved [31].

The steady-state winding damage can be expressed by:

$$D_w(t) = \frac{t}{L_w(\theta_{Cu})} \quad (7.7)$$

The transition from steady-state to dynamic simulation via linear damage accumulation gives the dynamic winding damage D_w with time-dependent winding temperature $\theta_{Cu}(t)$:

$$D_w(t) = \frac{1}{L_0} \int_0^t 2^{\frac{\theta_{Cu}(\tau) - TI}{HIC}} d\tau \quad (7.8)$$

The parameters on the temperature tolerance of the motor are taken from [74]. Assuming the highest tolerance class, H, the maximum allowable temperature TI is $180C^\circ$, HIC is equal to 10, meaning that each $10C^\circ$ rise above the maximum temperature may reduce the lifetime by one half. The lifetime of the engine is assumed to be 10 000 hours while operating at the maximum temperature.

Chapter 8

Results and Discussion

8.1 Electromagnetic Simulation - Power losses

In this section, the results from the electromagnetic simulations in RMxpert is presented. The detailed parameters of the electric motor used for analysis can be seen in the design sheet of the motor in Appendix B. The model was run at different operational states with different voltage and rpm values. In order to assess the normality of the results at more than just the rated power, extensive analyses were run at both $20kW$, $160kW$ and $200kW$. For the simulation of over-load cases, the model was run at levels at the rated power with low voltage.

The results shown are the power losses for different operations, focusing on the iron core (IC) losses and the armature copper (AC) losses. At $20kW$, $160kW$ and $200kW$, the analysis were run at $\pm 20\%$ of the rated voltage and rpm at 400 and 699, respectively. Over 100 different combinations of voltage and rpm were analysed, providing enough data to create a 3-dimensional curve fit of the losses shown in figure 8.6, 8.12 and 8.18. This curve fit was used to estimate losses in the thermal model. This is discussed further in the following sections. The table below shows the results of simulations for different power levels at rated voltage and rpm.

Power	Core Loss	Copper Loss
20 kW	787.248 W	1203.97 W
160 kW	787.248 W	7440.15 W
200 kW	787.248 W	15789.7 W

Table 8.1: Power losses at 20, 160 and 200 kW

As can be seen from table 8.1, the iron core losses is constant with changes in output power, while the armature copper losses are increasing significantly with a higher power output. The following figures show the results and curve fits for iron and copper losses at 20, 160 and 200 kW. Plots have been made to show how the changes in voltage and rpm affect the different losses. For 2D-plots with varying rpm, the voltage has been kept constant at 400 and vice versa. The 3D-plots also include another set of simulations where the voltage and rpm increase linearly at the same rate. The blue dots represent the results from analyses, while the coloured line or field represents the curve fit. For curve fitting,

the MATLAB curve fitting tool has been used. This tool can automatically find the best method in order to get the best fit possible.

8.1.1 Results

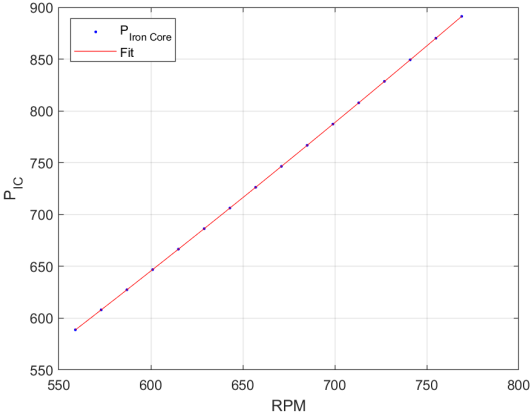


Figure 8.1: IC loss vs rpm at 20kW

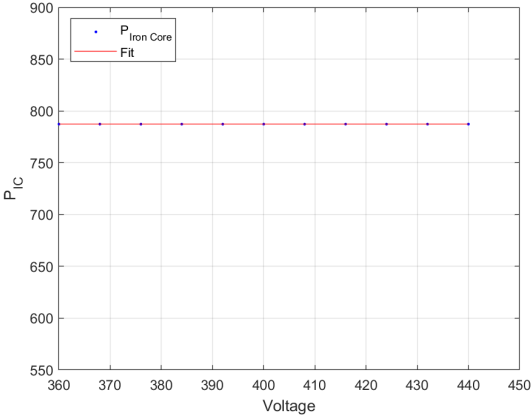


Figure 8.2: IC loss vs voltage at 20kW

From the graphs above, it is clear that the iron core losses increase with the rpm, but is not affected by changes in voltage.

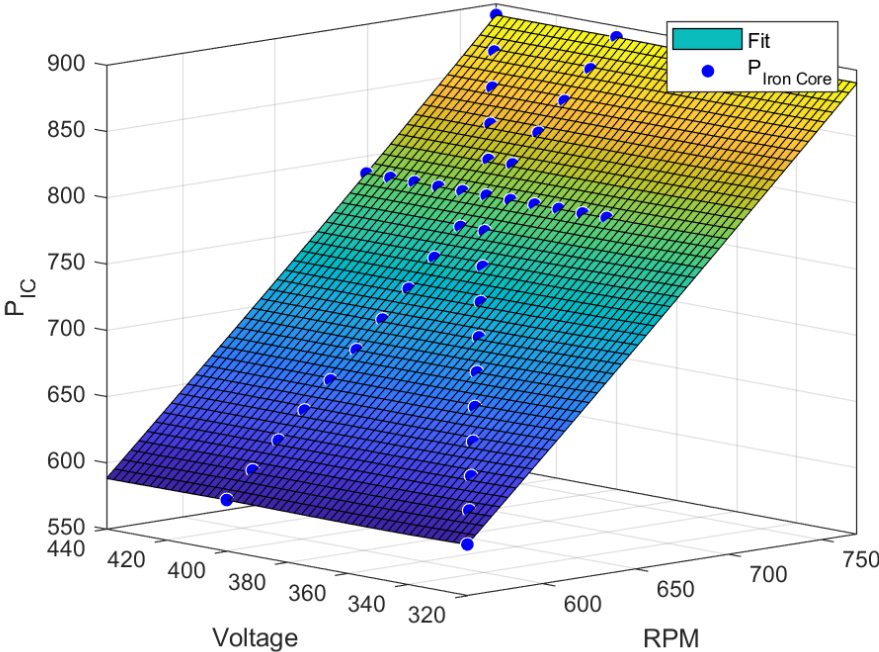


Figure 8.3: IC losses at 20 kW, 3D-Plot

The 3D-Plot of the iron core losses show that the losses increase linearly with the rpm and is constant for increased voltage.

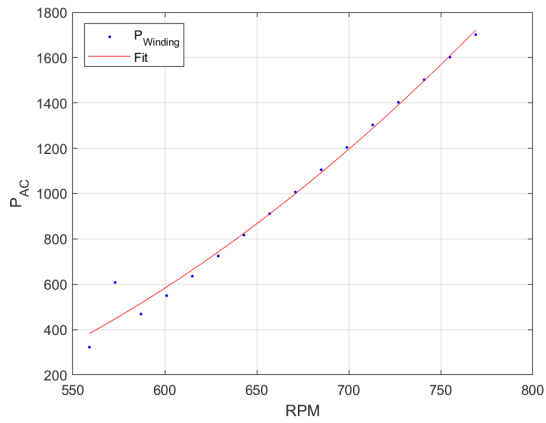


Figure 8.4: AC loss vs rpm at 20kW

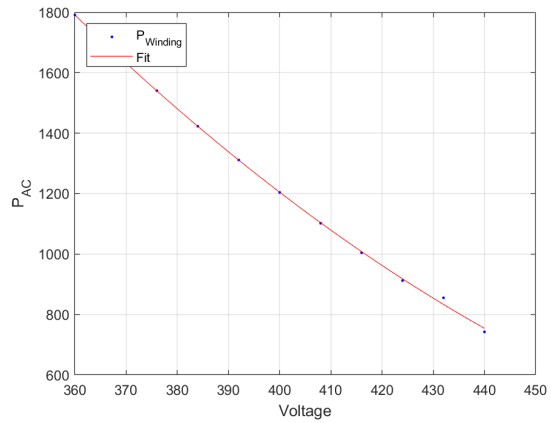


Figure 8.5: AC loss vs voltage at 20kW

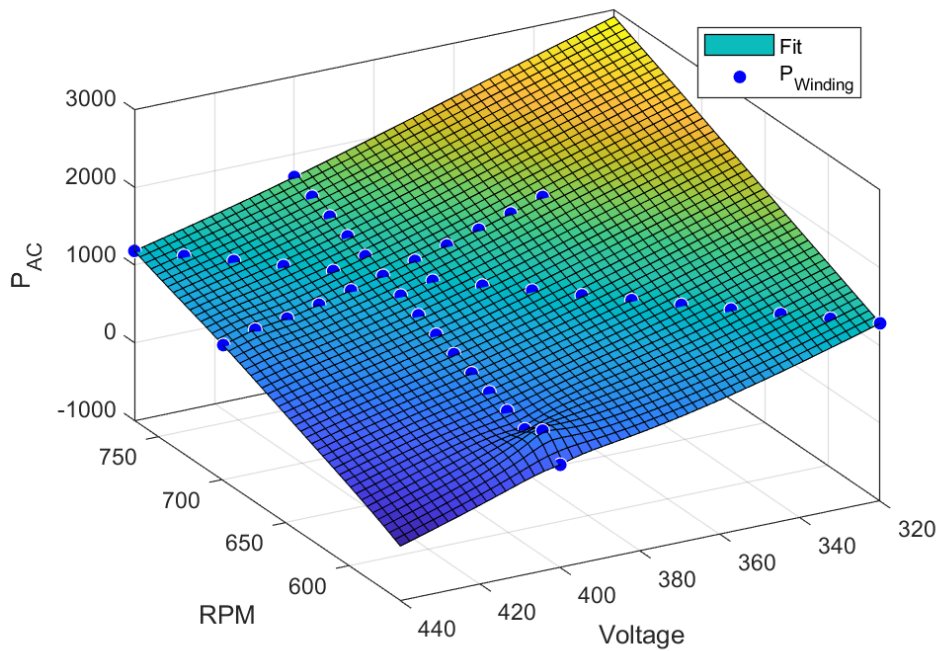


Figure 8.6: AC losses at 20kW, 3D-Plot

The figures above show the armature copper losses at 20 kW. Figure 8.4 shows that increasing rpm at rated voltage will cause an increase in AC-losses, while figure 8.5 shows that the AC-losses decrease with an increasing voltage at rated rpm. This can also be seen in the 3D-Plot.

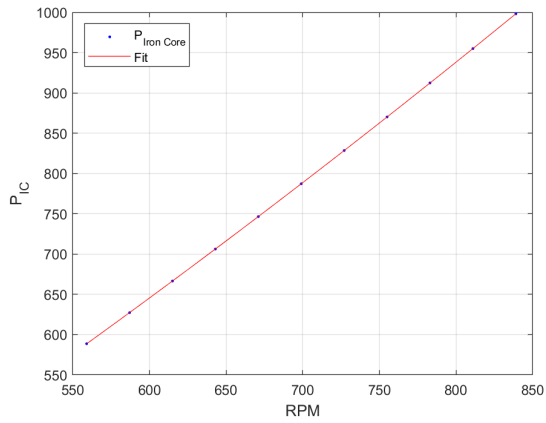


Figure 8.7: IC loss vs rpm at 160kW

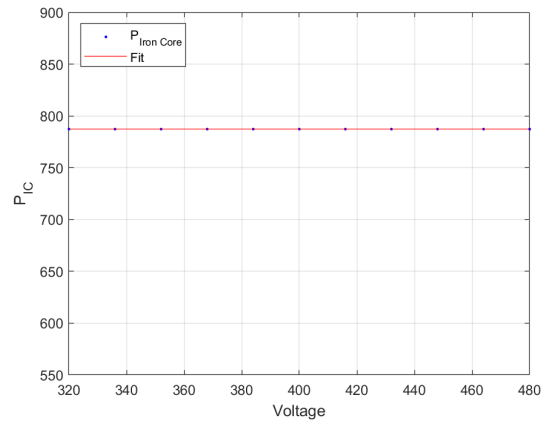


Figure 8.8: IC loss vs voltage at 160kW

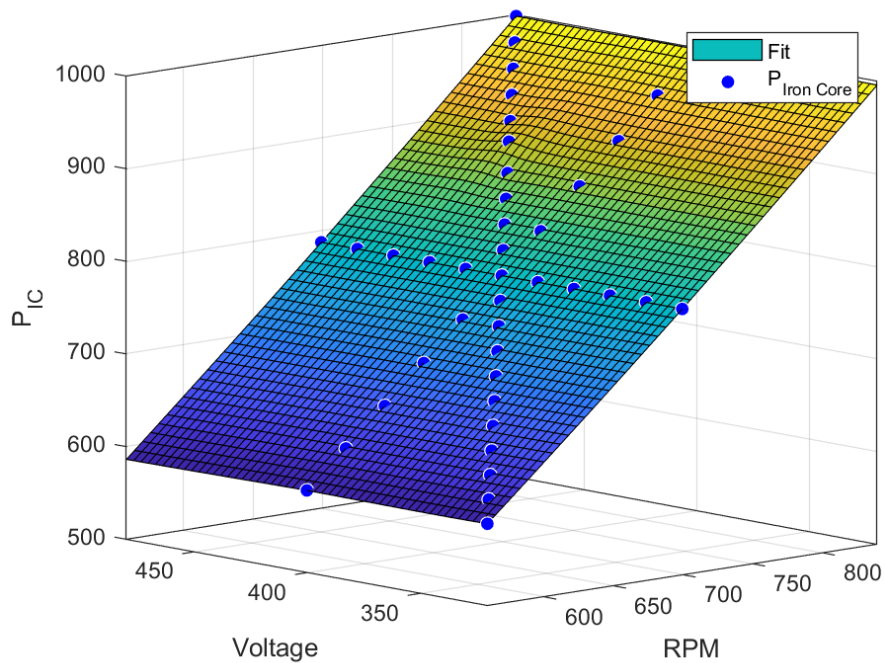


Figure 8.9: IC losses at 160 kW, 3D-Plot

The IC-losses at 160 kW show the same tendency as described for 20 kW.

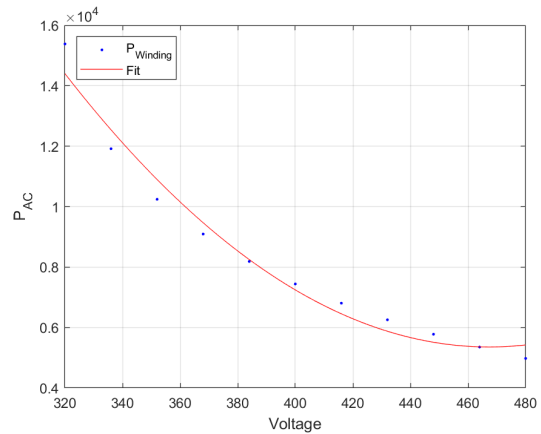
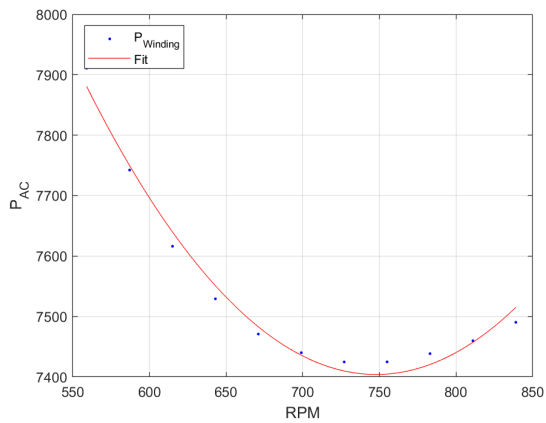


Figure 8.10: AC loss vs rpm at 160kW **Figure 8.11:** AC loss vs voltage at 160kW

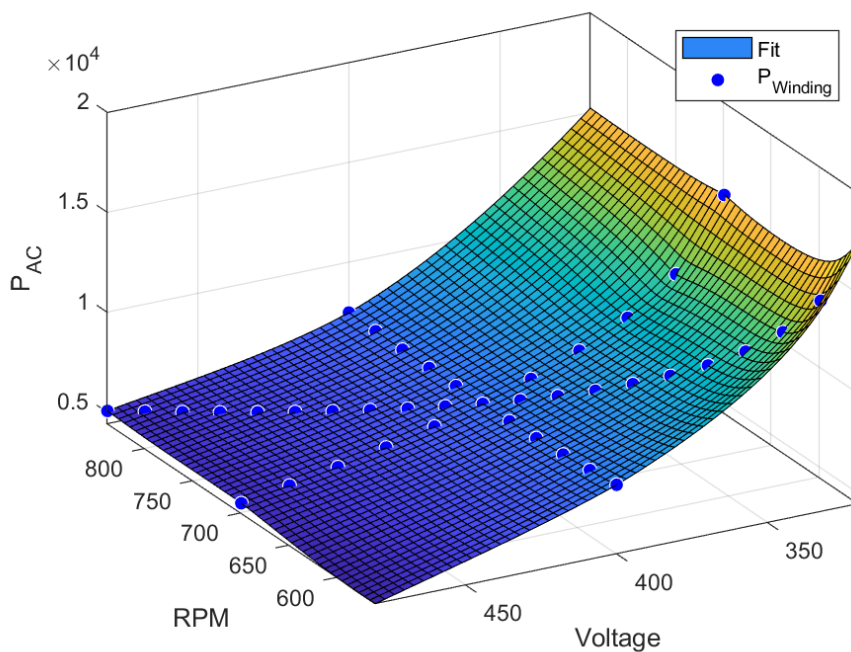


Figure 8.12: AC losses at 160kW, 3D-Plot

The AC-losses at 160 kW behave differently than at 20 kW. As can be seen in figure 8.10, the loss is decreasing with increasing rpm up to around the rated speed. At rpm higher than the rated speed, the loss starts to increase again. For varying voltage, the loss shows the same behaviour as with 20 kW power. From the 3D-plot, there is a clear tendency that the AC-losses are very high at low voltages for all levels of rpm.

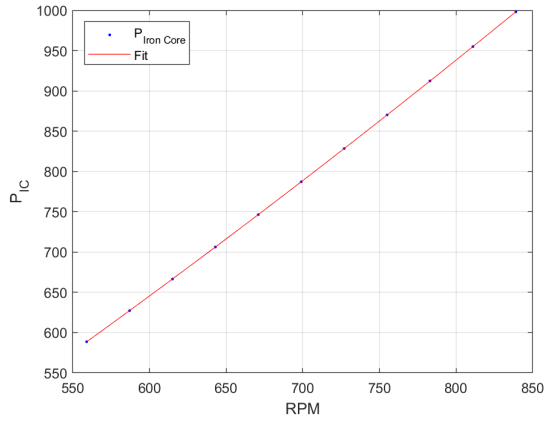


Figure 8.13: IC loss vs rpm at 200kW

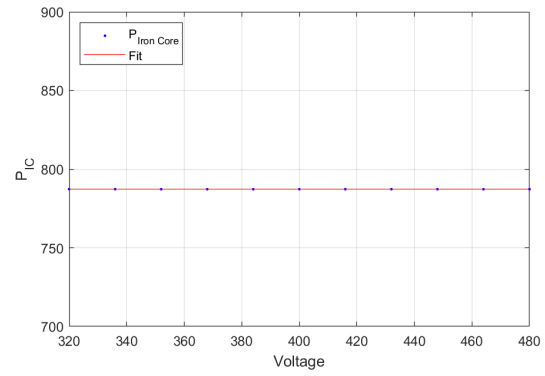


Figure 8.14: IC loss vs voltage at 200kW

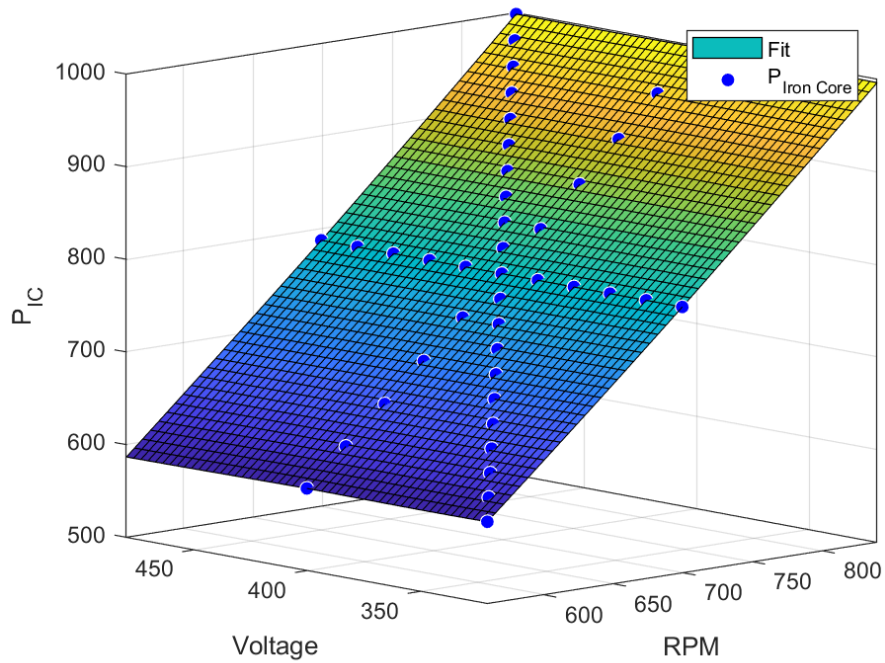


Figure 8.15: IC losses at 200 kW, 3D-Plot

The figures above show the IC losses at 200 kW. Comparing to the IC losses at 160 kW, it is evident that these losses are the same.

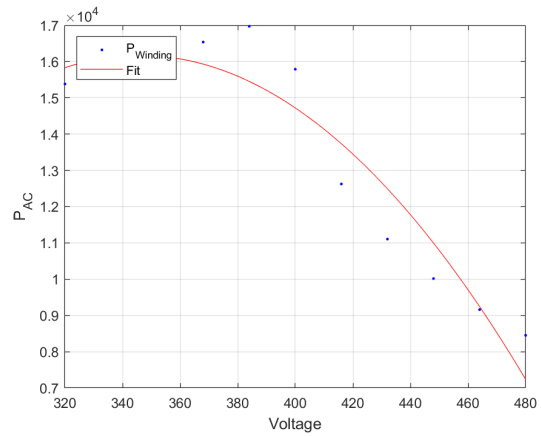
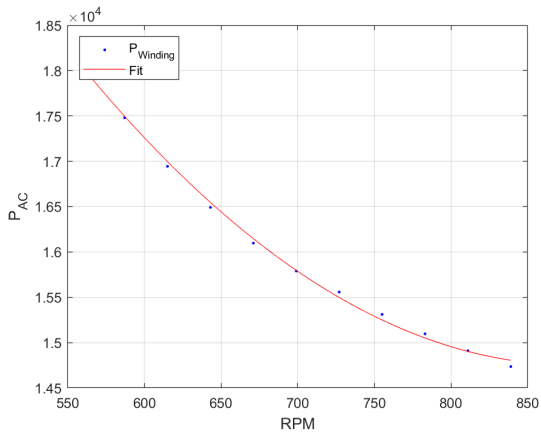


Figure 8.16: AC loss vs rpm at 200kW **Figure 8.17:** AC loss vs voltage at 200kW

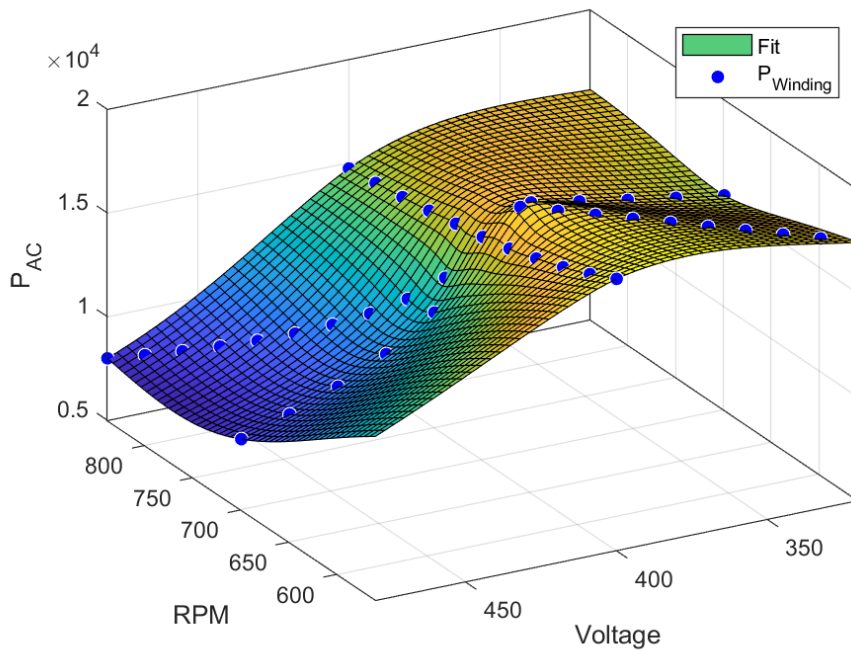


Figure 8.18: AC losses at 200kW, 3D-Plot

The figures above show the AC-losses at the rated power of 200 kW. The results are different than at both 20 and 160 kW, showing a more concave reduction with increasing voltages. This implies that the AC losses at rated speed and voltage at 200 kW is much higher than the same losses at 160 kW. This can be seen in figure 8.18.

8.2 Temperature Results

This section presents the results of different temperature simulations. Most simulations are done for 10^4 time-steps, with constant power, voltage and frequency through the simulation. The results include temperatures in different parts of the motor for several power outputs. There are also plots of the winding temperature for numerous combinations of voltage and rpm. The steady state temperatures at rated voltage and rpm for different power outputs can be seen in the table below:

Table 8.2: Temperatures in [C°] at rated voltage and speed for different power output

Power output	Stator core	Winding	Permanent Magnet	Rotor core
20 kW	26.7	30.9	20.4	19.0
160 kW	65.6	93.1	36.8	29.4
200 kW	117.7	176.3	58.9	43.4

From table 8.2 the temperature in the stator core and the windings increase significantly with increased power output. The winding temperature is by far the highest, as an effect of the increasing copper losses. The windings are also the furthest away from the cooling effect of the surrounding seawater. This effect, in combination with low losses, can be seen by the relatively low temperatures in the rotor core and permanent magnets. The results and ratios between motor parts seem reasonable when compared with relevant literature, for instance with [67]. The complete time-series plots of the simulations can be seen in figure 8.19, 8.21 and 8.23. The values displayed in the table are the temperature at the end of the simulation, i.e. at time-step $t = 10^4$.

Figure 8.19 shows the temperature simulation for 20 kW operation. The simulation starts at $t = 0$ with the temperature at all four nodes assumed to be equal to the seawater temperature of $15C^\circ$. The temperatures stabilize after around 3000 seconds or 50 minutes.

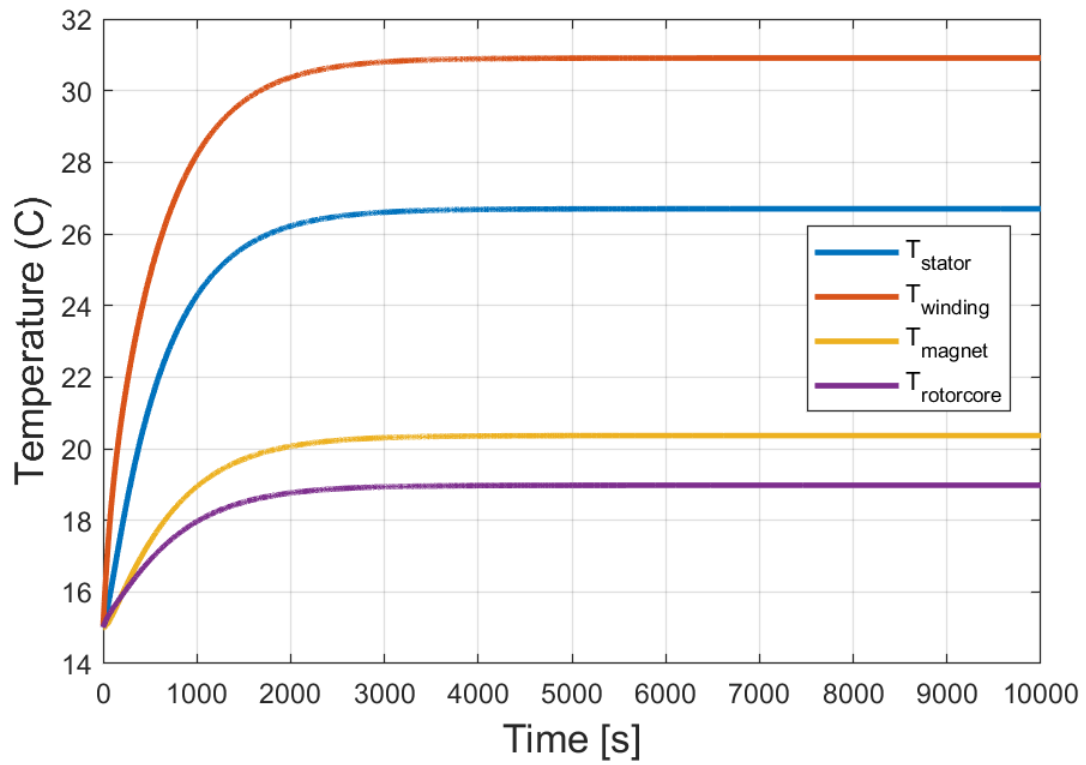


Figure 8.19: Temperature in 4 nodes at 20 kW

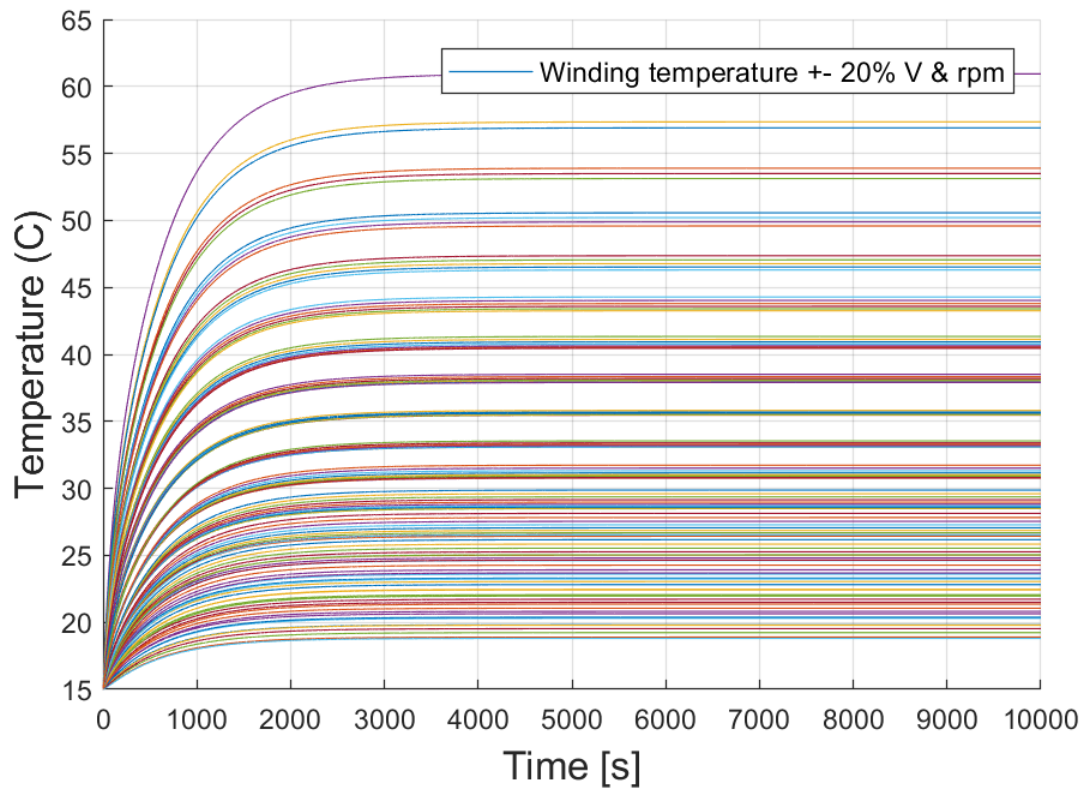


Figure 8.20: Simulations of winding temperature at 20 kW for different V and rpm

Figure 8.20 shows the simulation of winding temperatures at 20 kW for variations of voltage and frequency. The steady-state temperatures range from a minimum of $18.8C^{\circ}$ to $60.9C^{\circ}$, with a mean of $32.7C^{\circ}$. The distribution of the temperatures can be seen in figure 8.25.

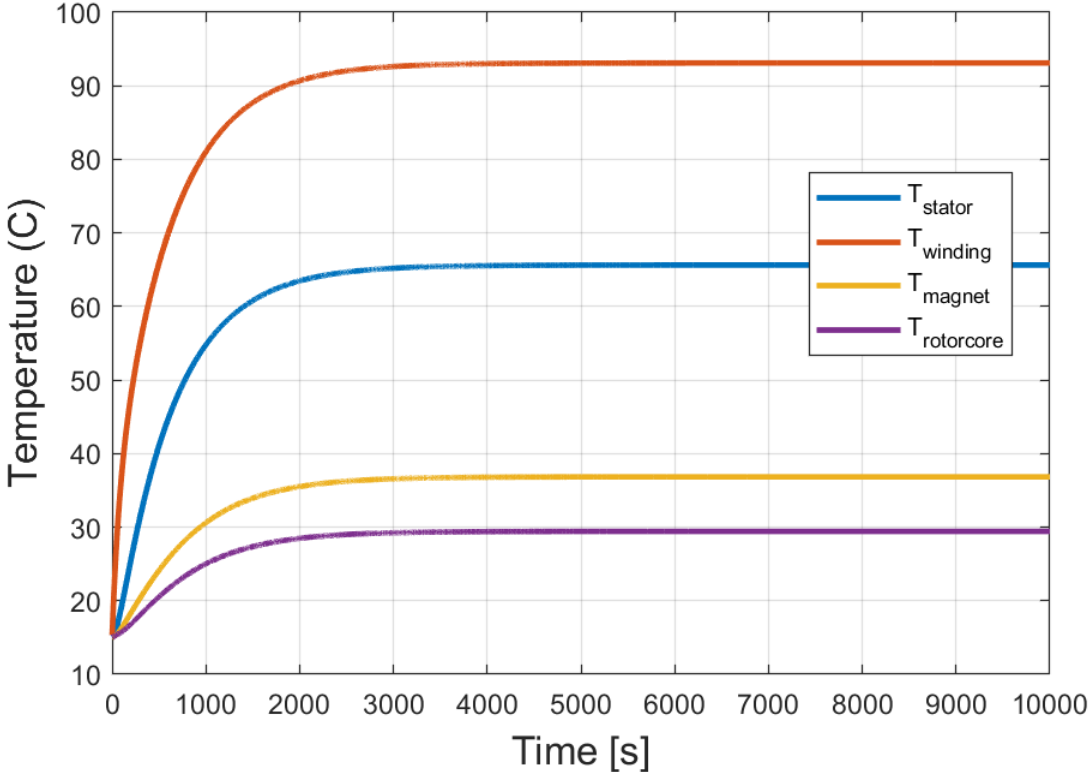


Figure 8.21: Temperature in 4 nodes at 160 kW

Figure 8.21 shows the temperatures in the motor at normal operation of 160 kW. The winding temperature has risen with around 60 degrees from figure 8.19, while the other temperatures have had a more moderate increase. This is an effect of the iron core losses remaining constant with an increase in power, while the copper losses increase. Hence, the increase in the stator, magnet and rotor-core temperature is due to heat transfer effects from the windings.

The winding temperatures at 160 kW for different voltages and frequencies show a big difference from min to max. The values range from $62.4C^{\circ}$ to $192.1C^{\circ}$ with a mean of $93.7C^{\circ}$. The minimum value occurs with a voltage of 480 and an rpm of 559, which is the highest voltage and lowest rpm tested for. The maximum temperature occurs with a voltage of 320 and an rpm of 559, which is the lowest level of both voltage and rpm tested for. The maximum temperature is over 30 degrees above the second highest temperature, indicating that the winding temperature is very sensitive at low voltage levels. The distribution of the temperatures can be seen in figure 8.26.

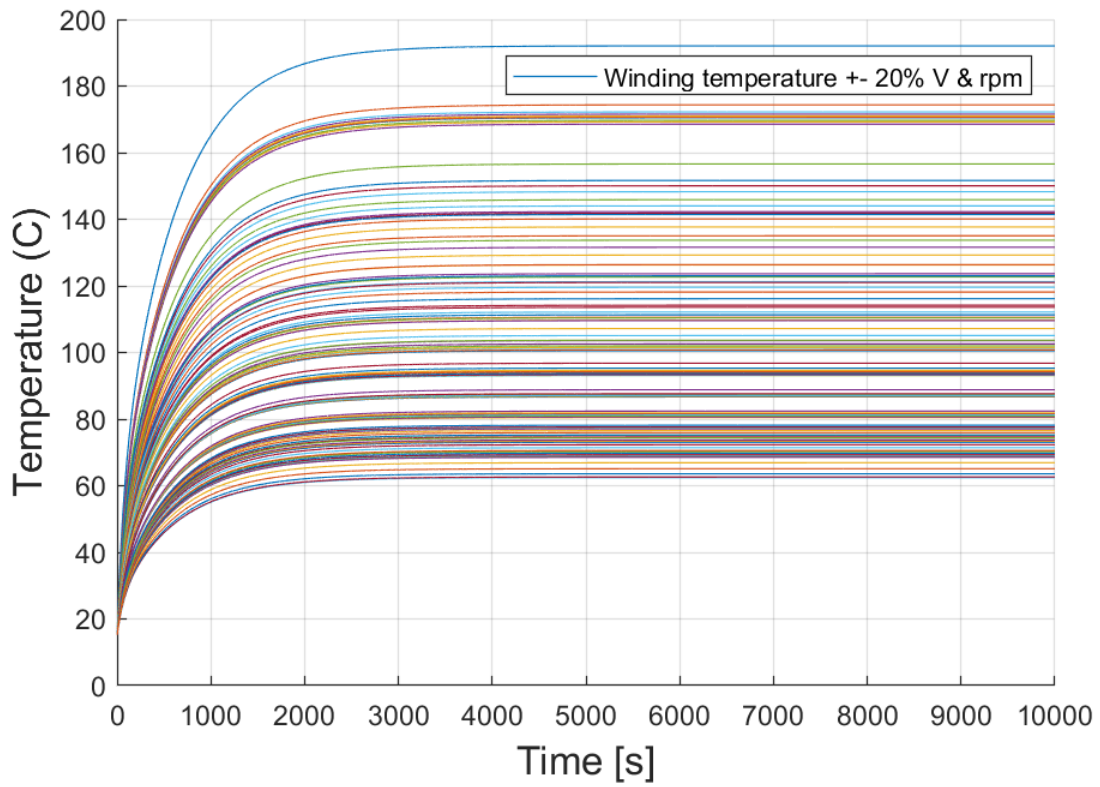


Figure 8.22: Simulations of winding temperature at 160 kW for different V and rpm

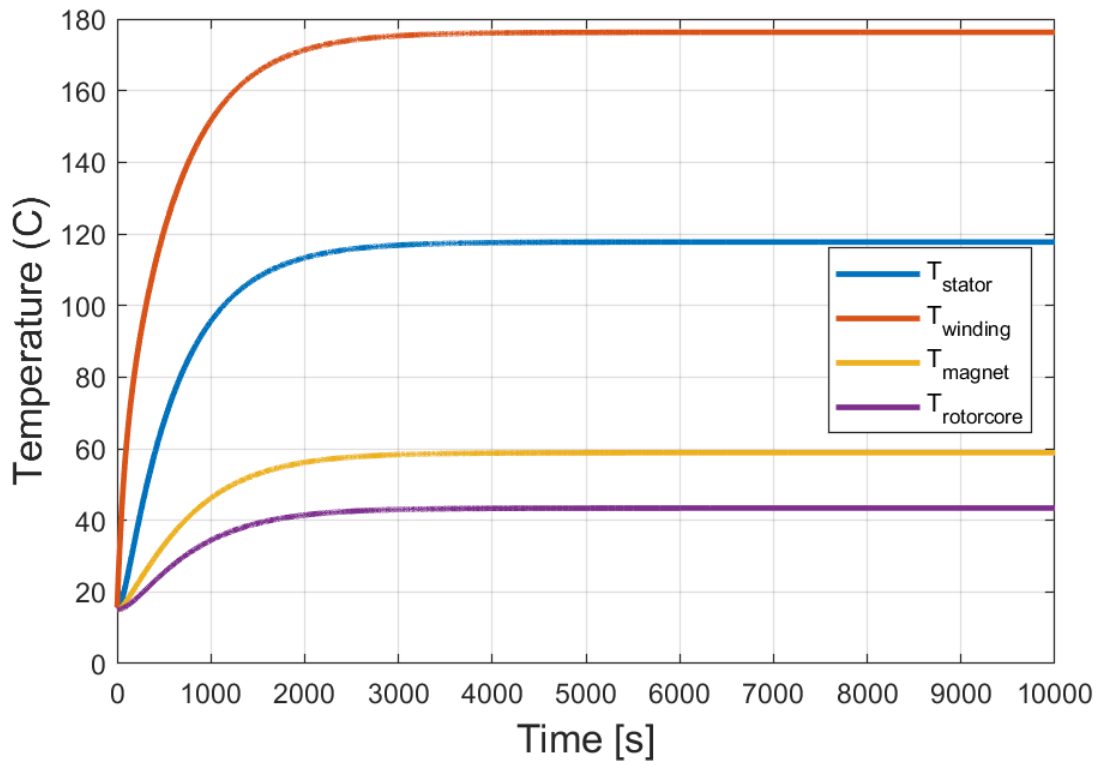


Figure 8.23: Temperature in 4 nodes at 200 kW

Figure 8.23 displays temperatures in the motor at the rated power of 200 kW. The winding and stator temperatures have almost doubled from the levels at 160 kW. As discussed earlier, this is an effect of the large copper losses at the rated power level.

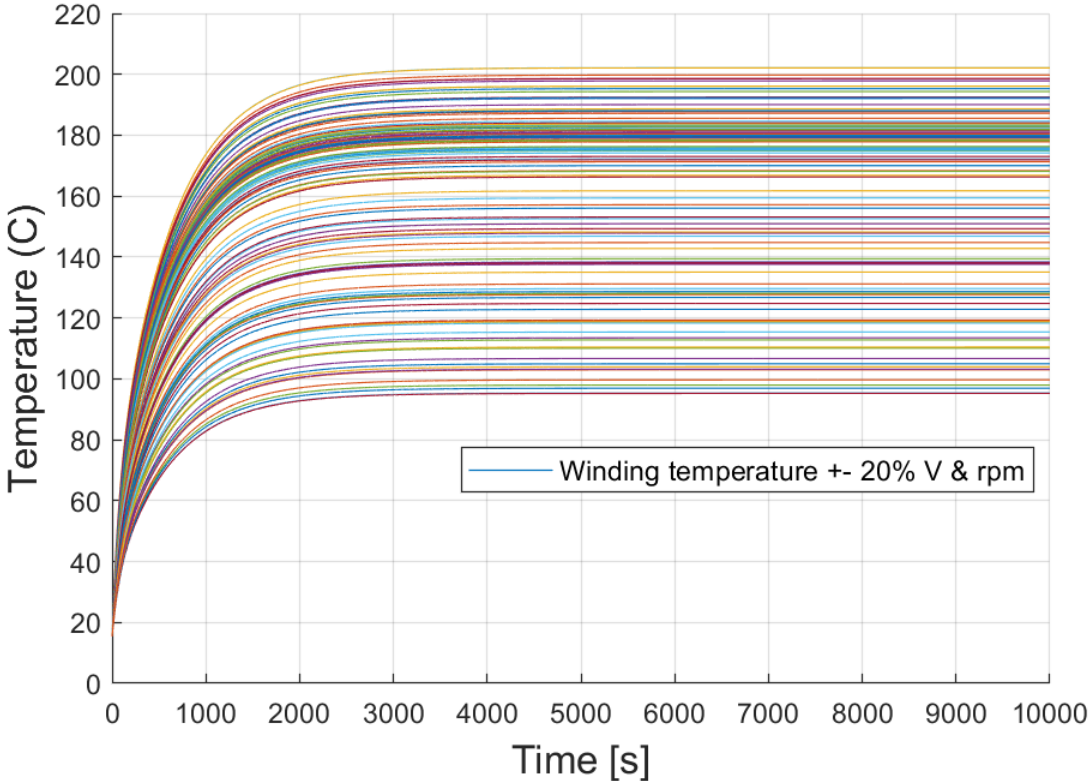


Figure 8.24: Simulations of winding temperature at 200 kW for different V and rpm

The winding temperatures at 200 kW for varying voltage and rpm has a range not too far from the range at 160 kW. The minimum value is $95.2C^{\circ}$ while the maximum value is $202.2C^{\circ}$. The same trend for low voltages and high temperatures can be seen here. However, comparing with the data at 160 kW, the mean is at $161.2C^{\circ}$ which is significantly higher than the mean at 160 kW. The distribution of the temperatures can be seen in figure 8.27. As discussed in section 7.5, the values exceeding $180C^{\circ}$ will be considered above the maximum limit, and from figure 8.24 there are some scenarios with low voltage and rpm causing the winding temperature to exceed this limit.

8.3 Distribution of Temperature Data

As described in section 7.6, the winding temperatures for different output power is analysed with the descriptive statistics tool in Excel. The objective with this analysis is to test the normality of the winding temperatures at constant power but with voltage and rpm varying with $\pm 20\%$. The key results from the analysis at each output power are displayed in table 8.3. A distribution plot for each operating point is also included.

The plot in figure 8.25 shows the distribution of the winding temperature at 20 kW. From table 8.3 one can see that the kurtosis is very close to zero, meaning that the "tailedness"

Table 8.3: Descriptive statistics of winding temperatures at different power outputs

	20 kW	160 kW	200 kW
Mean	32.8	103.5	161.2
Standard error	0.88	2.92	2.9
Standard deviation	9.7	32.1	30.8
Sample variance	94.0	1030.5	949.1
Kurtosis	-0.033	-0.178	-0.796
Skewness	0.745	0.890	-0.730
Range	42.1	129.6	106.9
Minimum	18.8	62.4	95.2
Maximum	60.9	192.1	202.2
Count	121	121	121

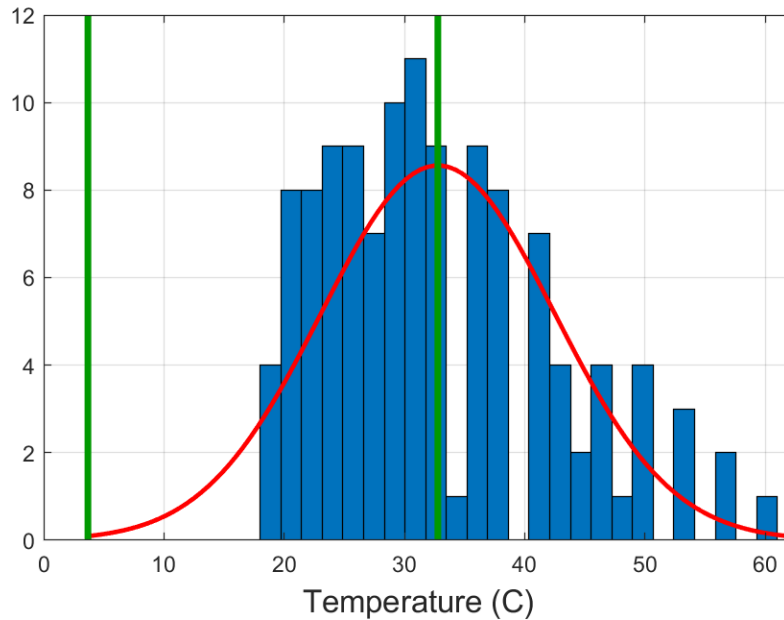


Figure 8.25: Distribution of winding temperatures at 20 kW

of the distribution is small. The skewness is positive, meaning that the distribution is asymmetrical with a tail towards the right. The values are well within the accepted range for normality.

Figure 8.26 shows the distribution at 160 kW. This is assumed the point of normal operation and will be the normal distribution used to detect faults when simulating the vessel running in cruising speed. The kurtosis and skewness are slightly higher than at 20 kW but is still well within the accepted range for normality.

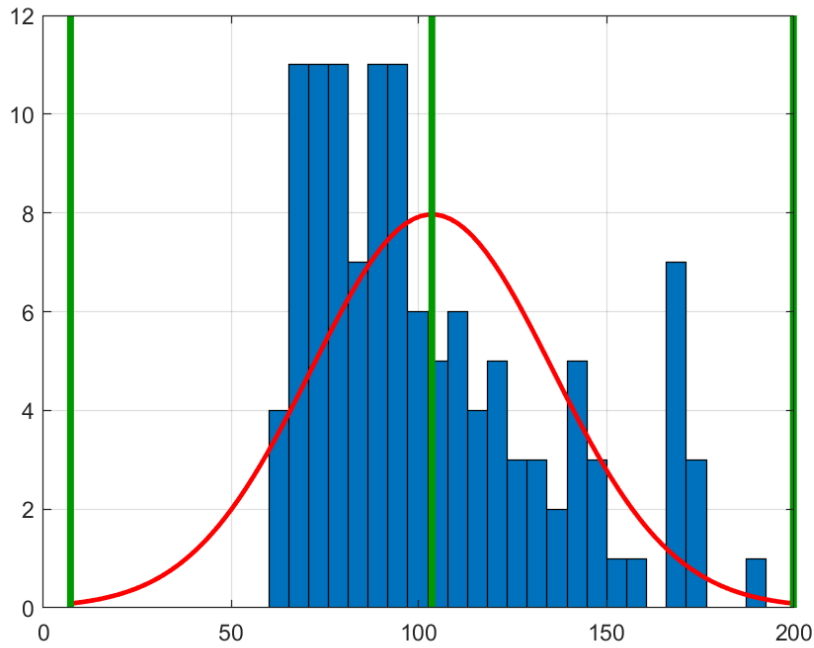


Figure 8.26: Distribution of winding temperatures at 160 kW

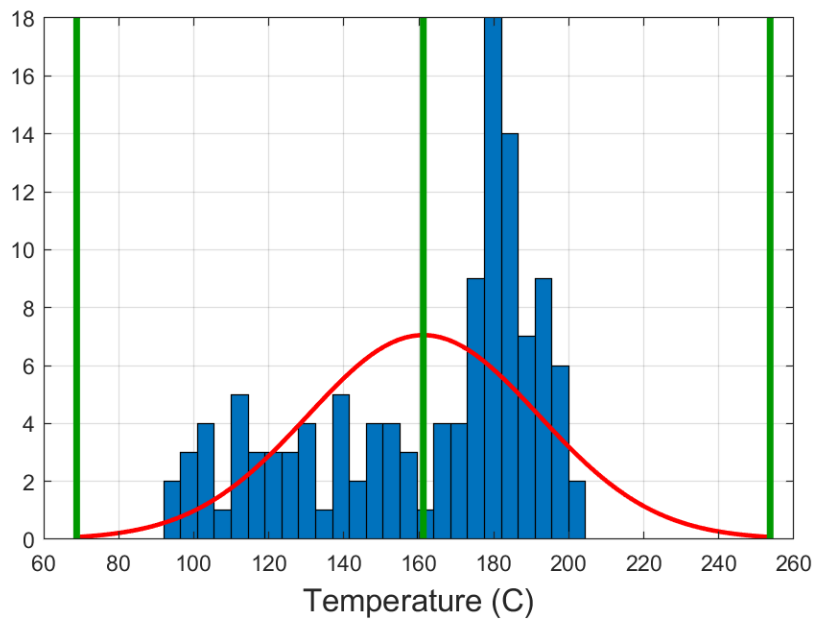


Figure 8.27: Distribution of winding temperatures at 200 kW

The distribution at 200 kW is displayed in figure 8.27 above. It shows a different development than at 20 and 160 kW, having a negative skewness and larger kurtosis value. We can see that the peak of the distribution is around $180C^{\circ}$, typically occurring at low voltages. From table 8.3, one can still see that the values of kurtosis and skewness are below one, and well within the accepted range of normality. With all the temperature distributions for different operation having a normal distribution, this method is possible to use for all operating phases.

8.4 Fault Detection

In this section, a time-series simulation with varying power level is presented. The simulation starts with normal operation at 160 kW with rated voltage and rpm. Halfway through, after 10 000 seconds, an overload scenario is simulated by increasing the power to 200 and dropping the voltage to around 300. The winding temperature from this simulation is run through the fault prediction algorithm, and each reading is given a score. As discussed in section 7.5, the maximum operating temperature allowed is assumed to be 180 degrees, corresponding to a threshold score at around 3. If this score is breached a faulty operation is indicated.

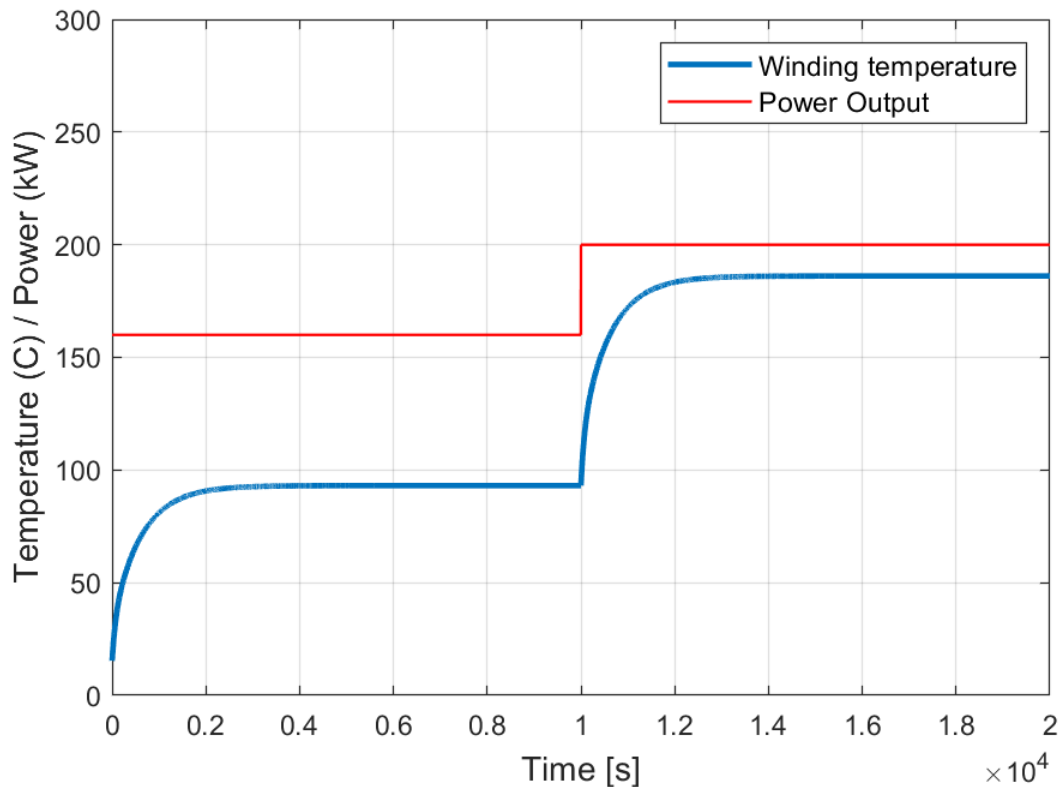


Figure 8.28: Simulation of temperature with overload scenario

Figure 8.28 shows the temperature and power output of the simulation. After around 2000 seconds the temperature stabilises at just under $100C^{\circ}$ as expected for normal operation at 160 kW. After 10 000 seconds, the power output is increased to a maximum of 200 kW, and a voltage drop to 320 V occurs. From the blue line, it can be seen that the winding temperature reaches levels above $180C^{\circ}$.

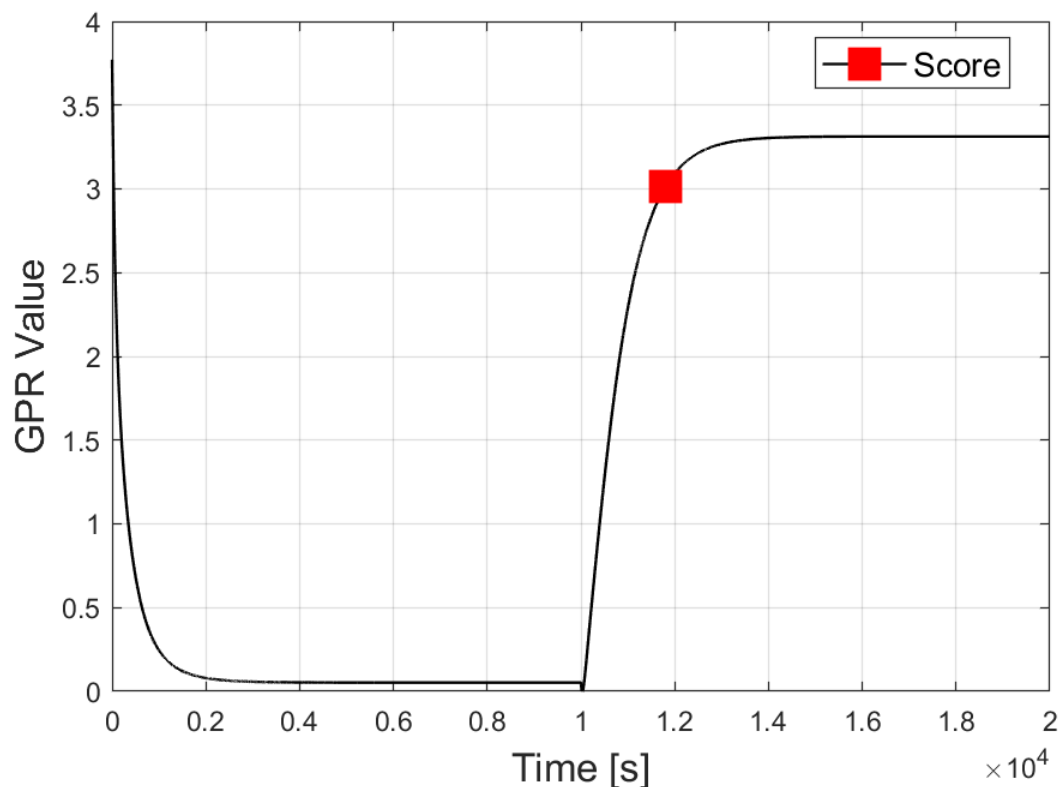


Figure 8.29: Score representing deviation from Gaussian distribution at normal operation

Figure 8.29 shows the penalty score of the results from the simulation in figure 8.28. As can be seen, the score is high and decreasing during the transient phase. To prevent this from causing a false positive, the first 1000 seconds is neglected. At the occurrence of the overload, the penalty immediately increases. The algorithm is made so that the threshold needs to be breached for 30 consecutive seconds, and the red square shows where this occurs. This shows that the algorithm has successfully identified a potential case of overloading. Results show that the temperature in the winding at the time the fault is identified is around $182C^o$, given the 30-second margin. This is assumed to be acceptable.

8.5 Lifetime Estimation

In this section, the expected lifetime and damage of the system for the simulation results above are presented. The methodology of this model is explained in section 7.5, along with the NEMA insulation class parameters of the motor.

Figure 8.30 shows the cumulative damage of the winding insulation during the simulation. Notice how the damage increases when the temperature increase, as expected.

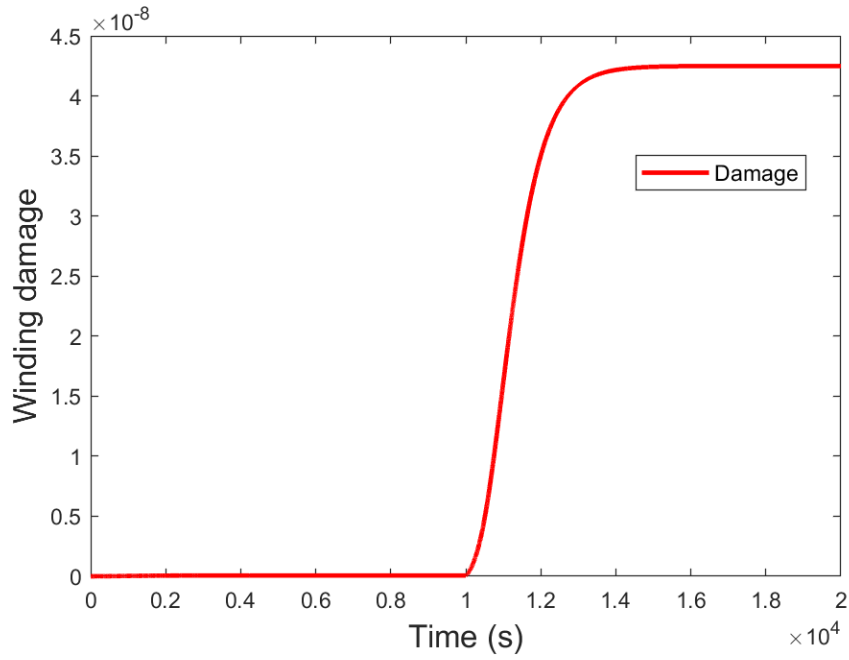


Figure 8.30: Cumulated winding damage

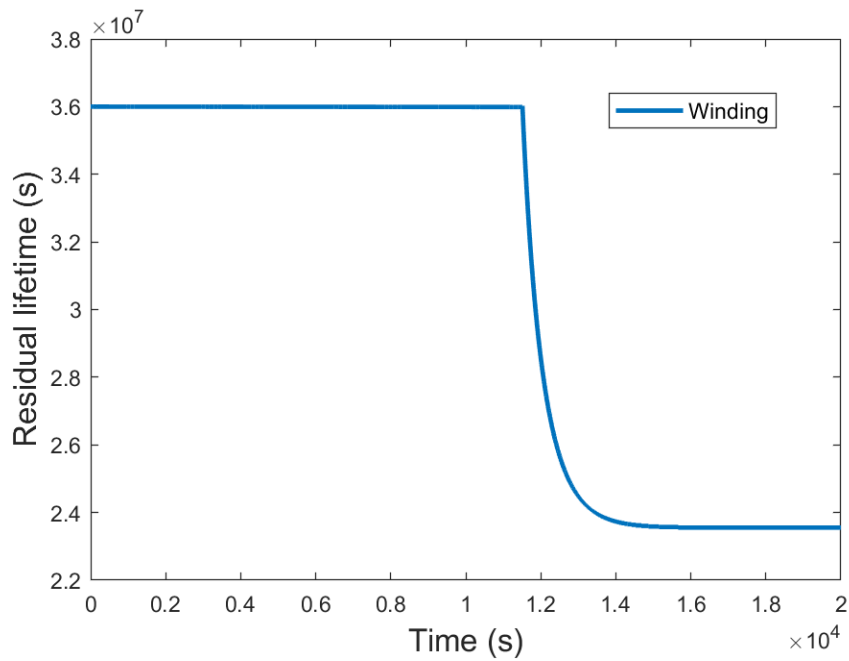


Figure 8.31: Residual lifetime for winding

Figure 8.31 shows the residual lifetime for the windings. The lifetime is calculated analogously with the results from the temperature simulation in figure 8.28. Notice how the expected lifetime of the motor decrease dramatically with the period of time where the temperature limit is breached.

8.6 Uncertainty

When running the analysis in RMXprt, an operating temperature needs to be set in addition to the output power, voltage and frequency. As the losses are calculated in order to find the temperature, this operating temperature causes some uncertainty, especially since the losses are affected by the temperature. The best approach would be to have an iterative process, where the simulated temperatures were fed to RMXprt. As of now, the operating temperature for the simulations is set to $100C^{\circ}$, which is around the mean temperature at normal operation.

Uncertainties regarding the Lumped Parameter Thermal Network are also present. When it comes to affecting the temperature, the resistances for convection and conduction as well as the capacitances has a large effect on the results. The capacitances are calculated by using parameters found in the design sheet of the motor and in material properties tables. The risk of the capacitance being very wrong is therefore assumed to be low. The resistance, however, requires very specific motor geometry as well as a coefficient for either conduction or convection. The coefficients for conduction for the same type of motor has been found in [61], and is assumed accurate. More uncertainty lies with the coefficient regarding the convection between the seawater and the metal because the table used only specifies a certain range. This is because of the effects the speed of the vessel and the temperature of the water have to the convection. Further study has to be carried out in order to verify this value. The resistance can easily be fitted more accurately if proper temperature data from a similar motor can be used for training.

The lifetime model is only as valid as the provided inputs from the thermal model. For example, the knowledge of bearing the exact temperatures at different points in the machine is crucial to get accurate results. Temperatures higher than predicted by the simulation will cause an enormous reduction in winding lifetime.

8.7 CM Methods

Condition monitoring of rotating electric machinery has received intense research interest for more than 40 years, and there are a lot of different methods available. With the exponential increase in electrically driven vessels, this will be of interest for the maritime industry. The condition monitoring approach should be minimalistic, take the minimum measurements necessary and by analysis extract a detection and diagnosis of the system or component. The methods that have demonstrated success and future potential have been evaluated against the specific AZ-PM Thrusters and the signals available.

Temperature detection has been a method that has been successful in use. It is a good global indicator of deterioration of electrical machines but has been neglected more recently because of newer, more attractive methods. However, temperature measurements should still be monitored, especially in combination with a more modern technique.

Vibration and shock pulse methods have traditionally been used extensively on electrical machinery and have proved themselves effective, especially for monitoring bearing deterioration [73]. These methods require specialized sensors with complex analysis, and the selection and location of the sensors are very important. As of now, there are no accessible

vibration signals. However, these exist, and access to this data will open up the possibility of using widely accepted techniques for monitoring of the AZ-PM Thrusters.

Literature has shown that comprehensive monitoring of an AZ-PM thruster can be achieved by measuring shaft flux, current, power and electrical discharge activity. These are signals that require complex analysis, but with a robust model, shaft flux, current and power signals are capable of detecting faults in both the electrical and mechanical parts of an electric propulsion system [73]. Power monitoring is a method that is comprehensive and can include all electrical terminal measurements for condition monitoring purposes using existing sensors. These sensors are equipped on Gunnerus, but the signals show faulty constant values, as well as having a sample rate that is far too low. Power monitoring has great potential when the motor is equipped with proper sensors with a high sampling frequency.

It is important to remember that since the motors operate with such variable speed, some key problems arise. If the speed of the drive remains constant for long periods at once, then spectral analysis of flux, voltage, current power or vibration can still be done [73]. For Gunnerus this might be possible, but such periods of steady operation will have to be identified. If the speed varies significantly, then non-stationary techniques will have to be used. These have been discussed specifically for permanent magnet motors in section 4.3. Using the power line as the communication channel for variable speed electric motors has been promising [73], and should be studied further.

AI and Machine Learning approaches applied to electrical machine drives have proven successful if they have comprehensive amounts of data available, as well as understanding the fundamental physical rules of the system. For Gunnerus, this approach might not be suitable, since the thrusters have had no known failures. Therefore, there exists no data on faulty states that these methods can use for learning. It is, however, possible to approach this problem with the method used in this case study. By combining physical modelling and data-driven techniques, one can model faulty states physically and use the results for training.

Chapter 9

Conclusions and Recommendations for Further Work

9.1 Concluding Remarks

The potential of having Digital Twins of vessels is undoubtedly huge, possibly saving the maritime industry a lot of time and money. The digital twin system should include a condition monitoring tool for fault detection of components and systems. As the world fleet is moving towards electric propulsion, preventing downtime issues related to these systems will become increasingly important. With vessels requiring high availability combined with complex, electrical systems, rise a maintenance challenge. Having an accurate condition monitoring tool could be the solution to this challenge.

This thesis has studied the literature on electrical propulsion systems and the condition monitoring techniques related to such systems on vessels. It has identified the requirements needed to build a dynamic model of such a system. This included a mapping of the required sensors as well as the different tools and methods to be used. The concept of digital twins, the technology behind it and its possible applications to the maritime industry has also been studied and presented in depth. Several condition monitoring methods have been researched. Signal-based, model-based and knowledge-based techniques of PMSM motors have been studied and discussed for possible integration with the digital twin of Gunnerus. Given a complete and high-resolution stream of sensor data from Gunnerus, a combination of a signal-based and model-based approach monitoring the power and vibration signals would be a good approach worth studying further. However, in light of the low resolution and poor quality of sensor data from the thrusters, a thermal model was pursued for further study.

The condition monitoring approach of the case study was a combination of a model-based and a data-driven solution. The satisfactory results from the electromagnetic analysis were used by the Lumped Parameter Thermal Network to simulate the thermal behaviour of the motor. Such simulations were done for different "normal" and faulty operational states, and the results gave insight into the temperature in four parts of the motor. With the lack of real-time temperature data to compare with, it is hard to verify the accuracy of the thermal model. However, when comparing with similar studies the results seem to be realistic and within the expected range. The results show that the winding temperature

breaches the maximum allowed temperature for insulation class H at maximum power output, in combination with a voltage drop. The other parts of the motor is well within this range.

The temperature data were analysed with regards to distribution and normality, showing that the data was within the range of normality for all the operating points considered. A state prediction algorithm was developed and tested using the normal distribution characteristics in combination with Gaussian process regression. This was done under the assumption that the faults could be characterized by changes in the mean and standard deviation of a time series. A simulation with an overload scenario was performed, and the incoming signals were given a score based on the deviation from the Gaussian distribution of a healthy motor at the same operating point. A threshold for identifying high temperatures had been defined, and the fault prediction algorithm managed to detect the faulty state caused by overload.

Since winding insulation failure due to high temperatures is one of the most frequently occurring electrical faults in a PMSM, a lifetime estimation based on the winding temperature was done for the same time-series simulation. The results show that operation over the allowed temperature limit has a large effect on the remaining lifetime of the motor. This tool can prove handy for simple estimation of the remaining life of the motor.

The method used in this thesis has proven to be a relatively simple and intuitive approach for fault detection of a PMSM. For a modern vessel with proper sensor data, a pure data-driven solution is expected to be the best approach in terms of cost and effectiveness. However, for vessels without proper thermal sensors, such a combination of model-based and data-driven condition monitoring can prove as a good alternative for control, fault detection and lifetime estimation.

9.2 Recommendations for Further Work

To improve the accuracy and minimise the uncertainty of the thermal simulations, fine-tuning of its parameters is required. A number of thermal resistances are nonlinear, depending on the speed or temperature of the component. The temperature also affects the losses of the motor, and therefore, the operating temperature of the motor should be introduced to the RMxprt and thermal model as a feedback loop. Another possible improvement is to perform a critical parameter tuning procedure, taking into account the uncertainties on the LPTN's parameters. This can be achieved by means of a tuning procedure based on experimental results or temperature sensor data. The procedure can be used to get an LPTN which is very accurate for time-varying loads. The first step of this procedure would be to determine the most critical model parameters to be adjusted with multiplicative correction factors. A general overview of the tuning of these factors would be as follows:

1. Experimental acquisition of temperature profiles for different operation.
2. Definition of an objective function representing the error between the LPTN predictions and experimental temperature profiles.
3. Use of an optimization algorithm that finds a set of optimal correction factors minimizing the objective function.

Another possible improvement of the solution is to include the permanent magnet temperature in the fault detection algorithm. As high temperatures in the magnets can cause demagnetization, this is a fault that can easily be added to the detection algorithm. This would require doing analysis on the distribution of the magnet temperature at different operating points.

For the digital twin paradigm to work as a real-time virtual sister vessel, a proper data flow system is required. Structured data flow with processing, storage etc. must seamlessly interact with the different models in order to work as a real-time tool for condition monitoring. The possible improvement of the Gunnerus Digital Twin must involve improving the sensors on board and sending data in real-time to the cloud. The vessel data can then be sent through the thermal model, fault prediction algorithm and lifetime estimation model for online condition monitoring.

In order to make the thermal model computational cost lower, transfer function approaches can be used for cost reduction with respect to the LPTN. A low computational cost (LCC) thermal model can be obtained from a polynomial approximation of the solution of the LPTN. The computational cost reduction with respect to the original model is a result of the LCC model not requiring computation of inverse matrices. The next step would then be to integrate this LCC with the digital twin infrastructure of R/V Gunnerus. This could be done by uploading the model as an application in Veracity. By doing this, it will be possible to include real-time thermal simulation in the digital twin viewer, and provide easy access to the fault detection and lifetime estimation results.

While the focus of this thesis was towards electrical thruster systems, many systems can take advantage of the digital twin paradigm. The opportunity of adding condition monitoring algorithms and system identification to other systems should be explored further. Examples include the overall dynamics of the vessel, the estimation of hull stress based on sensors in combination with AIS/weather data, and much more.

References

- [1] Alf Kåre Ådnanes, Asgeir J Sørensen, and Thomas Hackman. Essential characteristics of electrical propulsion and thruster drives in dp vessels. In *Proc. DP Conference. Houston, Texas*, 1997.
- [2] Luigi Alberti and Nicola Bianchi. A coupled thermal–electromagnetic analysis for a rapid and accurate prediction of im performance. *IEEE Transactions on Industrial Electronics*, 55(10):3575–3582, 2008.
- [3] Erik Andersson. Real time thermal model for servomotor applications. Technical report, Technical Report, ABB Corporate Research, Sweden, 2006.
- [4] Kurt M Becker and Joseph Kaye. Measurements of diabatic flow in an annulus with an inner rotating cylinder. *Journal of heat transfer*, 84(2):97–104, 1962.
- [5] Alberto Bellini, Fiorenzo Filippetti, Carla Tassoni, and Gérard-André Capolino. Advances in diagnostic techniques for induction machines. *IEEE Transactions on industrial electronics*, 55(12):4109–4126, 2008.
- [6] Theodore L Bergman, Frank P Incropera, David P DeWitt, and Adrienne S Lavine. *Fundamentals of heat and mass transfer*. John Wiley & Sons, 2011.
- [7] Aldo Boglietti, Andrea Cavagnino, Mario Lazzari, and A Pastorelli. A simplified thermal model for variable speed self cooled industrial induction motor. In *Conference Record of the 2002 IEEE Industry Applications Conference. 37th IAS Annual Meeting (Cat. No. 02CH37344)*, volume 2, pages 723–730. IEEE, 2002.
- [8] Aldo Boglietti, Andrea Cavagnino, and David Staton. Determination of critical parameters in electrical machine thermal models. *IEEE Transactions on Industry Applications*, 44(4):1150–1159, 2008.
- [9] Yung-Kang Robert Chin. *A Permanent Magnet Traction Motor for Electric Forklifts: Design and Iron Loss Analysis with Experimental Verifications*. PhD thesis, KTH, 2006.
- [10] Vincent Choqueuse, Mohamed Benbouzid, et al. Condition monitoring of induction motors based on stator currents demodulation. *INTERNATIONAL REVIEW OF ELECTRICAL ENGINEERING-IREE*, 10(6):704–715, 2015.
- [11] Anurag Choudhary, Deepam Goyal, Sudha Letha Shimi, and Aparna Akula. Condition monitoring and fault diagnosis of induction motors: A review. *Archives of Computational Methods in Engineering*, pages 1–18, 2018.

- [12] NJ Clarke. Marine electrical power systems. In *Second International Conference on Power Electronics, Machines and Drives (PEMD 2004)*., volume 1, pages 361–366. IET, 2004.
- [13] Sergio MA Cruz and AJ Marques Cardoso. Multiple reference frames theory: A new method for the diagnosis of stator faults in three-phase induction motors. *IEEE Transactions on Energy Conversion*, 20(3):611–619, 2005.
- [14] Alexander Danielsen-Haces. Digital twin development-condition monitoring and simulation comparison for the revolt autonomous model ship. Master’s thesis, NTNU, 2018.
- [15] AB Dehkordi, AM Gole, and TL Maguire. Permanent magnet synchronous machine model for real-time simulation. *International Conference on Power Systems Transients (IPST’05)*, (Vol. 5), 2005.
- [16] Georgios D Demetriades, Hector Zelaya De La Parra, Erik Andersson, and Håkan Olsson. A real-time thermal model of a permanent-magnet synchronous motor. *IEEE Transactions on Power Electronics*, 25(2):463–474, 2010.
- [17] David G Dorrell. Combined thermal and electromagnetic analysis of permanent-magnet and induction machines to aid calculation. *IEEE Transactions on Industrial Electronics*, 55(10):3566–3574, 2008.
- [18] Fang Duan and Rastko Živanović. Condition monitoring of an induction motor stator windings via global optimization based on the hyperbolic cross points. *IEEE Transactions on Industrial Electronics*, 62(3):1826–1834, 2015.
- [19] LLC. Engineers Edge. Convective heat transfer coefficients table chart. https://www.engineersedge.com/heat_transfer/convective_heat_transfer_coefficients__13378.htm, 2015. Accessed 01.02.19.
- [20] LLC. Engineers Edge. Specific heat capacity of metals table chart. https://www.engineersedge.com/materials/specific_heat_capacity_of_metals_13259.htm, 2015. Accessed 01.02.19.
- [21] Stein Ove Erikstad. Design patterns for digital twin solutions in marine systems design and operations. 2018.
- [22] GE. Ge digital twin: Analytic engine for the digital power plant. https://www.ge.com/digital/sites/default/files/download_assets/Digital-Twin-for-the-digital-power-plant-.pdf, Accessed 2018-12-05.
- [23] RD Geertsma, RR Negenborn, K Visser, and JJ Hopman. Design and control of hybrid power and propulsion systems for smart ships: A review of developments. *Applied Energy*, 194:30–54, 2017.
- [24] Dieter Gerling and Gurakuq Dajaku. Novel lumped-parameter thermal model for electrical systems. In *2005 European Conference on Power Electronics and Applications*, pages 10–pp. IEEE, 2005.

- [25] Mahdi Ghane, Amir R Nejad, Mogens Blanke, Zhen Gao, and Torgeir Moan. Statistical fault diagnosis of wind turbine drivetrain applied to a 5mw floating wind turbine. In *Journal of Physics: Conference Series*, volume 753, page 052017. IOP Publishing, 2016.
- [26] N Gindy and A Al-Habaibeh. Condition monitoring of cutting tools using artificial neural networks. In *Proceedings of the thirty-second international matador conference*, pages 299–304. Springer, 1997.
- [27] Y Han and YH Song. Condition monitoring techniques for electrical equipment—a literature survey. *IEEE Transactions on Power delivery*, 18(1):4–13, 2003.
- [28] Jan Fredrik Hansen and Frank Wendt. History and state of the art in commercial electric ship propulsion, integrated power systems, and future trends. *Proceedings of the IEEE*, 103(12):2229–2242, 2015.
- [29] G Henneberger, K Ben Yahia, and M Schmitz. Calculation and identification of a thermal equivalent circuit of a water cooled induction motor for electric vehicle applications. 1995.
- [30] Norden E Huang, Zheng Shen, Steven R Long, Manli C Wu, Hsing H Shih, Quanan Zheng, Nai-Chyuan Yen, Chi Chao Tung, and Henry H Liu. The empirical mode decomposition and the hilbert spectrum for nonlinear and non-stationary time series analysis. In *Proceedings of the Royal Society of London A: mathematical, physical and engineering sciences*, volume 454, pages 903–995. The Royal Society, 1998.
- [31] D Huger and D Gerling. An advanced lifetime prediction method for permanent magnet synchronous machines. In *2014 International Conference on Electrical Machines (ICEM)*, pages 686–691. IEEE, 2014.
- [32] ANSYS Inc. Ansys rmxprt. <https://www.ansys.com/products/electronics/ansys-rmxprt>, 2019. Accessed 05.06.19.
- [33] ANSYS Inc. Ansys twin builder. <https://www.ansys.com/products/systems/ansys-twin-builder>, 2019. Accessed 05.06.19.
- [34] Rolf Isermann and Peter Balle. Trends in the application of model-based fault detection and diagnosis of technical processes. *Control engineering practice*.
- [35] Sigrid Siksjø Johansen. On developing a digital twin for fault detection in drivetrains of offshore wind turbines. Master’s thesis, NTNU, 2018.
- [36] Sami Kanerva and Jan-Fredrik Hansen. State of the art in electric propulsion—viewpoint on redundancy. In *Electric Ship Technologies Symposium, 2009. ESTS 2009. IEEE*, pages 499–504. IEEE, 2009.
- [37] Subrata Karmakar, Surajit Chattopadhyay, Madhuchhanda Mitra, and Samarjit Sen-gupta. Induction motor fault diagnosis. *Publisher Springer Singapore*, 2016.
- [38] James L Kirtley, Arijit Banerjee, and Steven Englebretson. Motors for ship propulsion. *Proceedings of the IEEE*, 103(12):2320–2332, 2015.

- [39] Wired Brand Lab. Digital twin: Bridging the physical-digital divide. <https://www.ibm.com/blogs/internet-of-things/iot-digital-twin-enablers/>, 2017. Accessed 03.03.19.
- [40] Sang-Bin Lee, Thomas G Habetler, Ronald G Harley, and David J Gritter. An evaluation of model-based stator resistance estimation for induction motor stator winding temperature monitoring. *IEEE Transactions on energy conversion*, 17(1):7–15, 2002.
- [41] Chun Li, Fu-Chang Huang, and Yong-Qing Wang. An applicable real-time thermal model for temperature prediction of permanent magnet synchronous motor. *Proceedings of the Institution of Mechanical Engineers, Part I: Journal of Systems and Control Engineering*, 231(1):43–51, 2017.
- [42] Xiaodong Liang and Kenneth Edomwandekhoe. Condition monitoring techniques for induction motors. In *Industry Applications Society Annual Meeting, 2017 IEEE*, pages 1–10. IEEE, 2017.
- [43] Haitao Liao, Elsayed A Elsayed, and Ling-Yau Chan. Maintenance of continuously monitored degrading systems. *European Journal of Operational Research*, 175(2):821–835, 2006.
- [44] Jinhai Liu and Wei Chen. Generalized dq model of the permanent magnet synchronous motor based on extended park transformation. In *Future Energy Electronics Conference (IFEEEC), 2013 1st International*, pages 885–890. IEEE, 2013.
- [45] Li Liu and David A Cartes. A particle swarm optimization approach for automatic diagnosis of pmsm stator fault. In *American Control Conference, 2006*, pages 6–pp. IEEE, 2006.
- [46] Jehudi Maes and Jan A Melkebeek. Speed-sensorless direct torque control of induction motors using an adaptive flux observer. *IEEE Transactions on Industry Applications*, 36(3):778–785, 2000.
- [47] Johann Mayer, Dieter Gerling, and IEEE Staff Corporate Author. *Simulation of arbitrary fault-conditions in PM-machines by generalized unsymmetrical modeling*. 2012 XXth International Conference on Electrical Machines (ICEM). IEEE, 2012.
- [48] PH Mellor, D Roberts, and DR Turner. Lumped parameter thermal model for electrical machines of tefc design. In *IEE Proceedings B (Electric Power Applications)*, volume 138, pages 205–218. IET, 1991.
- [49] Omar Munoz-Ornelas, David A Elvira-Ortiz, Roque A Osornio-Rios, Rene J Romero-Troncoso, and Luis A Morales-Hernandez. Methodology for thermal analysis of induction motors with infrared thermography considering camera location. In *IECON 2016-42nd Annual Conference of the IEEE Industrial Electronics Society*, pages 7113–7118. IEEE, 2016.
- [50] Kevin P Murphy. *Machine learning: a probabilistic perspective*. MIT press, 2012.
- [51] Subhasis Nandi, Hamid A Toliyat, and Xiaodong Li. Condition monitoring and fault diagnosis of electrical motors—a review. *IEEE transactions on energy conversion*, 20(4):719–729, 2005.

- [52] Amir Rasekhi Nejad, Zhen Gao, and Torgeir Moan. Fatigue reliability-based inspection and maintenance planning of gearbox components in wind turbine drivetrains. *Energy Procedia*, 53:248–257, 2014.
- [53] Peter F Odgaard and Amir R Nejad. Frequency based wind turbine gearbox fault detection applied to a 750 kw wind turbine. In *Control Applications (CCA), 2014 IEEE Conference on*, pages 1383–1388. IEEE, 2014.
- [54] H Pestana. Future trends of electrical propulsion and implications to ship design. *Proc. Martech*, 2014.
- [55] Liliane Pintelon and Alejandro Parodi-Herz. Maintenance: an evolutionary perspective. In *Complex system maintenance handbook*, pages 21–48. Springer, 2008.
- [56] Rolls-Royce plc. New azimuthing permanent magnet thruster. <https://www.rolls-royce.com/~media/Files/R/Rolls-Royce/documents/marine-product-finder/rr-az-pm-broch190816.pdf>, 2016. Accessed 04.02.19.
- [57] Qinglin Qi and Fei Tao. Digital twin and big data towards smart manufacturing and industry 4.0: 360 degree comparison. *IEEE Access*, 6:3585–3593, 2018.
- [58] J Quiroga, DA Cartes, CS Edrington, and Li Liu. Neural network based fault detection of pmsm stator winding short under load fluctuation. In *Power Electronics and Motion Control Conference, 2008. EPE-PEMC 2008. 13th*, pages 793–798. IEEE, 2008.
- [59] J Quiroga, Li Liu, and DA Cartes. Fuzzy logic based fault detection of pmsm stator winding short under load fluctuation using negative sequence analysis. In *American Control Conference, 2008*, pages 4262–4267. IEEE, 2008.
- [60] Carl Edward Rasmussen. Gaussian processes in machine learning. In *Summer School on Machine Learning*, pages 63–71. Springer, 2003.
- [61] Astrid Røkke. Permanent magnet generators for marine current tidal turbines. *Doctoral thesis at NTNU*, 2017.
- [62] Roland Rosen, Georg Von Wichert, George Lo, and Kurt D Bettenhausen. About the importance of autonomy and digital twins for the future of manufacturing. *IFAC-PapersOnLine*, 48(3):567–572, 2015.
- [63] J Rosero, L Romeral, Esteban Rosero, and J Urresty. Fault detection in dynamic conditions by means of discrete wavelet decomposition for pmsm running under bearing damage. In *Applied Power Electronics Conference and Exposition, 2009. APEC 2009. Twenty-Fourth Annual IEEE*, pages 951–956. IEEE, 2009.
- [64] Javier A Rosero, Luis Romeral, Juan A Ortega, and Esteban Rosero. Short-circuit detection by means of empirical mode decomposition and wigner–ville distribution for pmsm running under dynamic condition. *IEEE Transactions on Industrial Electronics*, 56(11):4534–4547, 2009.
- [65] Funda Sahin, AM Tuckey, and AJA Vandenput. Design, development and testing of a high-speed axial-flux permanent-magnet machine. In *Conference Record of the 2001 IEEE Industry Applications Conference. 36th IAS Annual Meeting (Cat. No. 01CH37248)*, volume 3, pages 1640–1647. IEEE, 2001.

- [66] Benjamin Schleich, Nabil Anwer, Luc Mathieu, and Sandro Wartzack. Shaping the digital twin for design and production engineering. *CIRP Annals*, 66(1):141–144, 2017.
- [67] Claudio Sciascera, Paolo Giangrande, Luca Papini, Chris Gerada, and Michael Galea. Analytical thermal model for fast stator winding temperature prediction. *IEEE Transactions on Industrial Electronics*, 64(8):6116–6126, 2017.
- [68] Øyvind Smogeli. Digital twins at work in maritime and energy. <https://www.dnvgl.com/feature/digital-twins.html>, 2 2017. Accessed 12.01.19.
- [69] DA Staton. Thermal analysis of electric motors and generators, training course. *Motor Design Ltd*, 2007.
- [70] Dave Staton, Aldo Boglietti, and Andrea Cavagnino. Solving the more difficult aspects of electric motor thermal analysis in small and medium size industrial induction motors. *IEEE Transactions on Energy conversion*, 20(3):620–628, 2005.
- [71] Rangarajan M Tallam, Thomas G Habetler, and Ronald G Harley. Transient model for induction machines with stator winding turn faults. *IEEE Transactions on Industry Applications*, 38(3):632–637, 2002.
- [72] Fei Tao, Jiangfeng Cheng, Qinglin Qi, Meng Zhang, He Zhang, and Fangyuan Sui. Digital twin-driven product design, manufacturing and service with big data. *The International Journal of Advanced Manufacturing Technology*, 94(9-12):3563–3576, 2018.
- [73] PJ Tavner. Review of condition monitoring of rotating electrical machines. *IET Electric Power Applications*, 2(4):215–247, 2008.
- [74] Engineering ToolBox. Nema insulation classes. https://www.engineeringtoolbox.com/nema-insulation-classes-d_734.html, 2004. Accessed 07.06.19.
- [75] Zia Ullah and Jin Hur. A comprehensive review of winding short circuit fault and irreversible demagnetization fault detection in pm type machines. *Energies*, 11(12):3309, 2018.
- [76] PJ Van Spronsen and RL Tousain. An optimal control approach to preventing marine diesel engine overloading aboard karel doorman class frigates. *IFAC Proceedings Volumes*, 34(7):493–498, 2001.
- [77] B Venkataraman, B Godsey, W Premerlani, E Shulman, M Thaku, and R Midence. Fundamentals of a motor thermal model and its applications in motor protection. In *58th Annual Conference for Protective Relay Engineers, 2005.*, pages 127–144. IEEE, 2005.
- [78] Sethu Vijayakumar, Aaron D’souza, and Stefan Schaal. Incremental online learning in high dimensions. *Neural computation*, 17(12):2602–2634, 2005.
- [79] Wikipedia contributors. Induction motor — Wikipedia, the free encyclopedia, 2019. [Online; accessed 9-June-2019].

- [80] Wikipedia contributors. Nyquist–shannon sampling theorem — Wikipedia, the free encyclopedia, 2019. [Online; accessed 21-May-2019].
- [81] Wikipedia contributors. Synchronous motor — Wikipedia, the free encyclopedia, 2019. [Online; accessed 9-June-2019].
- [82] Yisha Xiang, C Richard Cassady, and Edward A Pohl. Optimal maintenance policies for systems subject to a markovian operating environment. *Computers & Industrial Engineering*, 62(1):190–197, 2012.
- [83] Ruqiang Yan and Robert X Gao. Hilbert–huang transform-based vibration signal analysis for machine health monitoring. *IEEE Transactions on Instrumentation and measurement*, 55(6):2320–2329, 2006.
- [84] Jingzhe Yang, Huiping Ye, Wei Zhou, et al. A review of permanent magnet synchronous motor fault diagnosis. In *Transportation Electrification Asia-Pacific (ITEC Asia-Pacific), 2014 IEEE Conference and Expo*, pages 1–5. IEEE, 2014.
- [85] Ali MD Younus and Bo-Suk Yang. Intelligent fault diagnosis of rotating machinery using infrared thermal image. *Expert Systems with Applications*, 39(2):2082–2091, 2012.
- [86] Junhong Zhang, Yunping Zou, and Youping Fan. Embedded neural network to model-based permanent magnet synchronous motor diagnostics. In *Power Electronics and Motion Control Conference, 2009. IPEMC'09. IEEE 6th International*, pages 1813–1817. IEEE, 2009.

Appendix A

Gunnerus Sensors

A	B	C	D	E	F	G
Sensor-signal	Quantity	UoM	System/component	Explanation	Sensor-module	Group
1	Motor_Voltage	V	AZ-PM thruster	Armature voltage	drive_ps	Electric motor for AZ-PM thruster, port side
4	Motor_Current_Total	A	AZ-PM thruster	Total current	drive_ps	Electric motor for AZ-PM thruster, port side
5	Motor_Current_U	A	AZ-PM thruster	Current in U-winding	drive_ps	Electric motor for AZ-PM thruster, port side
6	Motor_Current_V	A	AZ-PM thruster	Current in V-winding	drive_ps	Electric motor for AZ-PM thruster, port side
7	Motor_Current_W	A	AZ-PM thruster	Current in W-winding	drive_ps	Electric motor for AZ-PM thruster, port side
8	Motor_Frequency	Hz	AZ-PM thruster	Electric motor frequency	drive_ps	Electric motor for AZ-PM thruster, port side
9	Drive_Motor_Torque	kNm	AZ-PM thruster	Electric drive torque	drive_ps	Electric motor for AZ-PM thruster, port side
10	Drive_Motor_Power	kW	AZ-PM thruster	Electric drive power	drive_ps	Electric motor for AZ-PM thruster, port side
11	Drive_Running	bool?	AZ-PM thruster	Check if running	drive_ps	Electric motor for AZ-PM thruster, port side
12	Motor_Voltage	V	AZ-PM thruster	Armature voltage	drive_sb	Electric motor for AZ-PM thruster, starboard side
13	Motor_Current_Total	A	AZ-PM thruster	Total current	drive_sb	Electric motor for AZ-PM thruster, starboard side
14	Motor_Current_U	A	AZ-PM thruster	Current in U-winding	drive_sb	Electric motor for AZ-PM thruster, starboard side
15	Motor_Current_V	A	AZ-PM thruster	Current in V-winding	drive_sb	Electric motor for AZ-PM thruster, starboard side
16	Motor_Current_W	A	AZ-PM thruster	Current in W-winding	drive_sb	Electric motor for AZ-PM thruster, starboard side
17	Motor_Frequency	Hz	AZ-PM thruster	Electric motor frequency	drive_sb	Electric motor for AZ-PM thruster, starboard side
18	Drive_Motor_Torque	kNm	AZ-PM thruster	Electric drive torque	drive_sb	Electric motor for AZ-PM thruster, starboard side
19	Drive_Motor_Power	kW	AZ-PM thruster	Electric drive power	drive_sb	Electric motor for AZ-PM thruster, starboard side
20	Drive_Running	bool?	AZ-PM thruster	Check if running	drive_sb	Electric motor for AZ-PM thruster, starboard side
32	AzimuthFeedback	angle	AZ-PM thruster	Actual thruster direction	hcx_port_mp	Thruster control system, port side
33	AzimuthOrder	angle	AZ-PM thruster	Requested thruster direction	hcx_port_mp	Thruster control system, port side
34	LoadFeedback	percent	AZ-PM thruster	Thruster drive motor load	hcx_port_mp	Thruster control system, port side
35	RPMFeedback	percent	AZ-PM thruster	Actual thruster drive RPM	hcx_port_mp	Thruster control system, port side
36	RPMOrder	percent	AZ-PM thruster	Requested thruster drive RPM	hcx_port_mp	Thruster control system, port side
37	Ship_speed (round off GPS sf v	m/s	AZ-PM thruster	Velocity signal from speed log	hcx_port_mp	Thruster control system, port side
38	AzimuthFeedback	angle	AZ-PM thruster	Actual thruster direction	hcx_stbd_mp	Thruster control system,starboard side
39	AzimuthOrder	angle	AZ-PM thruster	Requested thruster direction	hcx_stbd_mp	Thruster control system,starboard side
40	LoadFeedback	percent	AZ-PM thruster	Thruster drive motor load	hcx_stbd_mp	Thruster control system,starboard side
41	RPMFeedback	percent	AZ-PM thruster	Actual thruster drive RPM	hcx_stbd_mp	Thruster control system,starboard side
42	RPMOrder	percent	AZ-PM thruster	Requested thruster drive RPM	hcx_stbd_mp	Thruster control system,starboard side
43	Ship_speed (round off GPS sf v	m/s	AZ-PM thruster	Velocity signal from speed log	hcx_stbd_mp	Thruster control system,starboard side

Figure A.1: Spreadsheet describing enabled sensors

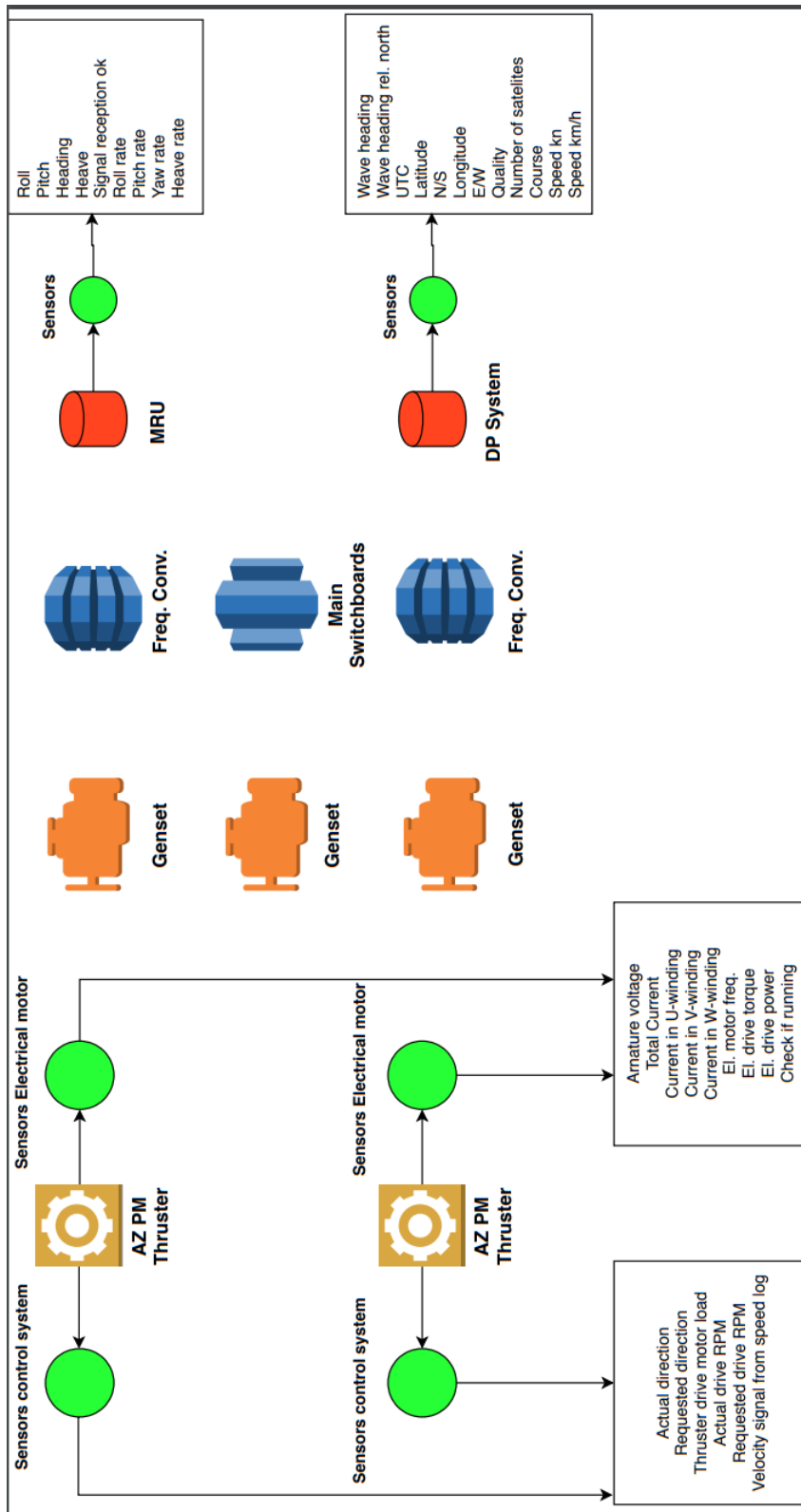


Figure A.2: Gunnerus sensor chart

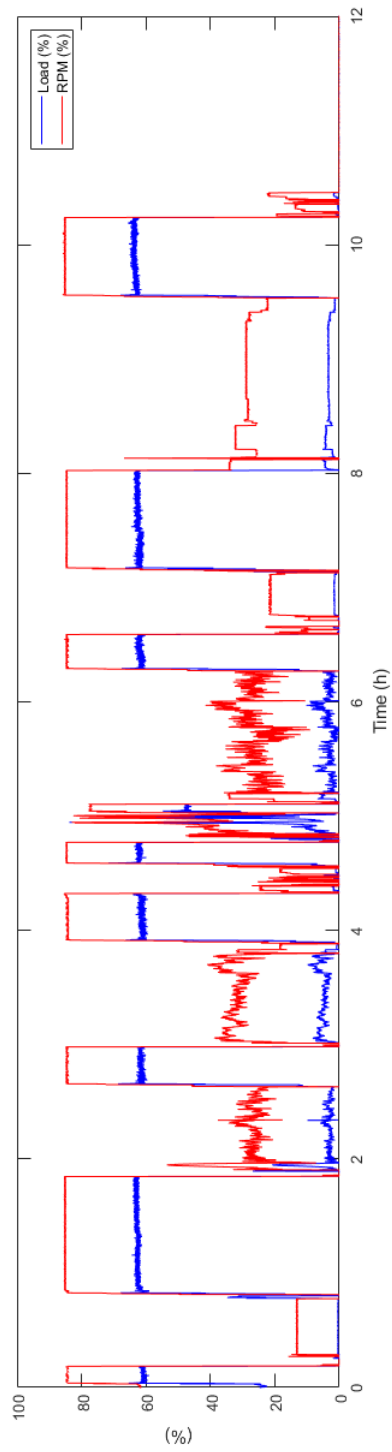


Figure A.3: Gunnerus operational profile 12 h

Appendix B

Motor Model

ADJUSTABLE-SPEED PERMANENT MAGNET SYNCHRONOUS MOTOR DESIGN	
File: Setup1.res	
GENERAL DATA	
Rated Output Power (kW):	160
Rated Voltage (V):	400
Number of Poles:	22
Frequency (Hz):	128.15
Frictional Loss (W):	12
Windage Loss (W):	0
Rotor Position:	Inner
Type of Circuit:	Y3
Type of Source:	PwM
Modulation Index:	0.8
Carrier Frequency Times:	100
One-Transistor Voltage Drop (V):	2
One-Diode Voltage Drop (V):	2
Operating Temperature (C):	100
STATOR DATA	
Number of Stator Slots:	132
Outer Diameter of Stator (mm):	650
Inner Diameter of Stator (mm):	540
Type of Stator Slot:	3
Stator Slot	
hs0 (mm):	1
hs1 (mm):	2
hs2 (mm):	35
bs0 (mm):	1
bs1 (mm):	8
bs2 (mm):	8
rs (mm):	0
Top Tooth Width (mm):	4.99579
Bottom Tooth Width (mm):	6.66163
Skew Width (Number of Slots):	0
Length of Stator Core (mm):	260
Stacking Factor of Stator Core:	0.97
Type of Steel:	M27_24G
Designed Wedge Thickness (mm):	2
Slot Insulation Thickness (mm):	0.3
Layer Insulation Thickness (mm):	0.3
End Length Adjustment (mm):	0
Number of Parallel Branches:	1
Number of Conductors per Slot:	2
Type of Coils:	21
Average Coil Pitch:	6
Number of Wires per Conductor:	3089
Wire Diameter (mm):	0.1798
Wire Wrap Thickness (mm):	0
Slot Area (mm ²):	290
Net Slot Area (mm ²):	249.58
Limited Slot Fill Factor (%):	99
Stator Slot Fill Factor (%):	80.0235
Coil Half-Turn Length (mm):	370.112
Wire Resistivity (ohm.mm ² /m):	0.0217

ROTOR DATA	
Minimum Air Gap (mm):	14.5
Inner Diameter (mm):	452
Length of Rotor (mm):	260
Stacking Factor of Iron Core:	0.97
Type of Steel:	M27_24G
Polar Arc Radius (mm):	255.5
Mechanical Pole Embrace:	0.75
Electrical Pole Embrace:	0.669128
Max. Thickness of Magnet (mm):	14
Width of Magnet (mm):	53.2286
Type of Magnet:	NdFe30
Type of Rotor:	1
Magnetic Shaft:	No
PERMANENT MAGNET DATA	
Residual Flux Density (Tesla):	1.1
Coercive Force (kA/m):	838
Maximum Energy Density (kJ/m ³):	230.45
Relative Recoil Permeability:	1.0446
Demagnetized Flux Density (Tesla):	0
Recoil Residual Flux Density (Tesla):	1.1
Recoil Coercive Force (kA/m):	838
MATERIAL CONSUMPTION	
Armature Wire Density (kg/m ³):	8900
Permanent Magnet Density (kg/m ³):	7550
Armature Core Steel Density (kg/m ³):	7650
Rotor Core Steel Density (kg/m ³):	7650
Armature Copper Weight (kg):	68.2047
Permanent Magnet Weight (kg):	32.1822
Armature Core Steel Weight (kg):	124.497
Rotor Core Steel Weight (kg):	43.9207
Total Net Weight (kg):	268.805
Armature Core Steel Consumption (kg):	464.778
Rotor Core Steel Consumption (kg):	357.906
STEADY STATE PARAMETERS	
Stator Winding Factor:	0.965926
D-Axis Reactive Inductance L _{ad} (H):	8.83453e-05
Q-Axis Reactive Inductance L _{aq} (H):	8.83453e-05
D-Axis Inductance L ₁ +L _{ad} (H):	0.000302736
Q-Axis Inductance L ₁ +L _{aq} (H):	0.000302736
Armature Leakage Inductance L ₁ (H):	0.000214391
Slot Leakage Inductance L _{s1} (H):	0.000198082
End Leakage Inductance L _{e1} (H):	1.42641e-05
Harmonic Leakage Inductance L _{d1} (H):	2.04482e-06
Zero-Sequence Inductance L ₀ (H):	0.000214391
Armature Phase Resistance R ₁ (H):	0.00973804
Armature Phase Resistance at 20C (ohm):	0.00741254

NO-LOAD MAGNETIC DATA	
Stator-Teeth Flux Density (Tesla):	1.26171
Stator-Yoke Flux Density (Tesla):	0.821522
Rotor-Yoke Flux Density (Tesla):	0.899672
Air-Gap Flux Density (Tesla):	0.471697
Magnet Flux Density (Tesla):	0.569672
Stator-Teeth By-Pass Factor:	0.000648476
Stator-Yoke By-Pass Factor:	6.14685e-06
Rotor-Yoke By-Pass Factor:	6.96993e-06
Stator-Teeth Ampere Turns (A.T):	16.668
Stator-Yoke Ampere Turns (A.T):	4.40781
Rotor-Yoke Ampere Turns (A.T):	3.77503
Air-Gap Ampere Turns (A.T):	5630.87
Magnet Ampere Turns (A.T):	-5656.19
Leakage-Flux Factor:	1
Correction Factor for Magnetic Circuit Length of Stator Yoke:	0.758299
Correction Factor for Magnetic Circuit Length of Rotor Yoke:	0.707432
No-Load DC Current (A):	7.29661
No-Load Input Power (W):	2918.64
Cogging Torque (N.m):	0.905381
FULL-LOAD DATA	
Maximum Line Induced Voltage (V):	398.3
Input DC Current (A):	427.451
Root-Mean-Square Phase Current (A):	504.655
Armature Thermal Load (A ² /mm ³):	505.315
Specific Electric Loading (A/mm):	78.5335
Armature Current Density (A/mm ²):	6.43439
Frictional and Windage Loss (W):	12
Iron-Core Loss (W):	787.248
Armature Copper Loss (W):	7440.15
Transistor Loss (W):	2218.31
Diode Loss (W):	508.058
Total Loss (W):	10965.8
Output Power (W):	160014
Input Power (W):	170980
Efficiency (%):	93.5865
Synchronous Speed (rpm):	699
Rated Torque (N.m):	2186.02
Torque Angle (degree):	50.817
Maximum Output Power (W):	200755
Torque Constant KT (Nm/A):	5.11446
WINDING ARRANGEMENT	
The 3-phase, 2-layer winding can be arranged in 6 slots as below:	
AAZZBB	

Figure B.1: Design sheet of PMSM

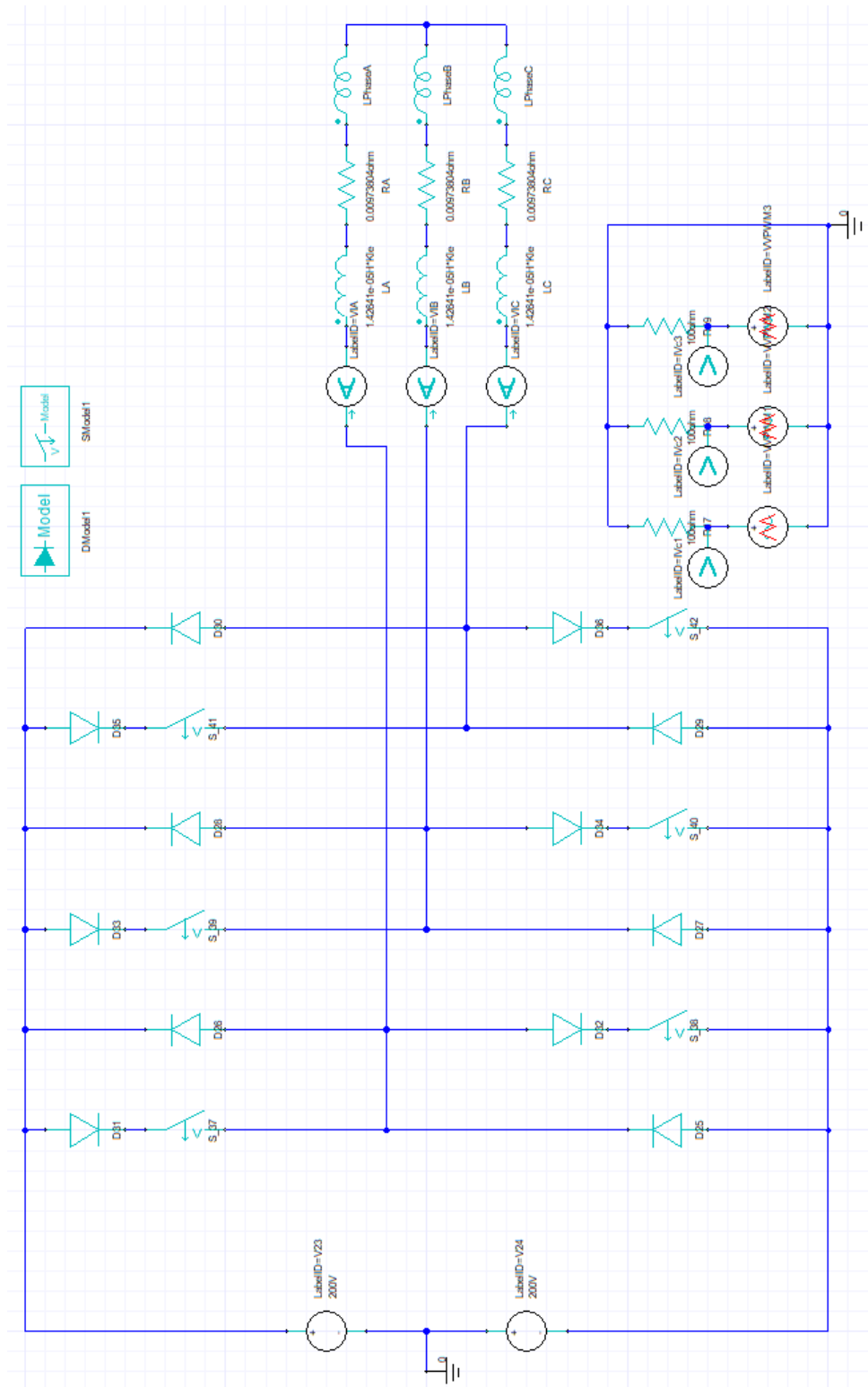


Figure B.2: Circuit of PMSM in Maxwell

